(2)

NAVAL POSTGRADUATE SCHOOL

Monterey, California

THESIS

PREDICTABILITY OF ICE CONCENTRATION ANOMALIES IN THE HIGH LATITUDES OF THE NORTH ATLANTIC USING A STATISTICAL APPROACH

by

Katharine Shanebrook Garcia

December 1988

Thesis Advisor: Robert H. Bourke
Co-Advisor: Laura D. Johnson

SECURITY CLASSIFICATION OF THIS PAGE

REPORT DOCUMENTATION PAGE

Form Approved OMB No 0704-0188

1a. REPORT SECURITY CLASSIFICATION: Unclassified	1b. RESTRICTIVE MARKINGS
2a. SECURITY CLASSIFICATION AUTHORITY	3. DISTRIBUTION / AVAILABILITY OF REPORT: Approved for public release; distribution unlimited
2b. DECLASSIFICATION / DOWNGRADING SCHEDULE	
4. PERFORMING ORGANIZATION REPORT NUMBER(S)	5. MONITORING ORGANIZATION REPORT NUMBER(S)
6a. NAME OF PERFORMING ORGANIZATION: Naval Postgraduate School; 6b. OFFICE SYMBOL (If applicable): Code 68	7a. NAME OF MONITORING ORGANIZATION: Naval Postgraduate School
6c. ADDRESS (City, State, and ZIP Code): Monterey, CA 93943 -5000	7b. ADDRESS (City, State, and ZIP Code): Monterey, CA 93943 -5000
8a. NAME OF FUNDING / SPONSORING ORGANIZATION; 8b. OFFICE SYMBOL (If applicable)	9. PROCUREMENT INSTRUMENT IDENTIFICATION NUMBER
8c. ADDRESS (City, State, and ZIP Code)	10. SOURCE OF FUNDING NUMBERS: PROGRAM ELEMENT NO; PROJECT NO; TASK NO; WORK UNIT ACCESSION NO

11. TITLE (Include Security Classification)
Predictability of Ice Concentration Anomalies in the High Latitudes of the North Atlantic Using a Statistical Approach

12. PERSONAL AUTHOR(S)
Garcia, Katharine S.

13a. TYPE OF REPORT	13b. TIME COVERED	14. DATE OF REPORT (Year, Month, Day)	15. PAGE COUNT
Master's Thesis	FROM _____ TO _____	1988 December	94

16. SUPPLEMENTARY NOTATION
The views expressed in this thesis are those of the author and do not reflect the official policy or position of the

17. COSATI CODES			18. SUBJECT TERMS (Continue on reverse if necessary and identify by block number)	
FIELD	GROUP	SUB-GROUP		
			Ice Concentration	Regression Analysis
			Sea Ice	Statistical Analysis
			Correlation Techniques	Arctic Climate

19. ABSTRACT (Continue on reverse if necessary and identify by block number)

Based on a 27 year data record from the COADS and SEIC data sets, a statistical analysis of ice concentration, sea surface temperature (SST), air temperature, U and V wind components, and sea level pressure anomaly data was conducted for five locations in the ice-covered waters of the North Atlantic. Spectral densities and autocorrelations of the time series for each variable were calculated to establish a measure of persistence and periodicity. Regression equations were formulated based on the above data sets to forecast both the winter and summer ice concentration anomalies for each location. The differing effects of land and ice boundaries, currents, storm passages and wind velocity anomalies on the ice concentration anomalies at each location were reflected by the parameters retained by each of the regression equations. In addition to ice concentration anomalies at various lags, the inclusion of meteorological and oceanographic parameters was shown to increase the total explained model variance, which should improve the accuracy of an ice concentration anomaly forecast at lead times of at least

20. DISTRIBUTION / AVAILABILITY OF ABSTRACT	21. ABSTRACT SECURITY CLASSIFICATION
☒ UNCLASSIFIED/UNLIMITED ☐ SAME AS RPT ☐ DTIC USERS	UNCLASSIFIED
22a. NAME OF RESPONSIBLE INDIVIDUAL: R. H. Bourke	22b. TELEPHONE (Include Area Code): 408-646-3270; 22c. OFFICE SYMBOL: 68Bf

DD Form 1473, JUN 86 — Previous editions are obsolete. — SECURITY CLASSIFICATION OF THIS PAGE

S/N 0102-LF-014-6603

19. Abstract continued:

one season over a forecast based on ice concentration anomaly persistence alone. How the COADS (Comprehensive Ocean-Atmosphere Data Set) SEIC (Sea Ice Concentration)

18. Subject terms continued:

COADS
SEIC
Ice forecasting
Greenland Sea
Barents Sea
Ice [illegible] Arctic
meteorology; Marine atmospheres.

16. Disclaimer continued:

Department of Defense or the U.S. Government.

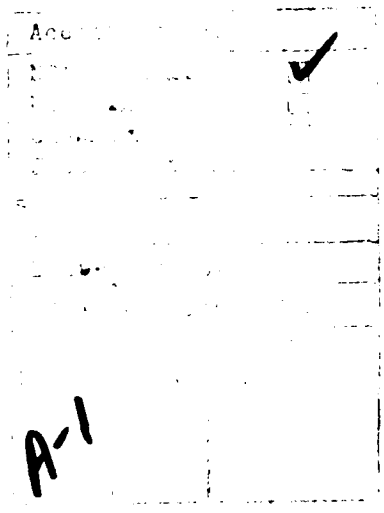

Approved for public release; distribution is unlimited.

Predictability of Ice Concentration
Anomalies in the High Latitudes
of the North Atlantic
Using a Statistical Approach

by

Katharine S. Garcia
Lieutenant, United States Navy
B.S., United States Naval Academy, 1980

Submitted in partial fulfillment of the
requirements for the degree of

MASTER OF SCIENCE IN METEOROLOGY AND OCEANOGRAPHY

from the

NAVAL POSTGRADUATE SCHOOL
December 1988

Author: Katharine S. Garcia
Katharine S. Garcia

Approved by: Robert H. Bourke
Robert H. Bourke, Thesis Co-Advisor

Laura D. Johnson
Laura D. Johnson, Thesis Co-Advisor

Curtis A. Collins
Curtis A. Collins, Chairman,
Department of Oceanography

Gordon E. Schacher
Gordon E. Schacher,
Dean of Science and Engineering

ABSTRACT

Based on a 27 year data record from the COADS and SEIC data sets, a statistical analysis of ice concentration, sea surface temperature (SST), air temperature, U and V wind components, and sea level pressure anomaly data was conducted for five locations in the ice-covered waters of the North Atlantic. Spectral densities and autocorrelations of the time series for each variable were calculated to establish a measure of persistence and periodicity. Regression equations were formulated based on the above data sets to forecast both the winter and summer ice concentration anomalies for each location. The differing effects of land and ice boundaries, currents, storm passages and wind velocity anomalies on the ice concentration anomalies at each location were reflected by the parameters retained by each of the regression equations. In addition to ice concentration anomalies at various lags, the inclusion of meteorological and oceanographic parameters was shown to increase the total explained model variance, which should improve the accuracy of an ice concentration anomaly forecast at lead times of at least one season over a forecast based on ice concentration anomaly persistence alone.

TABLE OF CONTENTS

ACKNOWLEDGEMENTS

I would like to thank Professors Robert Bourke and Laura Johnson for their guidance and critical support throughout this thesis project. Also, I would like to thank LCDR Gordon Fleming for adding his encouragement and special insight. Thanks also to Professor John Walsh for providing the digitized data used in this analysis. Finally, a special thanks goes to my husband, David B., for tolerating my absences and supporting me in so many ways throughout the entire time it took me to complete this thesis.

I. INTRODUCTION

The ability to forecast the presence and thickness of sea ice in the Arctic Ocean is gaining increased importance throughout the world. Route planning for commercial shipping and oil exploration is dependent on ice location and concentration for safe transit. Knowledge of the future location, thickness and concentration of the ice cover at a specific location in the Arctic Ocean would allow more specific route planning and could provide great cost and time savings by reducing the length of transits. Fishing fleets depend on open water for successful catches. The success of military operations and logistics may depend on icebreaker support. The ability for submarines to surface, either for operational or emergency considerations, is controlled by the presence and thickness of the ice cover.

Sea ice also affects the global climate. Parkinson et al., (1987) describe how sea ice significantly reduces the amount of solar radiation absorbed at the Earth's surface, and greatly reduces the exchange of heat, mass and momentum between the ocean and atmosphere. The freezing and melting processes of sea ice also affect the upper ocean through salt and heat fluxes.

The concentration and thickness of sea ice varies spatially and temporally over a broad range. When examining fluctuations varying on time scales of a season to several decades, the dominant signal in sea ice variability is the annual cycle (Parkinson et al., 1987). However, sea ice exhibits considerable interannual variability, or departure from monthly and seasonal means. To illustrate this extreme variability, minima and maxima extremes of ice cover for both summer and winter from 1953-1977 are shown in Figure 1.1. One may note that the range of the ice extremes covers a smaller area in the Greenland Sea as compared to the Barents

Sea. In the Greenland Sea, ice grows seaward away from the coast and southward towards Iceland. In exceptionally heavy ice years, ice will engulf the east and southeast coasts of Iceland (Wadhams, 1986). In the Barents Sea, a much larger area is affected as the growth of ice extends southward from the northern part of the sea over a broad area. However, the sea is never totally ice-covered, even in the most extreme years.

Limits of sea ice may also vary within short periods of time. Figure 1.2 demonstrates how rapidly ice can develop and disappear, even over large areas. During the winter of 1972-73, the ice edge was located just north of Svalbard near the end of November. By mid-December, the ice edge had retreated to north of 82°N, forming a large area of open water. By early January, the area had again become ice-covered.

Changing air temperatures, wind velocities and the composition of water and ice in the Arctic Ocean directly effect the air/ocean/ice boundary layer, which in turn effects the ice concentration. Oceanographic factors such as currents, bathymetry, water masses and heat fluxes from the surrounding air and water masses strongly affect interannual variability of ice concentration. However, since interannual fluctuations of atmospheric parameters are more pronounced than oceanic parameters the variations in sea level pressure, air temperatures and wind velocities may have the greatest impact on interannual ice concentration variations (Parkinson et al., 1987).

Sea ice forms, moves and melts in different regions of the Arctic in response to various forcing. Currents have a strong impact on the mean ice coverage in both the Greenland and Barents Seas. Cold currents transport and enhance ice growth and its spatial extent while warm currents melt the ice and/or preclude its formation. The southerly extent of the ice edge between regions of dissimilar temperatures can

vary as much as 30° of latitude. For example, cold currents maintain the broad area of ice along the east coast of Greenland whereas warm currents keep the North Cape of Norway free of sea ice. These effects are readily seen in the ice extremes depicted in Figure 1.1.

Other forcing functions that influence ice concentration include atmospheric pressure patterns, solar radiation and heat fluxes from deeper waters. One may also need to consider the nature of the ice cover, the presence of oceanic fronts and eddies, internal stresses and ice drift on ice concentration forecasts (Wadhams, 1986). These factors will affect ice concentrations more in different regions of the Arctic Ocean than others.

Various attempts at developing accurate methods of long range forecasting of sea ice in the Arctic Ocean have been made over the years with varying degrees of success. Both thermodynamic and numerical model forecasts have been developed. The U.S. Navy is currently using an ice forecasting model that is based on ocean currents and heat fluxes (Preller, 1985). State-of-the-art coupled ice-ocean models of the Arctic are limited by either the use of prescribed mass fluxes into the Arctic (Semtner, 1987) or by a damping of the ocean variables to a prescribed climatology (Hibler and Bryan, 1987). In a model of Arctic ice dynamics and thermodynamics (Hibler, 1979), the ice dynamics are coupled to the ice-thickness distribution by allowing the ice interaction to increase as the ice becomes thicker or consists of a lower proportion of thin ice. The forcing mechanisms discussed previously are subjected to such considerable time and spatial variability that development of a numerical model to accurately forecast ice concentration is quite difficult, and generally beyond the capability of input data bases to support such models.

Over the years several researchers have developed various statistical methods to forecast the ice concentration

anomaly, or departure from the monthly or seasonal mean. One previous study (Walsh and Johnson, 1979) has shown a tendency for ice anomalies to persist longer than sea surface temperature (SST) anomalies at high-latitudes.

Fleming (1987) found that both SST and ice concentration anomalies exhibited strong regional independence, and that their persistence was largest in geographically confined regions that are not influenced by strong currents. Also, he discovered that SST was a strong predictor of ice concentration in the Iceland Sea region and the northern portion of the Barents Sea.

Poor correlation of heavy ice years in Iceland with the total extent of sea ice in the Greenland Sea was discovered by Einarsson (1969). He concluded that the extent of ice toward Iceland was a local anomaly rather than a reflection of generally heavy ice conditions in the Greenland Sea. However, Bjornsson (1969) found that ice conditions in Icelandic waters were also dependent on the intensities of the low pressure cells over the Icelandic and Barents Seas.

A global climate model developed by Herman and Johnson (1978) found that a positive sea level pressure anomaly in the Barents Sea and Davis Strait, coupled with a negative anomaly in the North Atlantic Ocean between Iceland and Great Britain, produced maximum sea ice extent. Sanderson (1971) demonstrated that short-term ice-edge movements in the Greenland Sea were related to the mean wind anomaly. Good summaries of interactions between sea ice concentration and various atmospheric parameters are found in Herman and Johnson (1978) and Walsh and Johnson (1979).

The Soviets have long included meteorological parameters in their statistical forecasts. However, they often include data from regions other than the specific area being forecasted. SAIC (1987) summarized several statistical approaches the Soviets are experimenting with to produce long-range forecasts of sea ice. Sancevich (1976) claimed

that the summer ice anomaly in the western Soviet Arctic (Barents and Kara Seas) depended primarily on the winter ice accumulation from the eastern Soviet Arctic (East Siberian and western Chuckchi Seas), where the summer ice anomaly depended primarily on the amount of offshore airflow from May to August. For the Greenland Sea region Kirillov and Khromtsova (1974) discussed algorithms that could predict the monthly ice cover from May to August at lead times of two to six months. The major predictors for these equations included air temperature from Barentsburg and the export of Arctic ice through Fram Strait (which was computed from pressure differences).

Lebedev and Uralov (1972) included air temperatures from various Greenland stations, pressure gradients over nearby regions and early spring atmospheric pressures in their regression equations. These same investigators continued their work, and in 1977 presented equations for the Greenland Sea which included year-to-year persistence of the ice cover, October-February air temperatures from surrounding stations, and SST from the same months from two North Atlantic weather ships.

The recent availability of the Comprehensive Ocean-Atmosphere Data Set (COADS) provides an excellent data base for statistical analyses. See Slutz et al., (1985) for a complete description of this data set. COADS consists of various atmospheric and oceanic parameters measured over a long period of time, which permits a vast number of correlations to be calculated with sea ice concentration.

Instead of attempting forecasts of actual ice concentration, one could attempt to statistically develop long range forecasts of interannual variations of the ice concentration. Although persistence alone is a strong predictor for sea ice concentration, the inclusion of atmospheric and oceanic parameters may improve ice concentration forecasting (Walsh, 1986). Therefore, the objective of this study is to select

various regions in the Arctic Ocean, and determine which, if any, of several atmospheric and oceanic parameters from the COADS data base will increase the accuracy of a forecast of the ice concentration anomaly.

Regression equations to forecast ice concentration anomalies will be developed for each region for the winter and summer seasons. Ice concentration anomalies will be calculated using these regression equations, based on the same anomaly data used to develop these equations, and compared to the actual data. Finally, the forcing parameters retained by the various equations will be analyzed for similarities and trends between the locations. Because of the availability of the COADS data set, purely statistical methods will be used in this study, rather than numerical methods.

Chapter II describes the areas of interest for this study with a description of the North Atlantic climatology and oceanic characteristics. A description of the two data sets used in this study and how the initial data were manipulated are contained in Chapter III. The results of the statistical analyses are contained in Chapter IV. A discussion of these results follows in Chapter V, and finally, conclusions are found in Chapter VI.

(a)

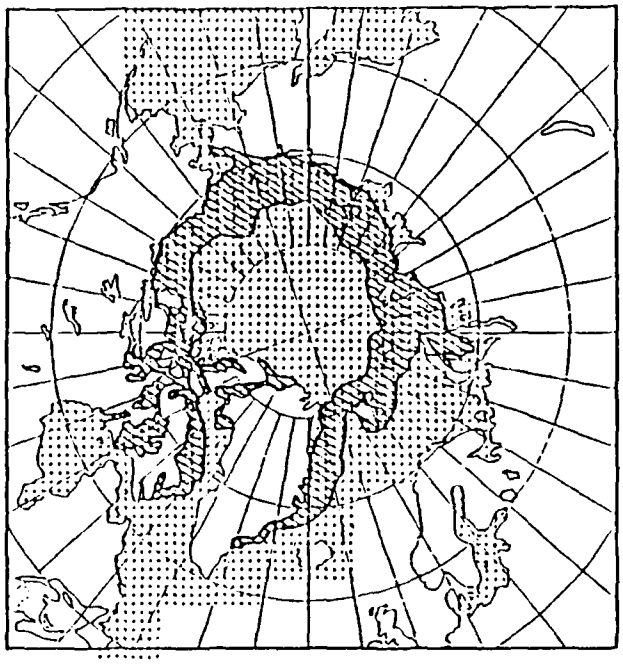

(b)

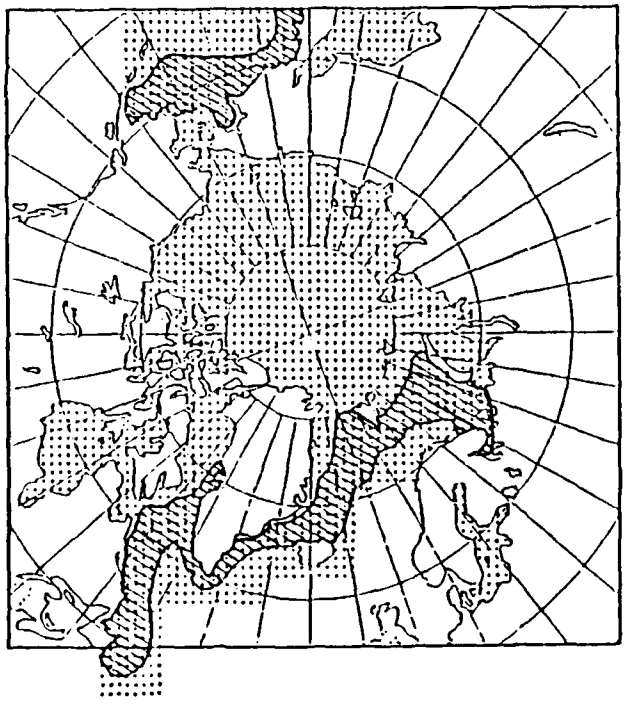

Figure 1.1 The shaded areas indicate the minimum and maximimum ice extent for (a) August and (b) February for the period 1953-1977. The dots indicate the area covered by the sea ice data set, while the hatched areas indicate the ice extremes (from Walsh and Johnson, 1979).

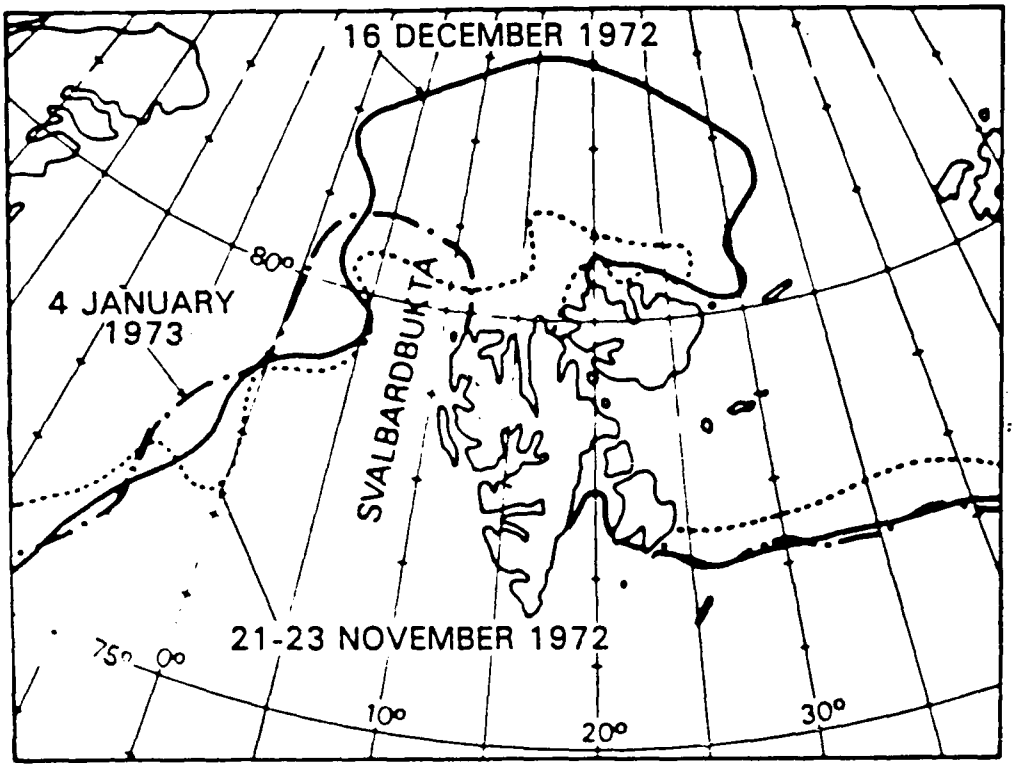

Figure 1.2 The rapid variation that may occur in ice edge location over a short period of time. The ice edge positions were deduced from Landsat images (from Wadhams, 1986).

II. THE ARCTIC WATERS

The focus of this work is to show the relationship, if any, between sea surface temperature (SST), air temperature, sea level pressure, wind speed and direction and ice concentration. Because so much variability in these parameters exists throughout the Arctic Ocean, a general understanding of the meteorological and oceanic features of the region is important to the analysis that follows. The regional discussions were derived principally from Parkinson et al., (1987), Welsh et al., (1986) and Wadhams (1986).

A. AREA SELECTION

Specific areas in different peripheral seas of the Arctic Ocean were chosen in order to observe the influence of the different variables which affect ice concentration. The variables chosen to analyze in this study, derived from the COADS data set, include SST, air temperature, wind velocity and sea level pressure. Other forcing functions that will be considered are ocean currents, advection of sea ice, and mesoscale eddies and heat fluxes. Since all of these functions undergo regional variations, the resulting ice concentration is also expected to vary regionally. Hence, grid points in five different areas were chosen where the different effects of the forcing could be observed. Grid points in regions where ice was absent or regions which experienced total ice coverage for long periods of time were avoided because of the potentially low correlations which would result. The selected grid points are plotted in Figure 2.1 and the locations are listed in Table I.

Of all the parameters that influence the ice concentration anomaly forecast, other ice concentration anomalies at various lags were expected to exert the strongest influence

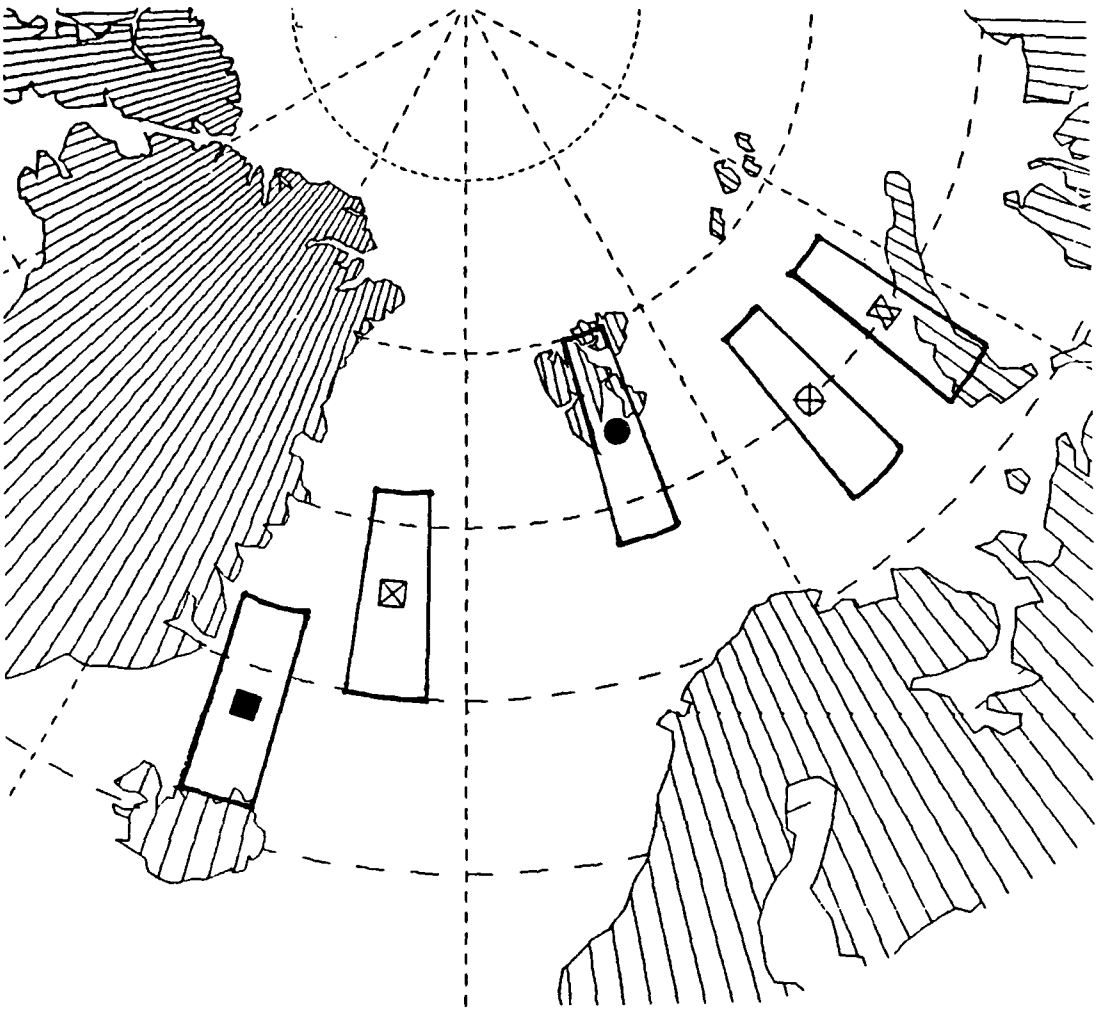

Figure 2.1. Chart depicting the five selected grid points.

TABLE I

POINT	LEGEND	POSITION	OCEAN AREA
1	⊠	73N 7W	EAST GREENLAND SEA
2	■	69N 17W	ICELAND SEA
3	●	77N 19E	SVALBARD
4	⊠	75N 41E	WEST BARENTS SEA
5	⊠	75N 53E	EAST BARENTS SEA

on the forecast. At grid point 1 in the Greenland Sea the ice concentration is predominately influenced by the alongshore/offshore winds and the transport of pack ice out of the Arctic by the Transpolar Drift Stream. Therefore, wind velocity and sea level pressure anomalies may be expected to show high correlation with the ice concentration anomalies. In the Iceland Sea at grid point 2, advection of warmer waters from the south by the Irminger Current or advection of pack ice from the north by the East Greenland Current could influence ice concentration. A strong SST correlation might be expected at this location due to the strong influence of advective features in this region.

Grid point 3 is located in a sheltered area with Svalbard and the Arctic ice pack to the north. Since this area is not influenced by a strong current, local effects such as SST and air temperature anomalies could possibly be expected to dominate. Grid point 4 in the western Barents Sea is in an open area, but along a major storm track. Therefore, sea level pressure and wind anomalies can be expected to dominate the ice concentration anomaly forecast. Finally, grid point 5 in the eastern Barents Sea near Novaya Zemlya is also near a land boundary. Since this region generally tends to record higher ice concentrations than the other regions, previous ice concentration anomalies (ice persistence) may likely be the most important factor in forecasting future anomalies.

B. REGIONAL DESCRIPTION OF THE GREENLAND SEA

1. Climatology

Patterns of wind direction and speed, sea level pressure and air temperature change dramatically between winter and summer in the Greenland Sea. Differences are also noted between the northern and southern regions, as the sea is crossed by the arctic front, which divides Arctic air to the north and Polar air to the south. Cyclones from the Atlantic Ocean often move along this front, modifying the wind speed and direction. Figure 2.2 illustrates how the

average low-pressure or storm track in the North Atlantic moves over the course of the year.

Three quasi-stationary pressure systems dominate the Greenland Sea: the Icelandic Low, the Arctic High centered over the polar pack and the high pressure region over Greenland. Figure 2.3 depicts the significant variation of atmospheric pressure between winter and summer. In winter the gradient is stronger, and pressures increase considerably from the south to the north. In summer, due to filling of the Icelandic Low and intensification of the Arctic High, the atmospheric pressure increases over the entire sea area. However, as this figure indicates, sea level pressure is significantly more uniform over the area in summer than in winter.

The averaged wind fields in the North Atlantic for representative months in winter and summer are shown in Figure 2.4. From the east Greenland coast to western Svalbard, the prevailing surface winds remain northeasterly in winter, but are much lighter and more easterly during summer.

Air temperatures vary widely throughout the Greenland Sea. In ice-free areas these temperatures are colder than the corresponding SST, indicating that heat transfer from the water to the air is a permanent and predominant feature in this area (Gatham, 1986). Figure 2.5 illustrates the strong effect of the Norwegian Atlantic Current on the extreme minimum and maximum air temperatures ever recorded. During summer temperatures are influenced by melting sea ice, but can reach 10°C in the southern portion of the Greenland Sea. Mean winter and summer air temperatures are shown in Figure 2.6.

2. Currents

Several currents are prominent in the Greenland Sea. A chart indicating the major ocean currents in the North Atlantic is included in Figure 2.7. The warm West

Spitsbergen Current in the eastern Greenland Sea is a northward flowing branch of the North Atlantic Current. The major part of this current turns westward, and then southward, forming a cyclonic circulation in the Greenland Basin. The southern limb of this circulation, the Jan Mayen Current, separates from the East Greenland Current (EGC), and bends eastward north of Iceland until it merges with the East Iceland Current.

The Transpolar Drift Stream is a major cold current originating under the polar ice cap and exiting the Arctic Ocean through Fram Strait, between Svalbard and Greenland. It passes down the east coast of Greenland as the strong southbound East Greenland Current (EGC). It transports cold, low saline Arctic Water out of the central Arctic Basin into the western Denmark Strait.

3. Ice

The location and concentration of sea ice in the Greenland Sea varies interannually and seasonally. The ice concentration in this sea is largely determined by the transport of the EGC and its branches, and to a lesser extent, by the East Spitsbergen Current (Welsh, 1986). The EGC transports thick multiyear ice from the central Arctic Basin. Different types of ice, including fast ice, pack ice and ice in the marginal ice zone, are located in the Greenland Sea, which are affected by various types of forcing.

Figures 2.8-2.9 show the variations between the maximum, mean and minimum ice edge limits in the North Atlantic for representative winter and summer months. The maximum retreat of ice is usually observed in late September when its edge, in the form of a narrow tongue, is wedged into the Greenland Sea from Fram Strait. Beginning in October, the ice edge steadily advances southward and seaward. Wadhams (1986) attributes this growth to both the increased drift rate of the EGC and the reduction in ice melting. After November, growth of new ice is greatly expedited by

eddy activity and storm passages along the ice edge, both of which tend to open the pack ice. The ice cover reaches its maximum extent in March or April, after which the ice begins retreating to the northwest.

Zubov (1945) described the relationship between ice drift and deformation due to the passage of cyclones. Depending on the intensity of the cyclonic low and its speed of translation, complex ice patterns could result. If a coastline or ragged fast-ice edge lies in the path of a passing cyclone, ice would be piled up against some portions of the boundary and drawn away from others.

Sea ice drifting in the East Greenland Current is subjected to many forces (Wadhams, 1986). In the marginal ice zone (MIZ) ice has much latitude of movement, leading to more frequent generation of open water areas through divergence and more rapid growth of new ice. However, as the ice drifts southward, this growth is somewhat offset by the warmer temperatures of the lower latitudes. Recent studies indicate that the ice drift rate accelerates through Fram Strait, but not down the east coast of Greenland (Wadhams, 1986). Measurements have shown that the lateral drift rate is fastest near the continental-shelf break, where an ice edge jet is present. Meanders and eddies in this jet can result in major deformation of the ice pack, leading to its breakup.

Ice found in the MIZ, usually in the form of floes of various size, tends to be broken up by long-period swells from the open ocean. Depending on the wind component, these floes would be advected either westward towards the margin or eastward into the open ocean (Wadhams, 1986). Mesoscale eddies could cause a decrease in ice concentration by drawing ice into warmer water causing them to melt, or by drawing floes from the ice pack toward the MIZ, where they could be broken up by waves. Wadhams (1986) also discussed the potential effects of upwelling on the MIZ. Studies predicted that wind blowing poleward along a north-south ice edge in

the East Greenland Sea will lead to upwelling by inducing divergence. Upwelling of warmer waters would inhibit growth of new ice outside the main ice edge, maintaining a sharp edge and melting any floes which might drift away.

B. REGIONAL DESCRIPTION OF THE BARENTS SEA

1. Climatology

The principal climatic characteristics of this region are determined by both its geographical location in the high latitudes and by the entry of warm Atlantic waters and moist marine air from the west. The sea is also under the influence of an arctic front, which separates cold Arctic air from the warmer, moister air of the temperate latitudes.

In winter, when the Siberian High is formed and the Icelandic Low is intensified, the arctic front is accentuated. Rather strong cyclonic activity develops over the central part of the Barents Sea, causing the sea level pressure to be depressed and strong winds to blow from southwesterly to southeasterly. In summer the Icelandic Low fills and the Siberian High is destroyed. The arctic front weakens and a region of increased pressure forms over the Barents Sea resulting in stable cool weather. Figure 2.3 depicts these variations between the winter and summer sea level pressures.

Wind speeds usually remain under 9 m/s throughout the year (Figure 2.4), but the direction varies over the region. In winter winds are southwesterly in the southern part of the sea. They turn southerly near Novaya Zemlya, forming a cyclonic rotation as they become easterly in the northern regions. During summer this rotation is not as evident as the winds are lighter. Air temperatures (Figure 2.6) in winter are below freezing throughout the entire sea, although they differ considerably from one area to another. In summer temperatures are warmer in the southern part of the sea due to the influence of the warm North Cape Current.

2. Currents

The Barents Sea has a shore boundary only to the south, which is dissected by numerous fiords, gulfs and bays. The western coast of the islands of Novaya Zemlya to the north is covered by glaciers which descend to the shore, where some of them flow into the sea forming occasional icebergs. Since the Barents Sea is relatively shallow (500 m), with a complex bottom topography, surface currents tend to be confused (Wadhams, 1986).

The Norwegian Atlantic Current transports relatively warm Atlantic water into the Barents Sea, which has a profound influence on the ice cover of this sea. As it advances eastward, one branch, the North Cape Current, subdivides into further branches. One, the Murman Current, turns northeast toward Novaya Zemlya and then northwest. The cold East Spitsbergen Current flows southwestward, transporting ice from the Arctic basin. This current also closes the cyclonic gyre in the Barents Sea. Figure 2.7 depicts these currents.

3. Ice

The Barents Sea is almost entirely ice-free during the summer. In the winter it never freezes completely because the waters of the warm North Cape Current in the southwestern part of the sea maintain temperatures above zero throughout the year. Figures 2.8-2.9 show the large seasonal variation of the ice edge between Svalbard and Novaya Zemlya. Ice formation begins in the northern part of the sea in September, although a major ice advance from the north occurs in October. By February, Novaya Zemlya is engulfed by ice (Wadhams, 1986).

The ice cover attains its maximum development by April when about 75% of its surface is covered by ice (Welsh et al., 1986). Retreat of the ice then begins, reaching its minimum extent in September. When arctic air flows over the

sea, sharp cooling is observed, whereas thaws occur when there are intrusions of warm air from the Atlantic.

Because the Transpolar Drift Stream transports large quantities of multiyear pack ice to the east of Svalbard and into the Barents Sea, it is an area of highly variable ice concentration and ice thickness. Also, because of the high percentage of open water found in this sea, winds, currents and waves strongly influence ice conditions (Welsh et al., 1986). Evidence has shown that the ice is quite dynamic, as the complex current system causes ridging and deformation (Wadhams, 1986).

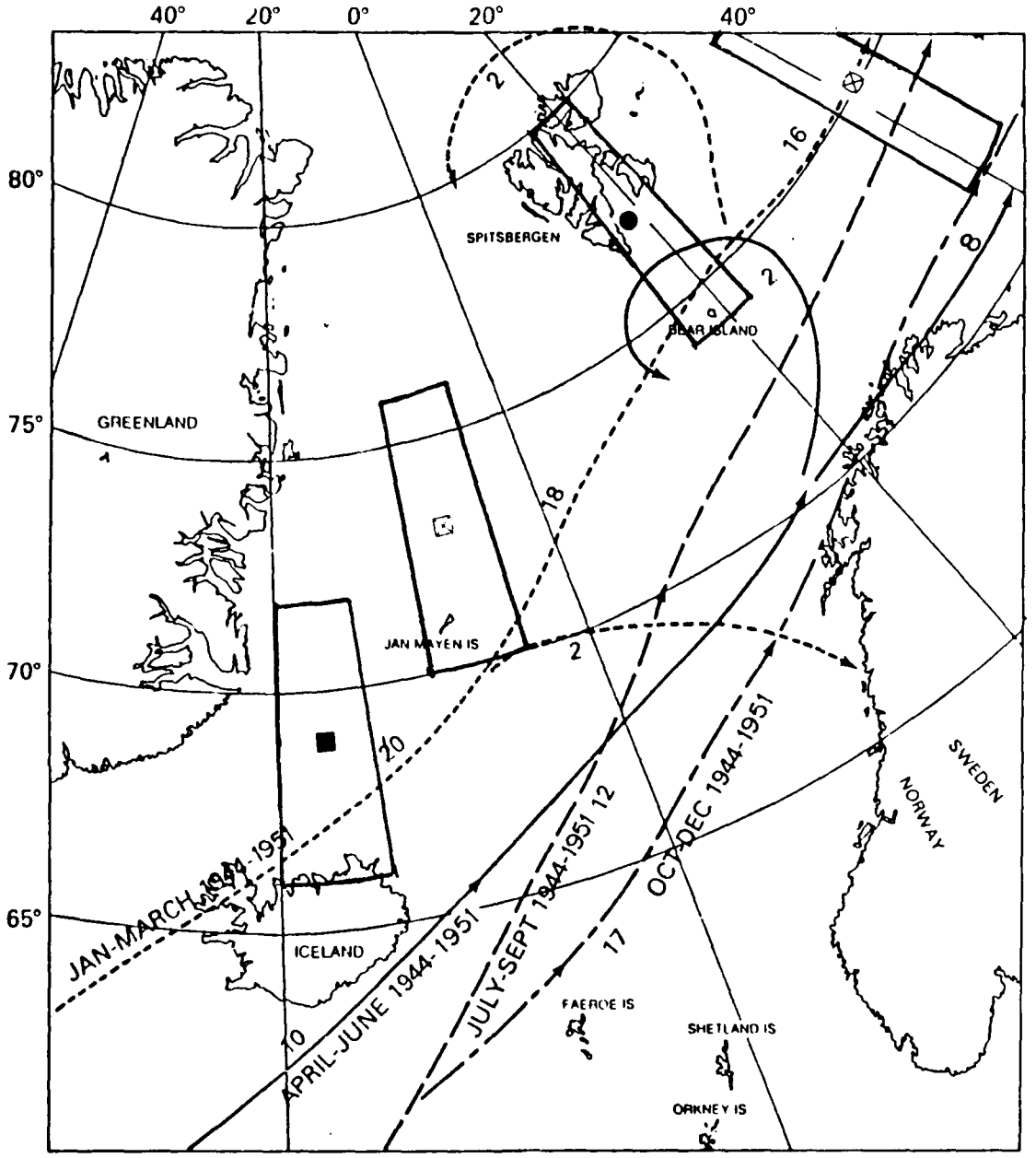

Figure 2.2 Mean tracks of low-pressure centers, i.e., severe storms. The numbers along the tracks indicate the relative frequency of the storms during the years indicated (from Gatham, 1986).

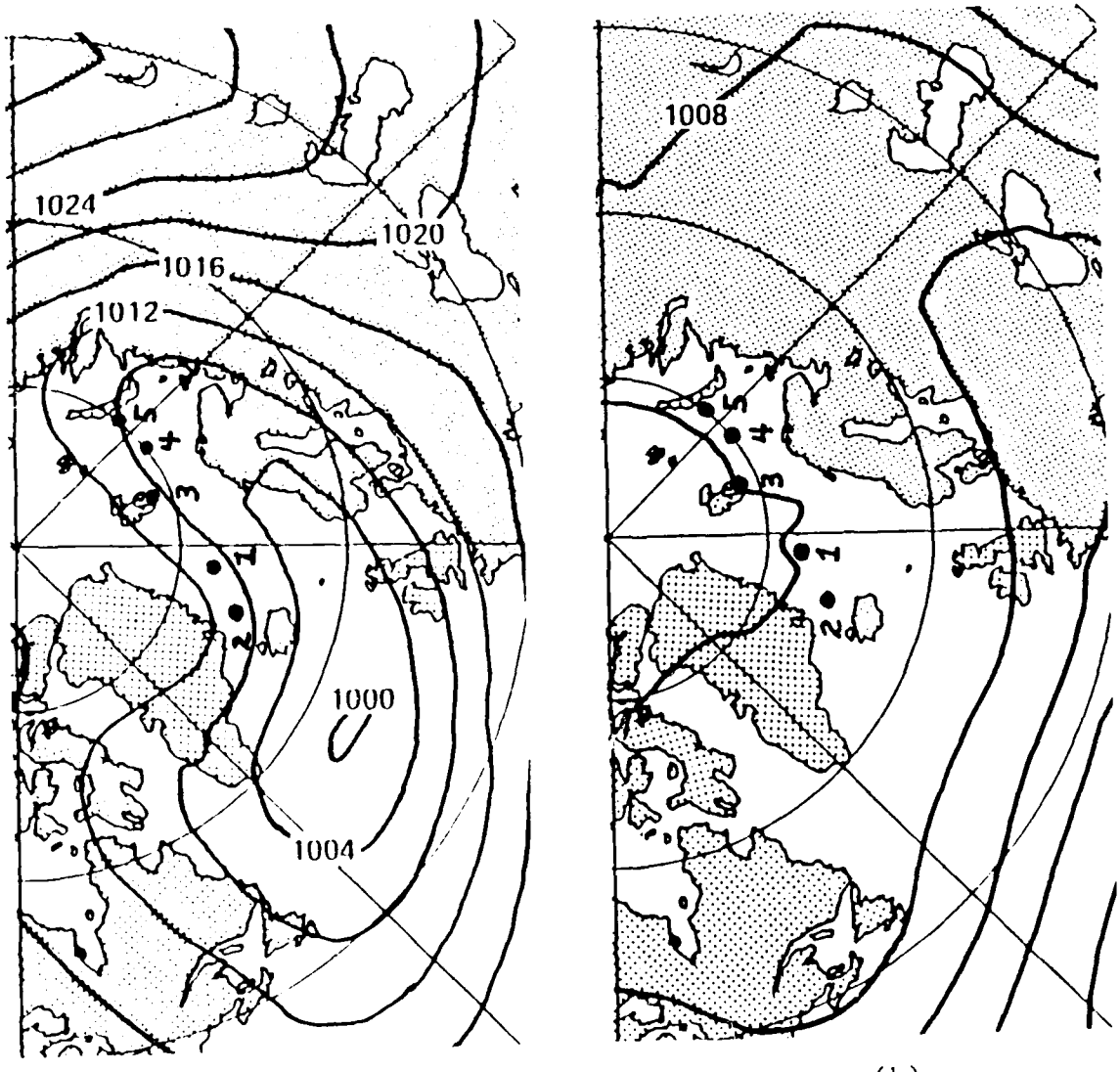

Figure 2.3 Mean sea level pressure in the North Atlantic for (a) winter and (b) summer. Pressure is in mbars (from Herman, 1981).

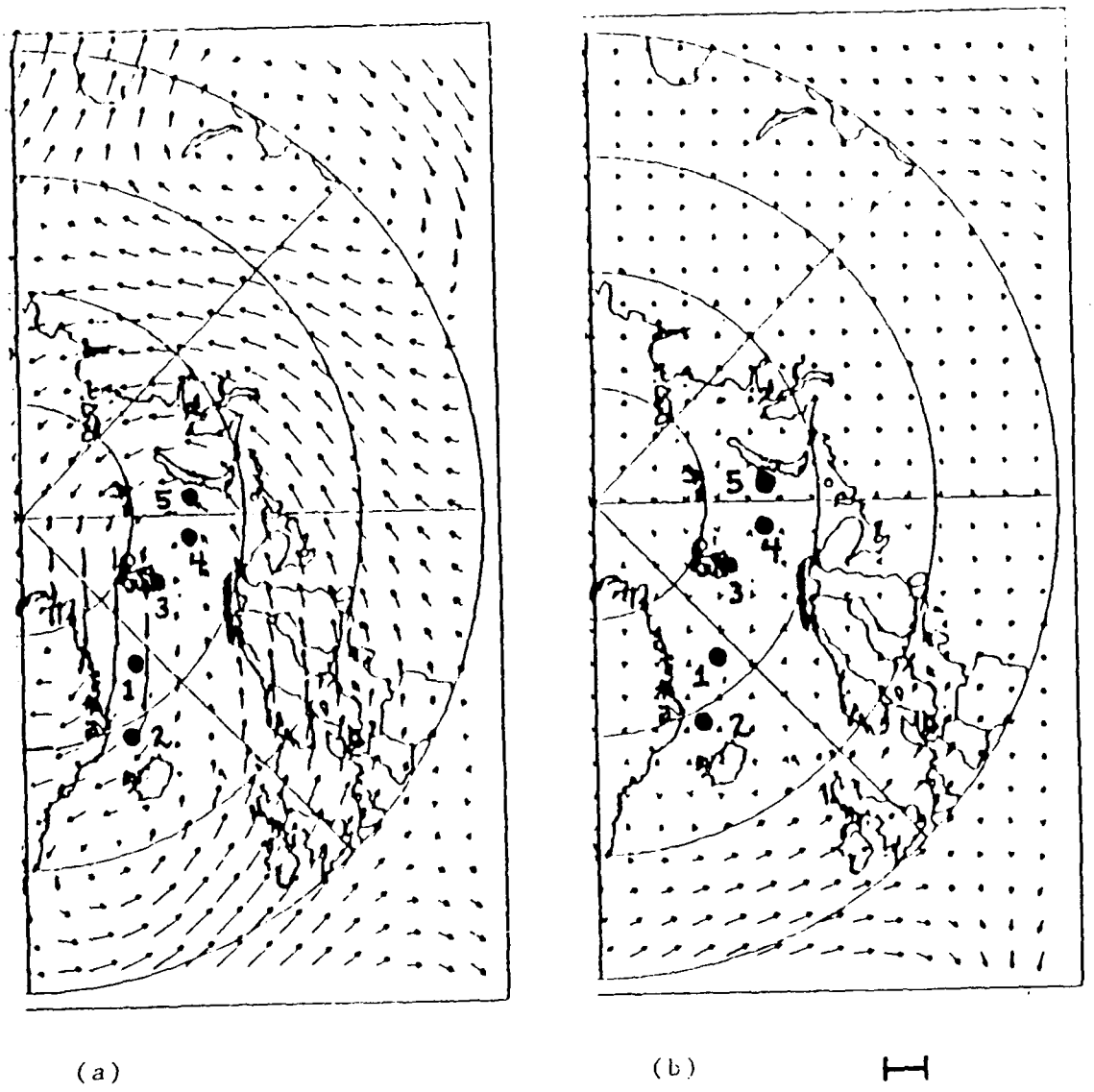

Figure 2.4 Mean wind fields over the North Atlantic from 1973-1976 for (a) January and (b) July. The scale arrow represents 10 m/s (from Parkinson et al., 1987).

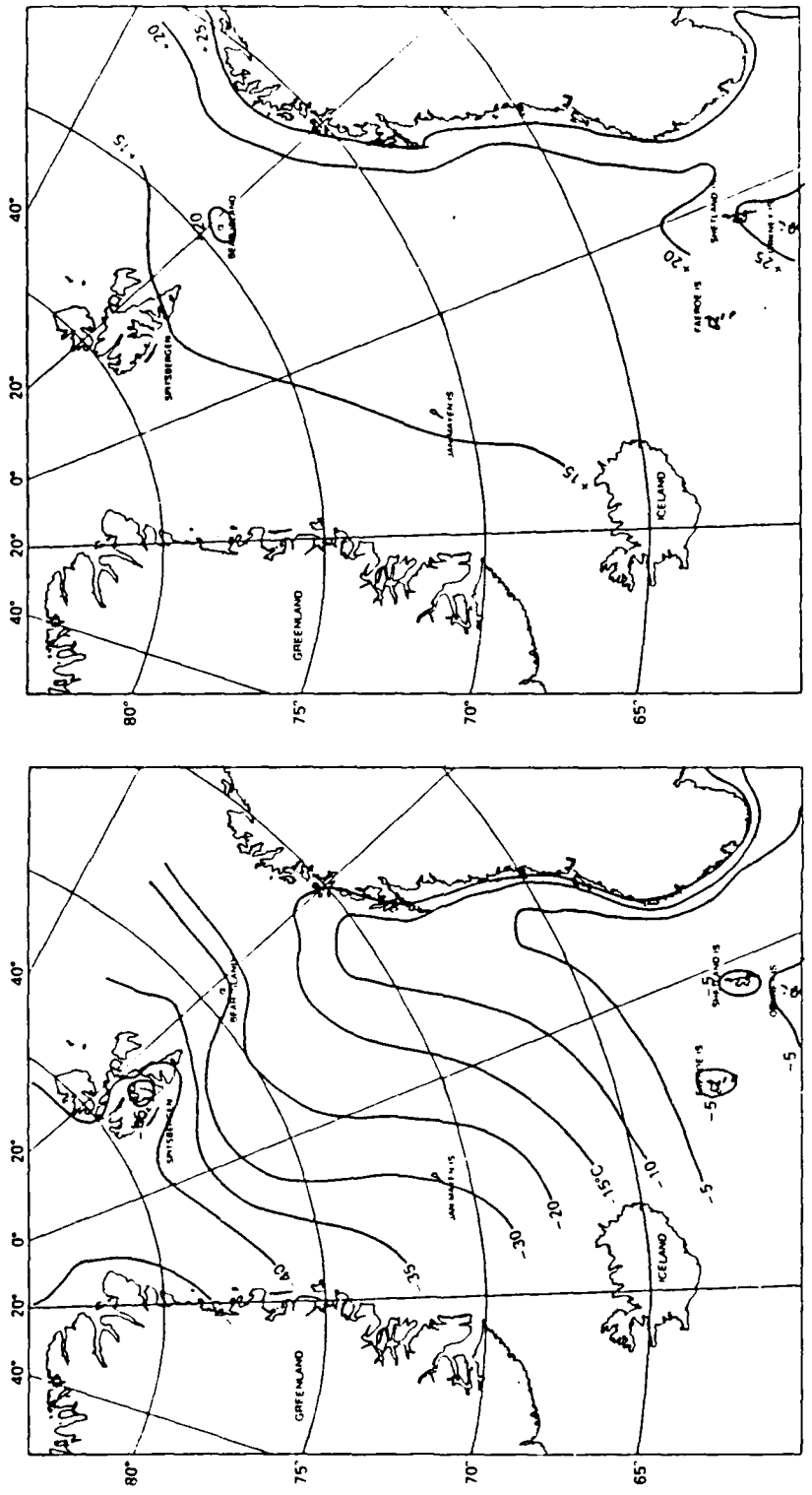

Figure 2.5 Extreme air temperatures recorded in this portion of the North Atlantic. Minimum (a) and maximum (b) temperatures are in °C (from Gatham, 1986).

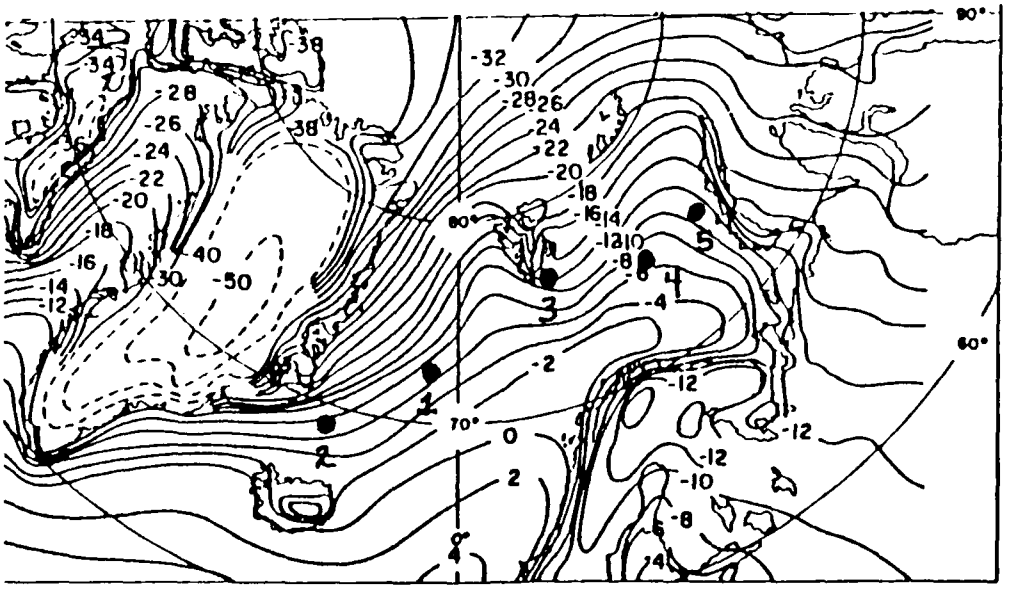

(a)

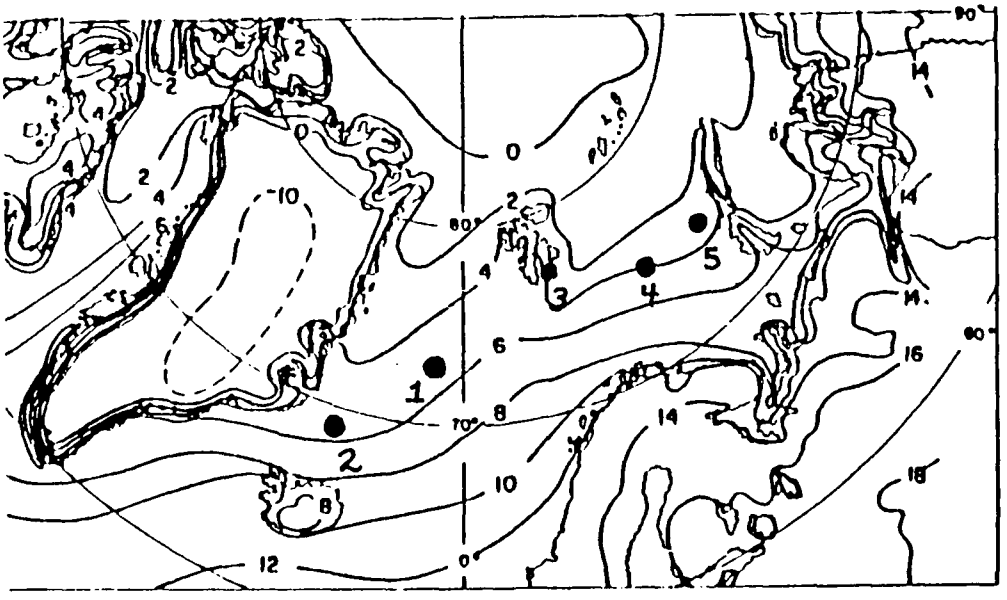

(b)

Figure 2.6 Mean air temperatures (in °C) for (a) February and (b) July (from Sater et al., 1971).

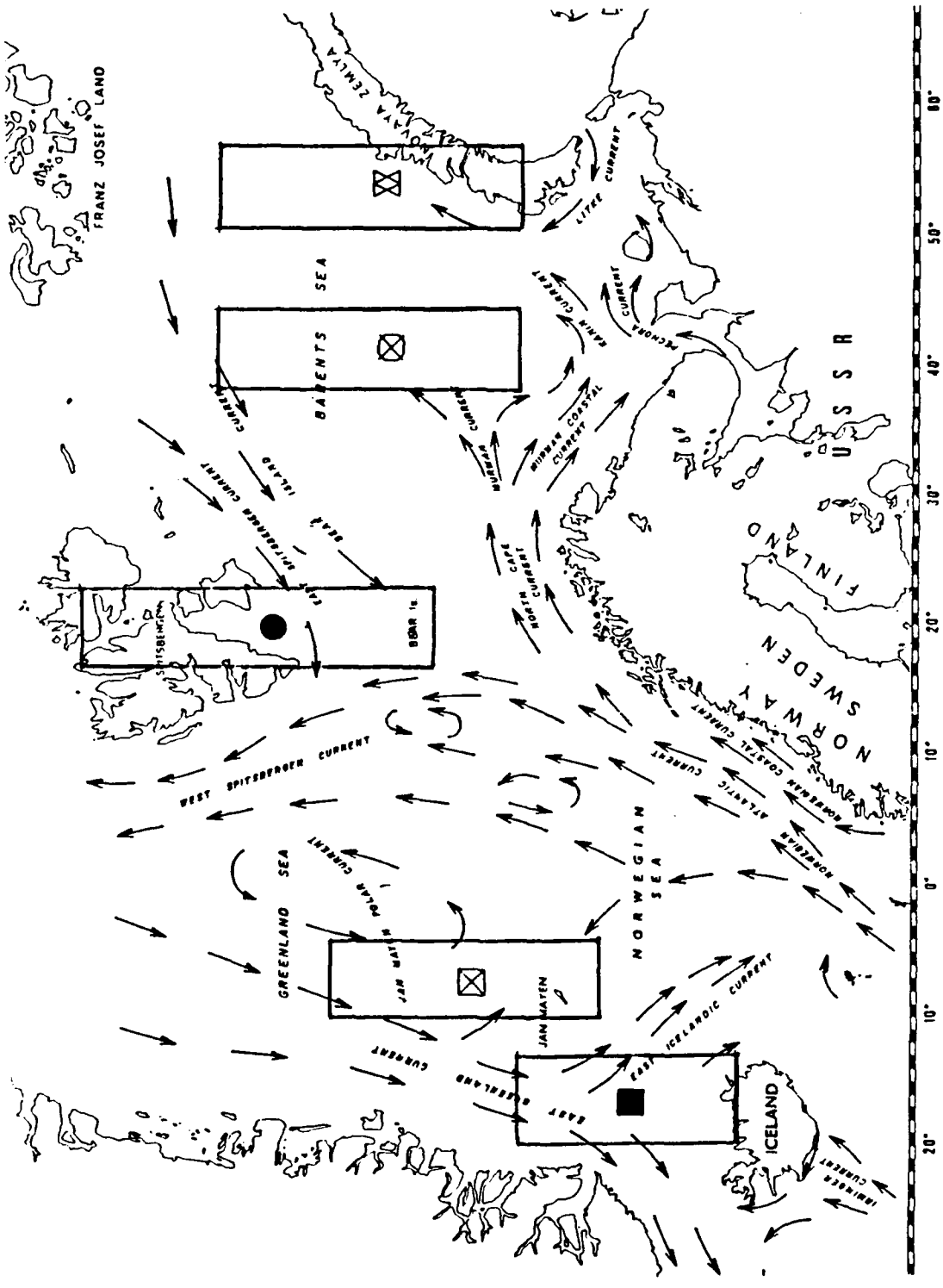

Figure 2.7 Large-scale surface circulation of the North Atlantic (from Johannessen, 1986).

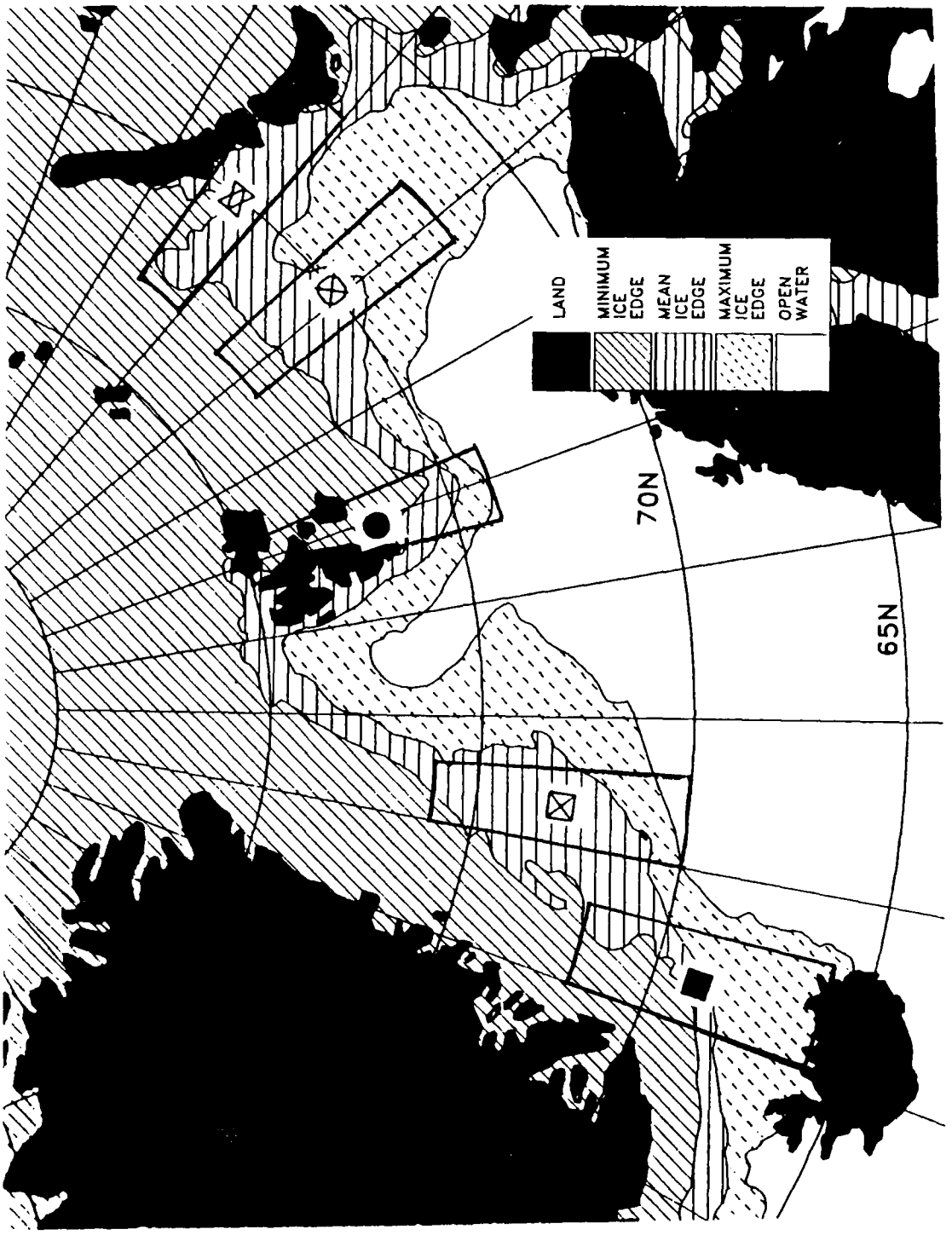

Figure 2.8 The average maximum, mean and minimum ice edge limits for 15 April in the North Atlantic for the years 1972-1982 (from NOCD, Asheville, 1986).

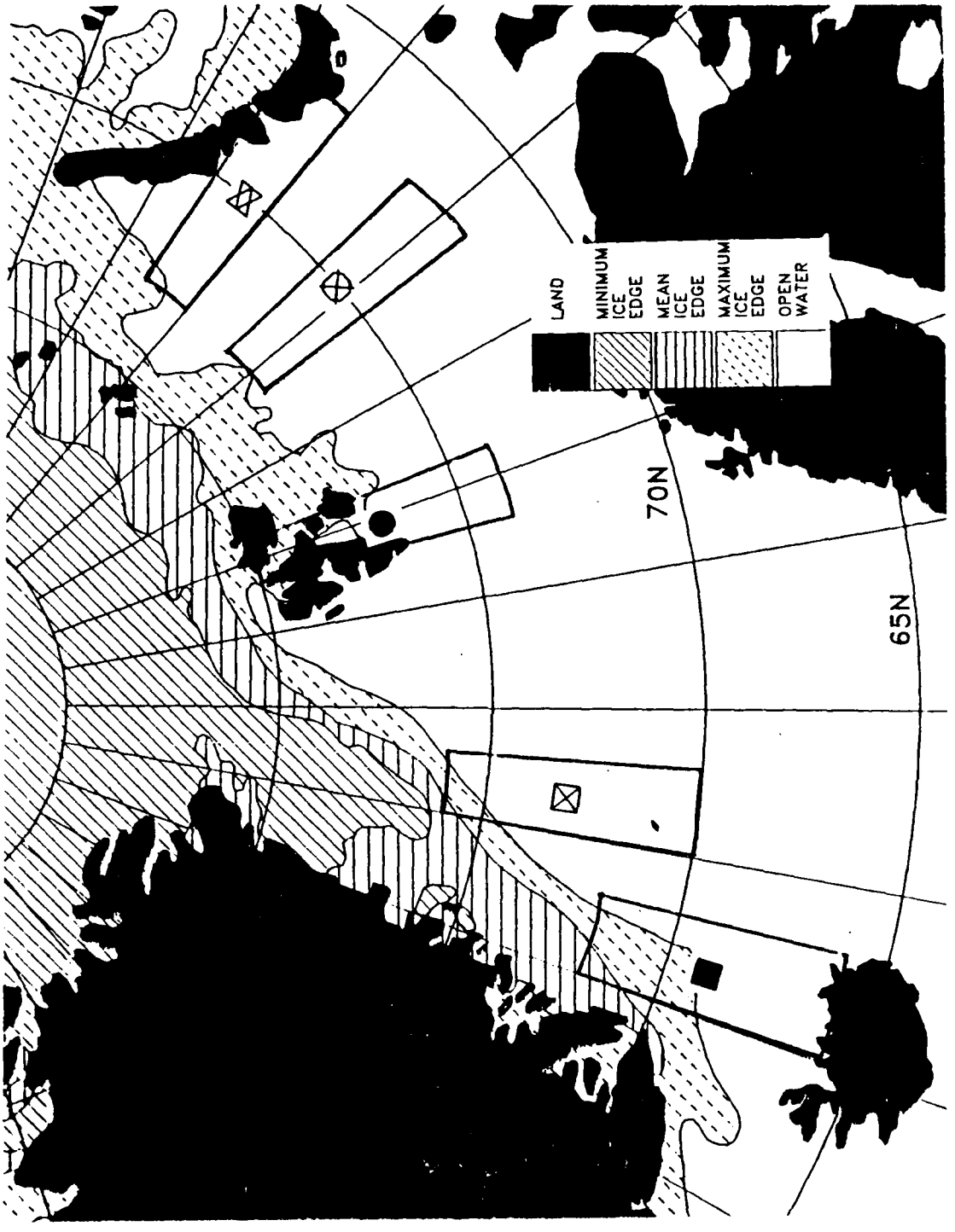

Figure 2.9 The average maximum, mean and minimum ice edge limits for 15 September in the North Atlantic for the years 1972-1982 (from NOCD, Asheville, 1986).

III. DATA

The statistical analyses performed in this study were based on two different data sets. A modified COADS (Comprehensive Ocean-Atmosphere Data Set) data base provided monthly-averaged sea surface temperatures (SST), air temperatures, east (U) and north (V) components of the surface winds and sea level pressure. The SEIC (Sea ice concentration) data base contained sea ice concentrations in tenths determined for the end of each month.

A. COADS

The following information describing the COADS data set is from Slutz et al. (1985). The COADS data set contains approximately 70 million reports from ships of opportunity, ocean weather ships, buoys and bathythermographs. The data have been assimilated, sorted, edited and summarized statistically for every month for the years 1854-1984 in 2° latitude by 2° longitude boxes over the world's oceans. Data sources are noted in Table I.

COADS is considered to be the most complete data set of environmental parameters now available for the ocean/atmosphere boundary. However, Slutz et al. (1985) suggest that careful attention must be paid to the sometimes serious, and usually poorly understood, limitations inherent in any data set of this type.

In using this data caution must be observed due to the historical changes that instrumental, observational and coding methods have undergone over the past 130 years. Also, navigational procedures and accuracy, ship construction and data density have seen great changes over this time frame. Most of these changes have gone unrecorded in the data sets from which COADS has been derived. These inhomogeneities are compounded by the significant percentage of errors that are

TABLE I

DATA SOURCES FOR COADS
(from Slutz et al., 1985)

	Million Reports (approx.)	**Source**
Atlas	38.6	NCDC
HSST (Historical Sea Surface Temperature Data Project)	25.20	NCDC, Germany
Old TDF-11 Supplements B and C	7.00	NCDC
Monterey Telecommunications	4.00	NCDC
Ocean Station Vessels, and Supplement	0.90	NCDC
Marsden Square 486 Pre-1940	0.07	NCDC
Marsden Square 105 Post-1928	0.10	NCDC
National Oceanographic Data Center (NODC) Surface, and Supplement	2.00	NCDC
Australian Ship Data (file 1)	0.20	Australia
Japanese Ship Data	0.13	M.I.T.
IMMPC (International Exchange)	3.00	NCDC
South African Whaling	0.10	NCAR
Eltanin	0.001	NCDC
'70s Decade	18.00	NCDC
IMMPC (International Exchange)*	0.90	NCDC
Ocean Station Vessel Z*	0.004	NCDC
Australian Ship Data (file 2)*	0.20	Australia
Buoy Data*	0.30	NCDC
'70s Decade Mislocated Data*	0.003	NCDC
	100.00**	

* Additions solely to 1970-1979 decade

** The approximate total includes 26.58 million relatively certain duplicates, and some seriously defective or mis-sorted reports, which were removed by initial processing steps.

inherent at every stage of observation, recording, transmission and processing. Additionally, Slutz et al. (1985) emphasize a few known problems where errors could enter:

1. SST measurements. Temperatures measured by engine intake have been shown by Ramage (1984) to be approximately 0.5°C higher than those measured by bucket.

2. Wind speed and direction. The "old" Beaufort scale was used to bracket each estimated speed at a value in m/s. The mixture of speeds and different compass codes estimated by sea state versus those actually measured yields potentially inhomogeneous data.

3. Diurnal effects. The data sets identify how much daylight had occurred prior to each observation. However, effects discussed by Ramage (1984), such as insolation, heating from the ship and cloud cover biases are not taken into account.

4. Duplication. Numerous duplicate entries of single observations were included in data files, which obviously leads to unwanted biases. Although 25% of the original data were rejected because of duplication, others undoubtedly remain.

B. SEIC

The SEIC data set contains monthly ice concentrations in tenths and was compiled by Walsh and Johnson (1979) from existing sea ice distribution observations. The original data sources are listed in Table II. The data set contains monthly values from 1953-1984, and was recently updated with the digitized ice data for 1972-1984 from the United States Navy/NOAA Joint Ice Center (Gross, 1986). A 58 x 80 cartesian grid covers those portions of the Arctic seas where ice was observed during any month. Each grid box is 60 nm by 60 nm; this 110 km spacing was chosen to permit resolution of year-to-year fluctuations.

Walsh and Johnson (1979) noted that the SEIC, like the COADS, had limitations. These include:

1. Data acquisition. The data set covers time periods both before and after satellite observations. Different observational methods cause nonuniformity in the data interpretation.

2. Concentration classifications. Ice conditions can vary considerably over relatively small areas. Ice observing agencies such as the British Meteorological Office and the United States Naval Oceanographic Office tend to group the concentrations into categories such as "very open" (1/10 - 3/10) and "open" (4/10 - 6/10).

TABLE II

DATA SOURCES FOR SEIC
(Walsh and Johnson, 1979)

U.S. Navy Fleet Weather Facility, 1976-1977: Arctic Sea Ice Analyses, Eastern and Western (weekly charts), Suitland, MD.

_____, 1976a: Eastern Arctic Sea Ice Analyses, 1972-75. ADA 033344, Suitland, MD.

_____, 1976b: Western Arctic Sea Ice Analyses, 1972-75. ADA 033345, Suitland, MD.

British Meteorological Office, 1959-77: Monthly Ice Charts, HMSO, London (1959 charts in Mariners Weather Log, vols. 3-4).

U.S. Naval Oceanographic Office, 1953-71: Report(s) of the Arctic Ice Observing and Forecasting Program. Tech. Reps. TR-49 through TR-52, TR-66, TR-69: Spec. Pubs. SP-70 through SP-81, Washington, DC.

Canadian Meteorological Service, 1966-71: Ice Summary and Analysis, 1964-69 (Yearbooks), Toronto, Ontario.

Arbok Norsk Polarinstitut, Oslo,1963-71: Sea ice and drift speed observations (Annual reports). Also, T. Lunde, 1965: Ice conditions at Svalbard, 1946-1963. Arbok Norsk Polarinstitut (1963).

Danish Meteorological Institute, 1957-1968: The Ice Conditions in the Greenland Waters (Yearbooks), Charlottenlund, Copenhagen.

U.S. Navy Hydrographic Office, 1958: Oceanographic Atlas of the Polar Seas. Part II. Arctic.H. O. Publ. No. 705, Washington, DC.

Danish Meteorological Institute. 1953-56: The state of the ice in the Arctic Seas. Appendices to Nautical-Metorological Annuals (Yearbooks), Charlottenlund, Copenhagen.

Jokill, 1953-67: Reports of sea ice off the Icelandic coasts (Annual reports). Icelandic Glaciological Society, Reykjavik.

When the source charts were digitized, the center value of these classification groups was used.

3. Overlapping data. When more than one source covered the same area, discrepancies were sometimes observed. In these cases the mean value of the observations was digitized.

C. Data Set Manipulation

In order to observe the diverse effects of oceanographic and meteorological effects on ice concentration throughout the Arctic Ocean, specific areas which could demonstrate these diversities were selected for evaluation. Also, since the two data sets did not cover similar time frames nor had the same grid scales, they had to be modified before any statistical analyses could be conducted.

1. Temporal and Spatial Considerations

The 27-year time period from January 1953 to December 1979 was chosen since ice data records for several regions of the Arctic seas did not become essentially continuous until 1953.

Since the grid sizes of the two data sets were not compatible, the ice grid was manipulated in order to use the maximum amount of data. Each ice grid data point was assigned to the nearest latitude and longitude. Then, the latitude and longitude of each of the five grid points from the COADS grid (see Table 2.1) were determined and matched to the nearest corresponding ice grid point. Since data reports were often sparse in the higher latitudes, spatial averaging was performed in order to smooth the data and hopefully improve the statistical analyses. On the COADS grid, the center value and surrounding eight values were averaged, while on the ice grid the center value and surrounding 24 values were averaged. This produced averages covering approximately the same area on both grids. In the cases where land was encountered at any of the surrounding points, such values were not included in the average.

2. Time Series

The entire time series of the averaged data were plotted in order to note the seasonal cycles and any other notable characteristics. Figures 3.1 - 3.12 are representative time series plots of data from grid points 2 and 4. Annual cycles are quite obvious in the ice concentration and temperature plots, but not as prominent in the wind and pressure plots. In Figures 3.3 and 3.9, missing air temperature data throughout the time series is quite evident.

Long-term climatic changes, or trends, may adversely influence the statistical analyses of data. Since Oort (1987) detected long-term cooling of SST in the mid-latitudes in the COADS data, these data sets were examined for linear trends. Leaving a trend in a time series of data may lead to considerably exaggerated autocorrelations and cross-correlations (Walsh, 1986). Using a linear model, a unique trend equation was calculated for each parameter. These are the lines plotted on the time series on Figures 3.1 - 3.12. A slight overall cooling trend is noted at grid point 2, while a stronger warming trend is seen at grid point 4. On Figure 3.3, the warming trend indicated is misleading due to the missing data. The trends may also be exaggerated on Figures 3.8 and 3.9 for the same reason. To remove the trend, the averaged data were subtracted from the linear equation leaving the residuals.

Since the main objective of this work was to forecast ice concentration "anomalies", it was necessary to remove some of the persistence inherent in geophysical time series. Therefore, monthly averages of the residuals were calculated and then subtracted, leaving monthly anomalies. This procedure removed, or at least significantly reduced, the annual cycle from the data. The computed statistics then represented patterns of the monthly anomalies. Otherwise, the statistics would simply represent the normal seasonal cycle, and the correlations would be quite large and misleading.

Also, interannual fluctuations of the parameters would be more readily observed when just the anomalies were used. These resulting "anomaly" time series are also plotted in Figures 3.1 - 3.12.

Finally, a three month sequential mean was calculated for the ice concentration, sea surface temperature and sea level pressure anomaly data. This was done as the time averaging reduced the short-term noise, allowing better determination of the correlation signal (Fleming, 1987, p. 41).

3. Final Data Sets

Data sets for each grid point were constructed in order to develop regression equations to forecast ice anomaly values on a seasonal basis. These sets included the detrended anomaly values of: ice concentration, sea surface temperature, air temperature, sea level pressure, east and north vector wind components, and the three month sequential means of ice concentration, sea surface temperature and sea level pressure. These values were then lagged from one to thirteen months. The regression equations were calculated using the lagged values only.

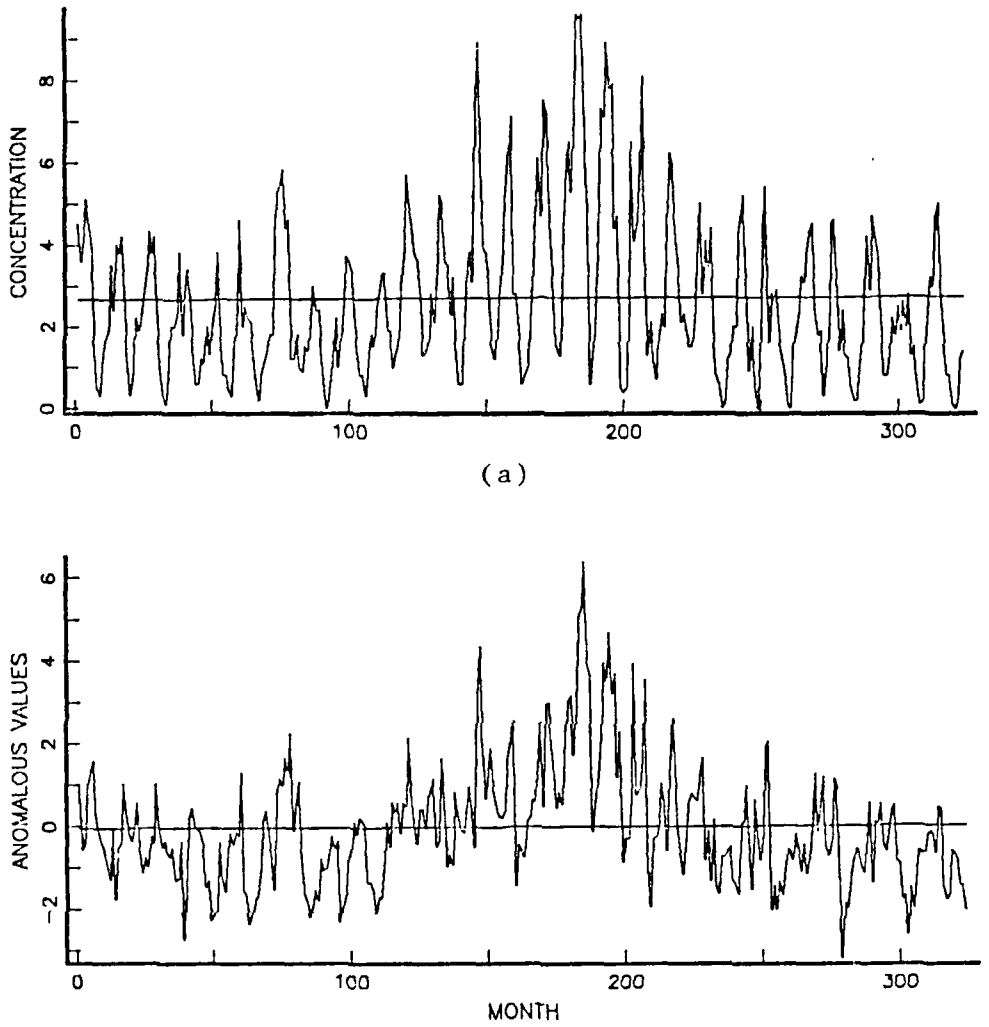

Figure 3.1 Time series of the (a) spatially averaged and the (b) detrended anomalous ice concentration data at grid point ?. The straight line through the data indicates the trend.

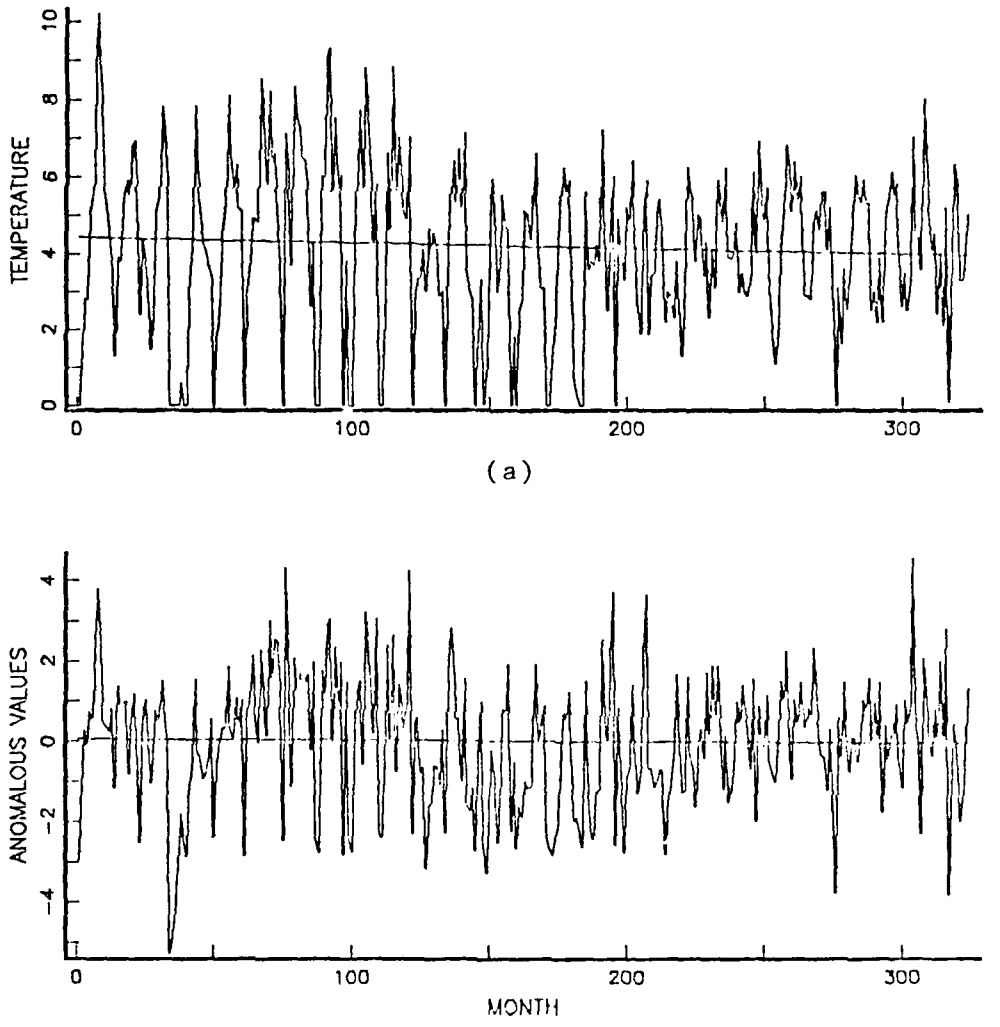

Figure 3.2 Time series of the (a) spatially averaged and the (b) detrended anomalous SST data at grid point 2. The straight line through the data indicates the trend.

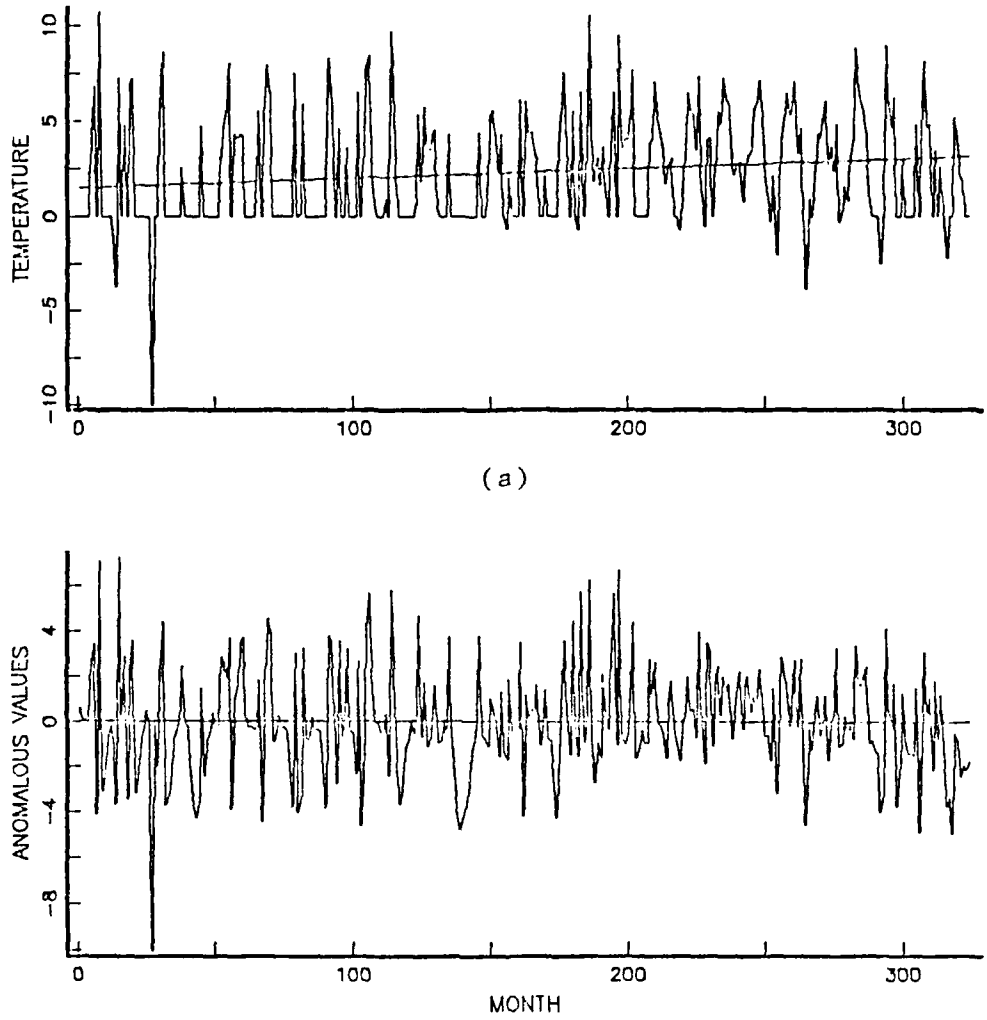

Figure 3.3 Time series of the (a) spatially averaged and the (b) detrended anomalous air temperature data at grid point 2. The straight line through the data indicates the trend.

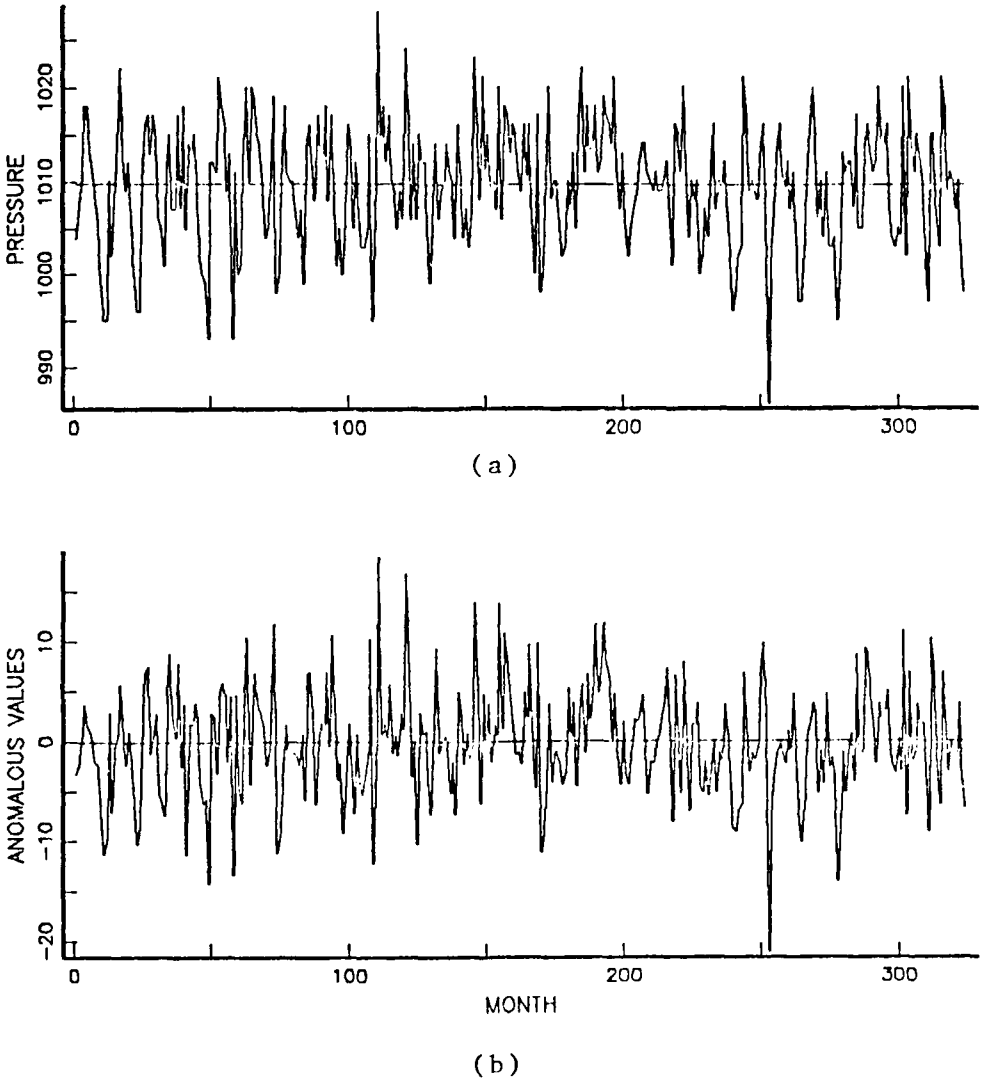

Figure 3.4 Time series of the (a) spatially averaged and the (b) detrended anomalous sea level pressure data at grid point 2. The straight line through the data indicates the trend.

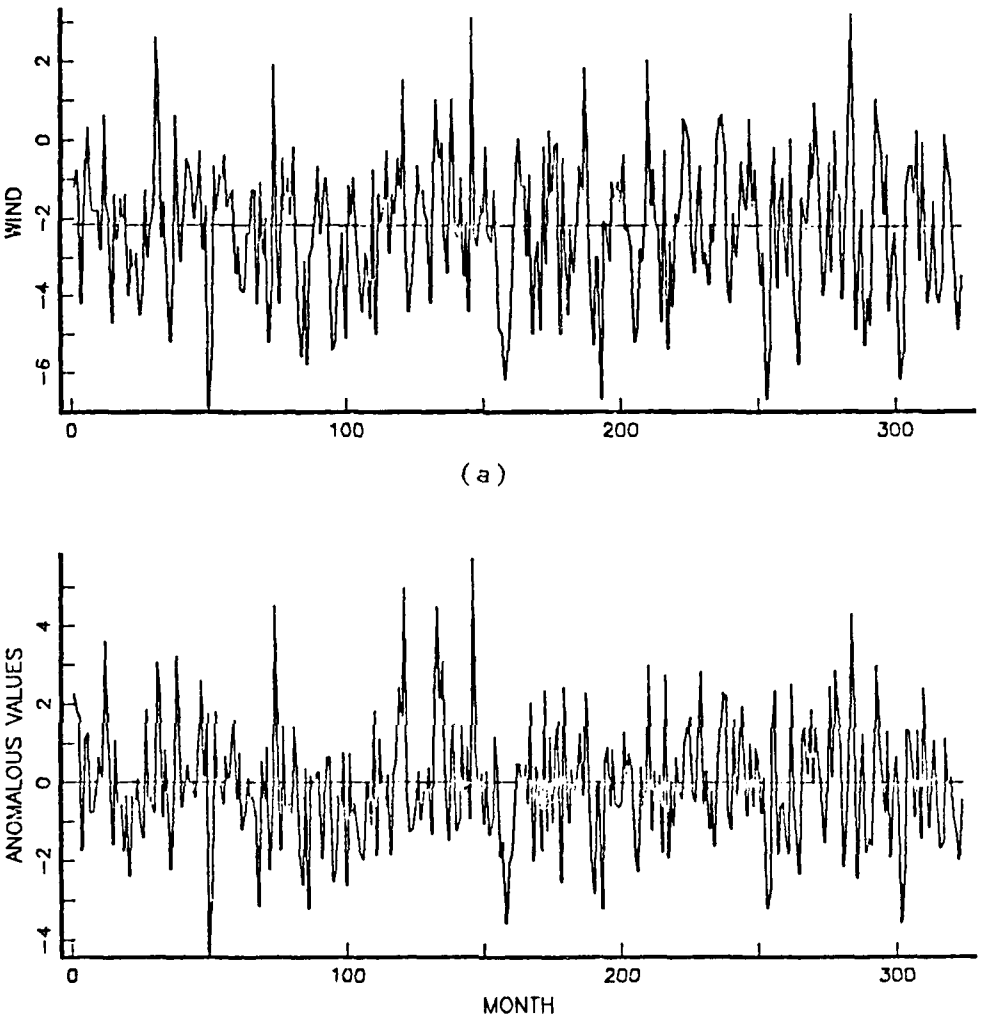

Figure 3.5 Time series of the (a) spatially averaged and the (b) detrended anomalous U wind component data at grid point 2. The straight line through the data indicates the trend.

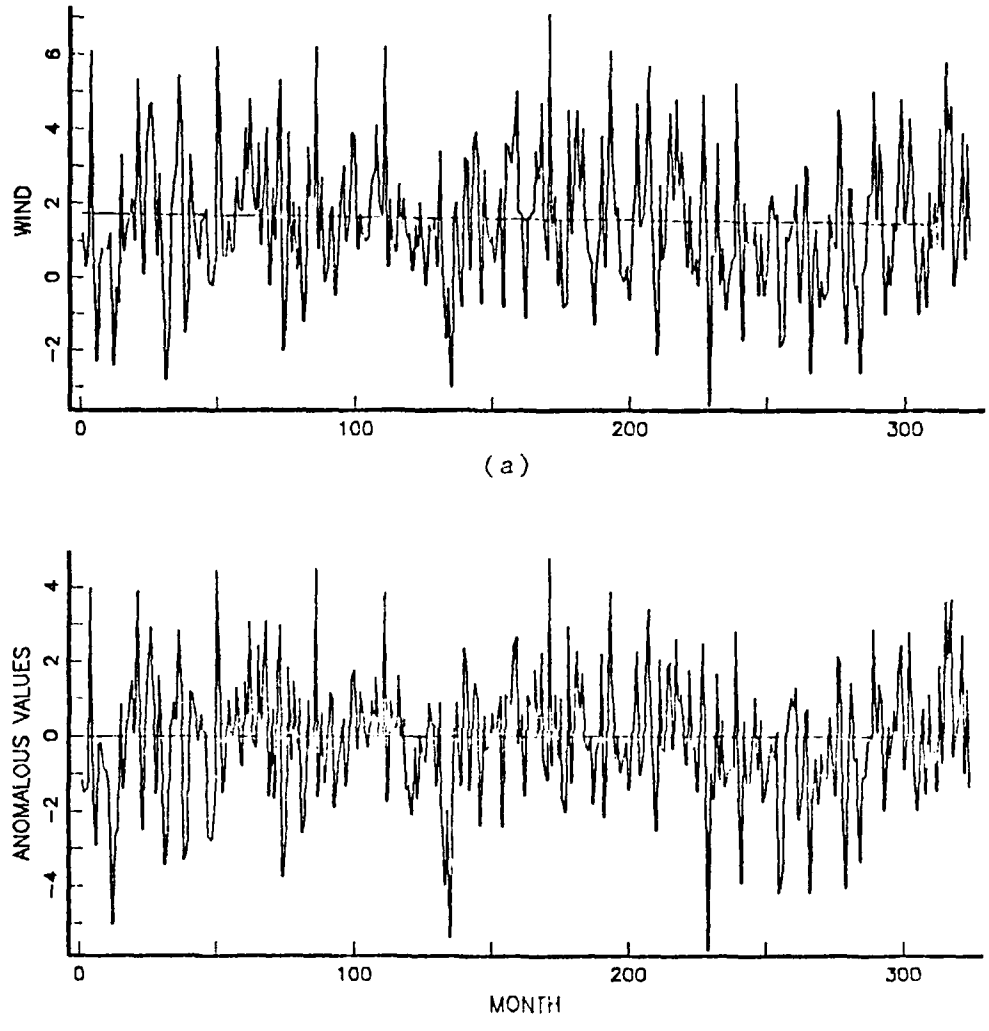

Figure 3.6 Time series of the (a) spatially averaged and the (b) detrended anomalous V wind component data at grid point 2. The straight line through the data indicates the trend.

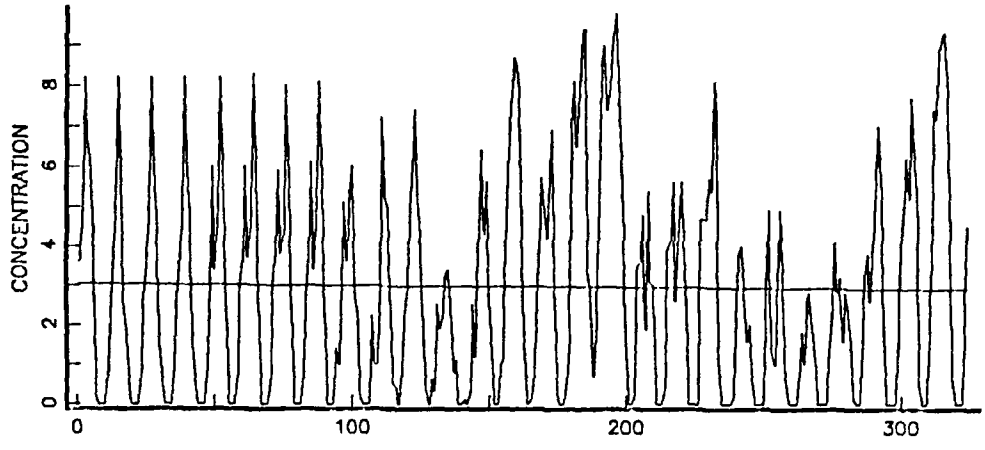

(a)

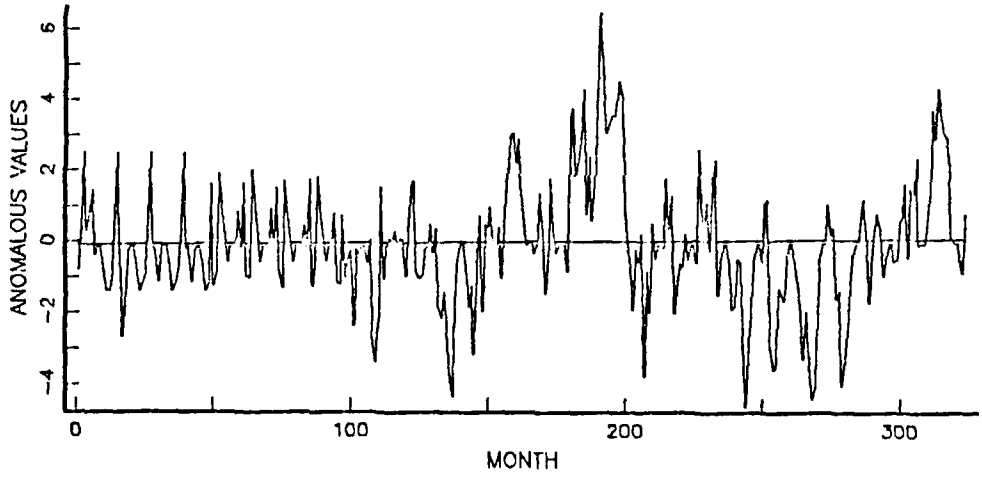

(b)

Figure 3.7 Time series of the (a) spatially averaged and the (b) detrended anomalous ice concentration data at grid point 4. The straight line through the data indicates the trend.

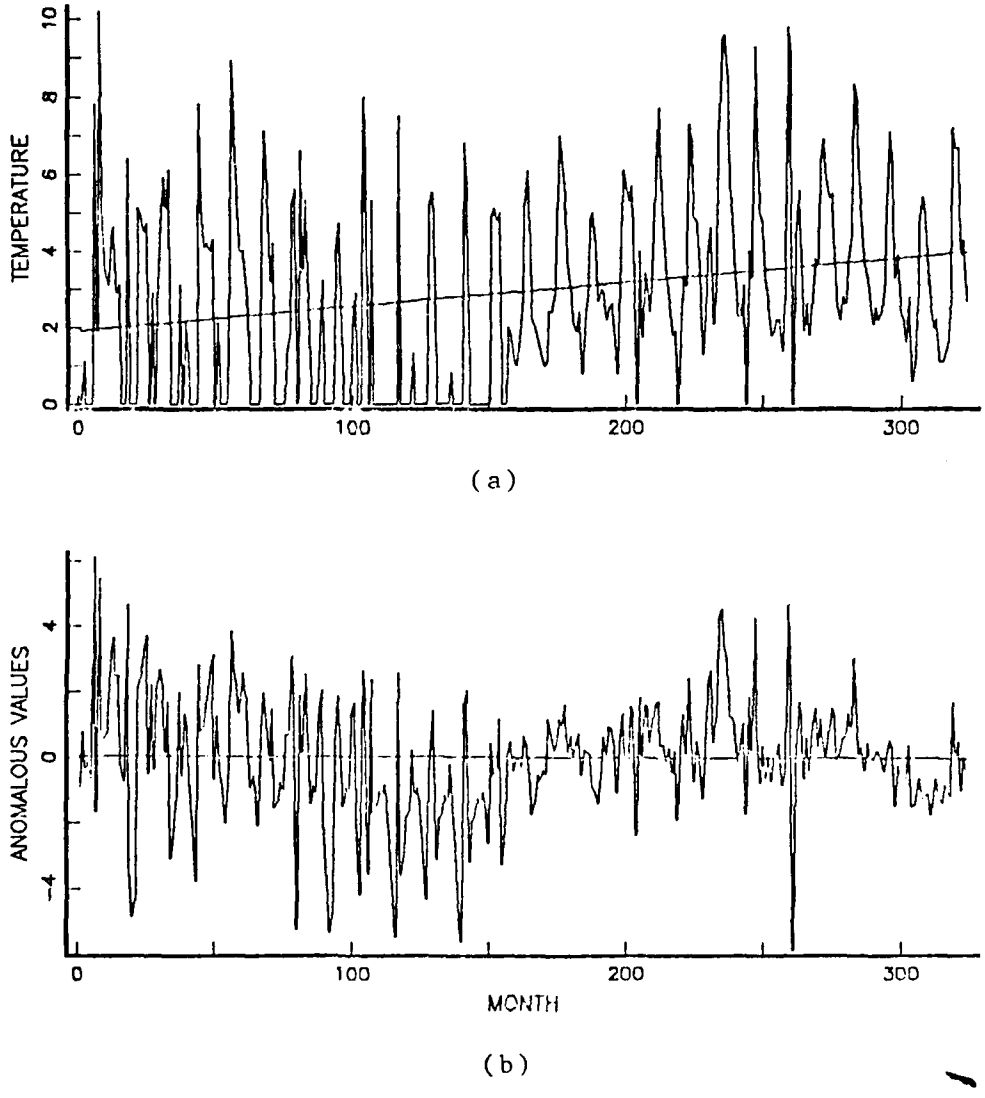

Figure 3.8 Time series of the (a) spatially averaged and the (b) detrended anomalous SST at grid point 4. The straight line through the data indicates the trend.

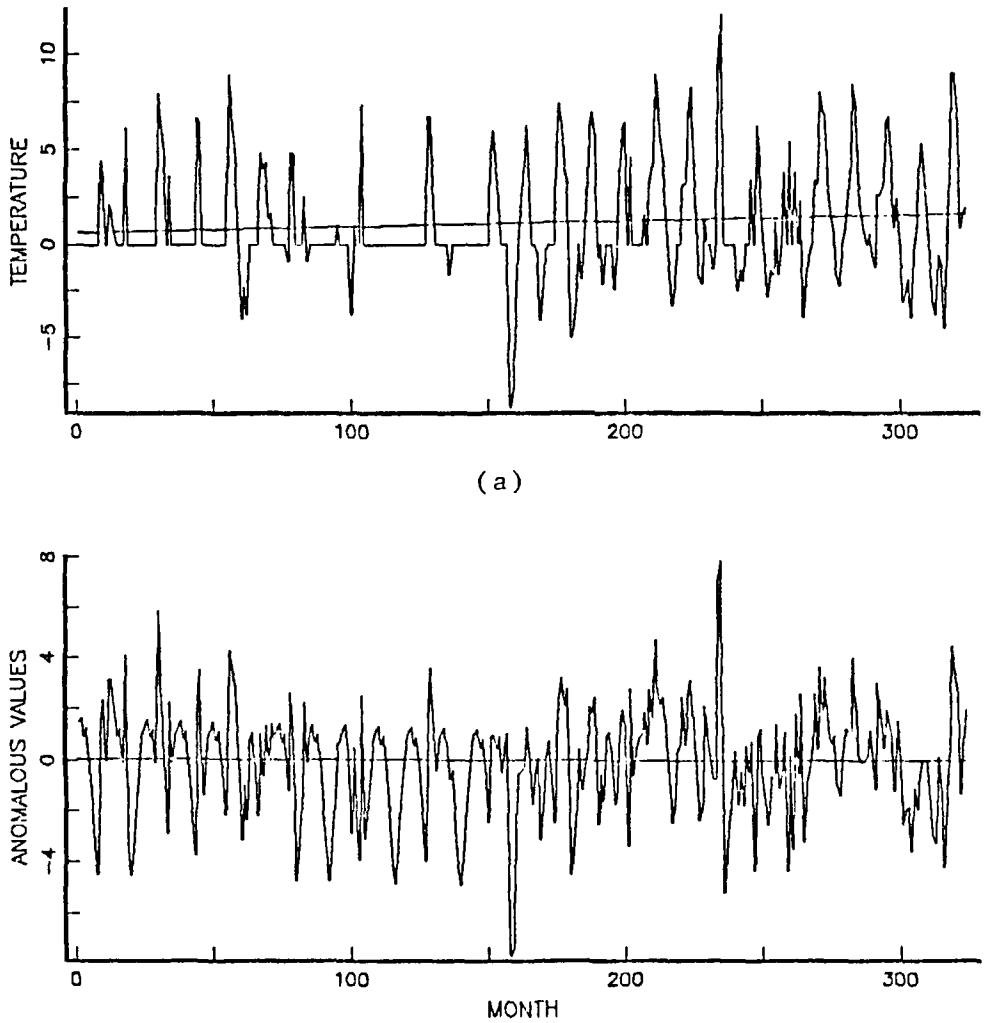

Figure 3.9 Time series of the (a) spatially averaged and the (b) detrended anomalous air temperature data at grid point 4. The straight line through the data indicates the trend.

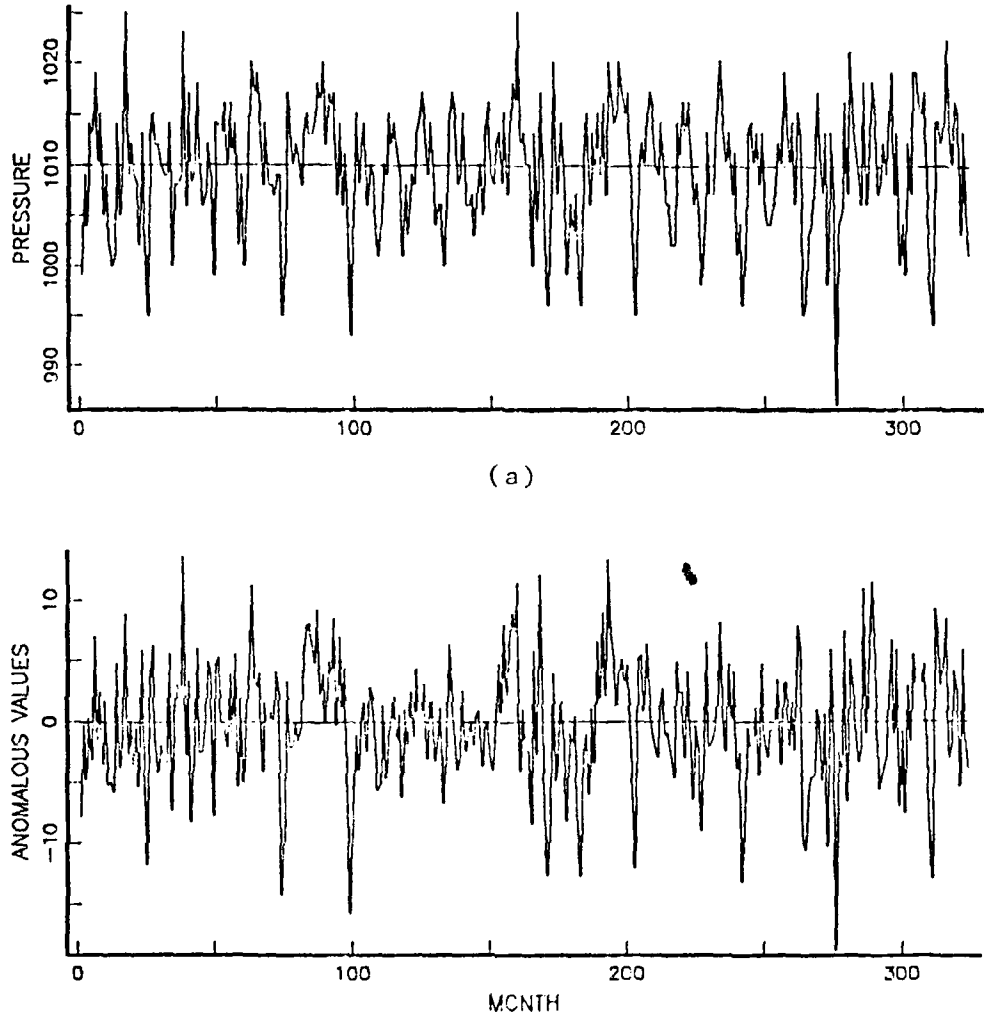

Figure 3.10 Time series of the (a) spatially averaged and the (b) detrended anomalous sea level pressure data at grid point 4. The straight line through the data indicates the trend.

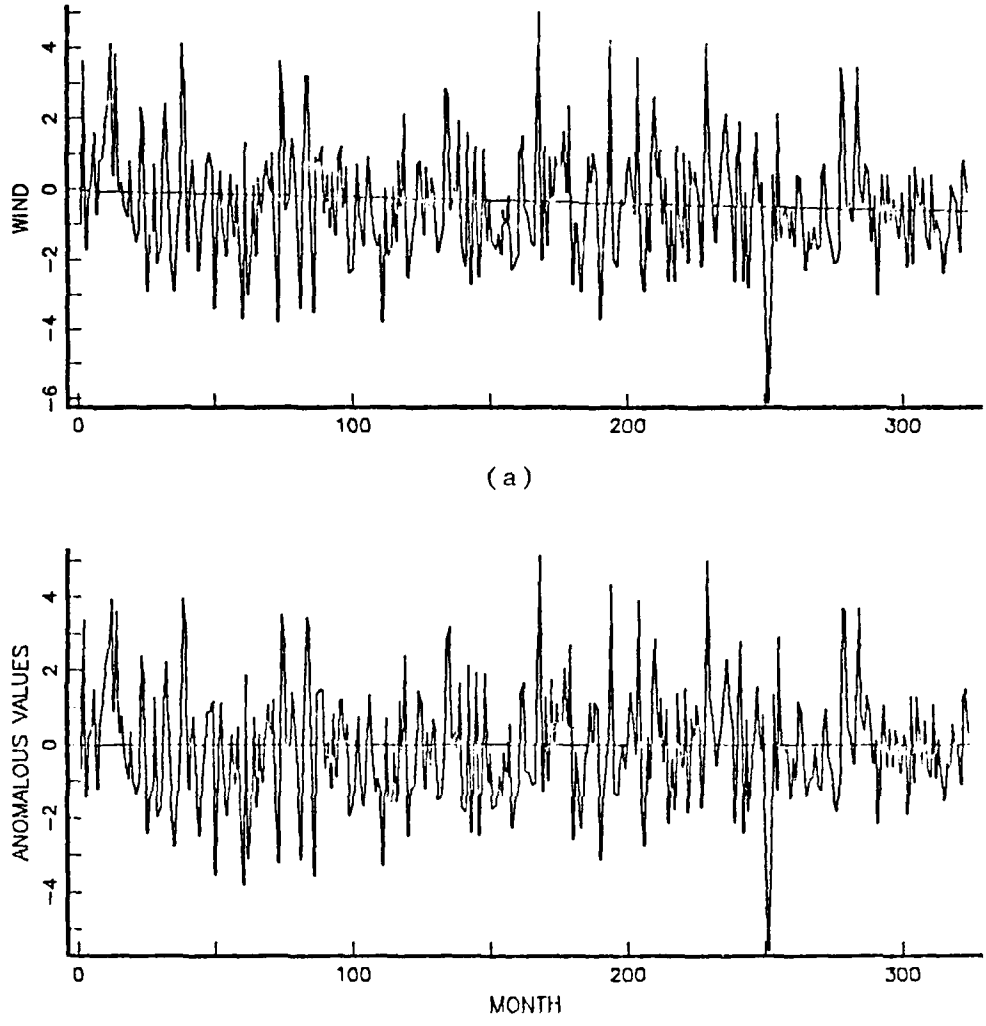

Figure 3.11 Time series of the (a) spatially averaged and the (b) detrended anomalous U wind component data at grid point 4. The straight line through the data indicates the trend.

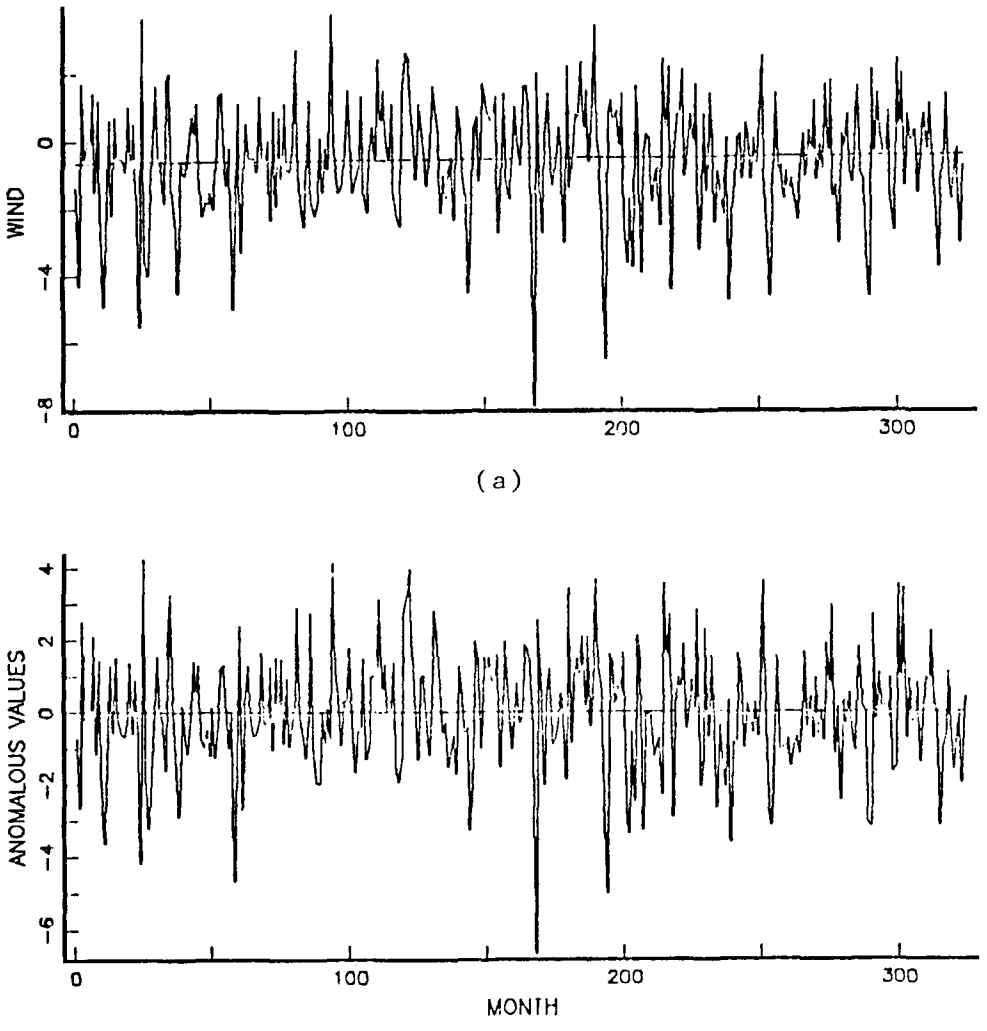

Figure 3.12 Time series of the (a) spatially averaged and the (b) detrended anomalous V wind component data at grid point 4. The straight line through the data indicates the trend.

IV. RESULTS

Various types of statistical analyses were performed on the COADS and SEIC data sets. The estimated spectral density for each spatially averaged and anomaly time series was plotted to observe dominate frequencies. Seasonal autocorrelations for the ice concentration and the SST anomalies were calculated for each area to determine if the degree of persistence varied spatially during the two major seasons. Stepwise regression equations were determined to calculate a seasonal ice anomaly for each location. The results varied both seasonally and regionally.

A. ESTIMATED SPECTRAL DENSITIES

The estimated spectral density, also known as the power spectrum, provides the distribution of the variance of a time series over all possible frequencies. Spectral densities based on the entire time series of each spatially averaged parameter were calculated both for the averaged and the detrended anomaly data. For these spectra the units of frequency are $month^{-1}$, since all the data are based on monthly averages. Because the mean parameter time series still contain seasonal cycles, the largest amplitudes were expected to be seen at a frequency of 0.083 $month^{-1}$, which represents the twelve month annual cycle. To overcome the strong annual signal, the spectral densities were recomputed after detrending the data and removing the monthly anomalies. Figures 4.1 - 4.3 are representative spectral density plots from grid point 2.

A pronounced spike is present at 0.083 $month^{-1}$ on all of the spectral density plots except for some of the wind component data. At grid points 4 and 5 in the Barents Sea, the spectral densities of the U wind component show a widely distributed variance (Figures 4.4 and 4.5). At these

locations spectral peaks are noted at approximately five and nine month cycles, but not at 12 months. Also at grid point 4, the V wind component exhibits a pronounced five month cycle as well as weaker nine and 12 month cycles. In spite of the lack of a strong annual peak, the monthly averages were still subtracted from these data in order to maintain consistency with the other parameters used in the regression equations.

The spectral density plots of the detrended anomaly data show significant overall reduction in the magnitude of the variance. Since the large spikes at twelve months have been removed or significantly reduced, other cycles become more obvious. Note that since the scale of the y-axis has changed on these plots, the remaining spikes appear more pronounced, although their magnitude has not changed appreciably.

Long cycles of 120 to 240 months (10 to 20 years) are evident in the ice concentration and the SST anomaly data at all of the grid points. Walsh (1987) cites examples of other researchers, some from very early publications, who have discovered multiyear cycles in sea ice concentration. Four to five year periodicities of both Iceland Sea (Meinardus, 1906) and Greenland Sea ice severity were noted (Kelly, 1979). Also, seven year cycles of ice concentration have been noted in areas of the North Atlantic (Kelly, 1979). Although apparent cycles such as these have been reported by various investigators, they clearly do not represent regular periodic fluctuations. Walsh also astutely notes that the variety of purported cycles in the two to ten year range will accommodate virtually any multiyear interannual fluctuation.

The spectra of the meteorological anomaly parameters also exhibited some long term cycles. The sea level pressure data show a cycle from 0.28 to 0.31 month^{-1}, or 32 to 36 months, at all of the grid points. At grid point 2, a large magnitude of variance at 108 months appeared in the V wind component (Figure 4.3).

One major limitation of the analyses of these spectral densities is the problem of "aliasing" of the high-frequency fluctuations, which are unresolvable, onto the low-frequency fluctuations, which are resolvable. In these time series, higher frequency fluctuations may consist of those with time scales shorter than one month, which may include diurnal changes.

B. AUTOCORRELATIONS

The autocorrelation of a variable is a direct indication of its temporal persistence. Since the persistence of an oceanographic anomaly varies both seasonally and spatially, plotting its autocorrelation directly illustrates the length of the anomaly's persistence.

In order to examine the variation of an anomaly's persistence in different seasons, specific months were selected to represent the summer and winter seasons. Since the Arctic region is typified by long winters and short summers, time series of the five winter months (December to April) and three summer months (July to September) were created. Extended persistence of meteorological parameters was not expected because of their inherently short time scales. Therefore, only autocorrelations of ice concentration and SST anomalies were plotted. See Figures 4.6 - 4.10.

As discussed previously, Walsh and Johnson (1979) found a tendency for ice concentration anomalies to persist for several months and for this persistence to be greater than that for SST in high latitudes. Therefore, persistence of the ice concentration anomalies was expected to exceed that of the SST anomalies for these areas. However, significant differences were seen at the various grid points. These differences will be discussed in the following chapter.

C. STEPWISE REGRESSION MODEL

In order to statistically forecast the ice concentration anomaly for a given area and time period, a stepwise

regression model was developed. For the development of each model equation in this study, the detrended anomalies of ice concentration, SST, air temperature, U and V wind components, and sea level pressure were included as well as the sequential three month mean ice concentration, SST and sea level pressure anomalies, all lagged from one to 13 months. The resulting regression equations indicate which parameters are most highly cross-correlated with the ice concentration anomaly values.

The stepwise regression model was chosen because it introduces the variables into the model one at a time in order to reach the optimum equation. Walpole (1985) describes how this statistical model evolves and the interpretation of the F statistic used to determine the goodness of fit of the regression equation. The first variable chosen is that which gives the largest regression sum of squares when performing a simple linear regression with the ice concentration anomaly, or equivalently, that which gives the largest value of R^2, or variance. The subsequent variables are individually chosen such that when inserted into the model, they give the largest increase in R^2 over that found in the first step. As each new variable is entered into the regression equation through a significant increase in R^2 (as determined by the F test), each prior variable is also subjected to the F test to ensure its continued effectiveness.

If a variable is determined to be unimportant because of relationships that exist between it and other variables entering at later steps, it will be removed from the equation. This procedure continues until a stage is reached for which no additional variables can be inserted or deleted.

For the development of these regression equations, a confidence level of 0.05 was used as a test level. The closer a value is to 0.00 in the PROB>F column in the

following regression tables, the more statistically significant the variable is to the equation.

All seasonality was removed in calculating the regression equations by weighing all the same months together, e.g., all Januarys, all Februarys, etc. were separately considered by the model. Initially, the regression equations were developed to forecast a three month mean ice concentration anomaly for winter and summer at each grid point. Therefore, lags of one and two months were not included in the calculation of the regression equations. The forecasted mean ice concentration anomalies from January to March for winter and July to September for summer were chosen for analysis. The results of the regression analysis are tabulated in Tables I-V. Although other variables were included in the equations, only those explaining 5% or more of the variance still unexplained by the previous parameters are displayed.

The number following each variable indicates the lag behind the forecast month. Therefore, for a winter forecast based on the last month of the season (March), Ice3 indicates the December ice concentration anomaly value. An M preceding the lag number indicates that it is a three month sequential mean value. Therefore, for a winter forecast, SSTM8 indicates the SST anomaly averaged from May to July (July being the lag 8 month behind March).

In general, the most important contributor to the total explained variance was the ice concentration anomaly value lagged at three months. However, oceanic and meteorological parameters were also found to be important contributors to the regression equations. For various seasons and locations, a wide variety of parameters comprised the different prediction equations.

At grid point 1, the ice concentration anomaly and SST anomalies from preceding seasons are the only predictors in the regression equation for winter. Of all the equations, the least amount of total variance, only 50%, was explained

by these variables. In summer various wind component, SST and sea level pressure anomalies, lagged for periods greater than five months, were included in the regression equation.

At grid point 2, the averaged ice concentration anomaly from fall explained most of the variance of the model in winter. Also included in the equation were June's U and V wind component anomalies. In summer three different ice concentration anomalies accounted for most of the total explained model variance.

At grid point 3, the most important predictor in winter was the SST anomaly from the previous winter. Additionally, wind and sea level pressure anomalies at long lags were the other significant contributors; no ice variables were included in the equation. The ice concentration and sea level pressure anomalies from June and the sea level pressure anomaly from winter were retained by the regression equation for summer.

The winter regression equation for grid point 4 included variables from recent months. Besides the ice concentration anomaly lagged at three months, the equation included the U wind component and SST anomalies from November and the sea level pressure anomaly from October. Ice concentration anomalies dominated the regression equation for summer. These anomalies from December, early winter and the previous summer explained 61% of the total model variance. The V wind component from March and sea level pressure anomaly from fall were the other most significant contributors to the model.

At grid point 5, ice concentration anomalies dominated both regression equations. In winter the ice concentration anomaly lagged at three and four months, June's air temperature, November's U wind component and the previous winter's SST anomalies explained most of the total model variance. In summer, November's SST and March's U wind component anomalies supplemented various ice concentration anomalies to form the regression equation.

D. TEST RESULTS

The ice concentration anomaly for each season at each grid point was calculated using the 27-year anomaly time series using the regression equations determined above. In order to graphically display the results, the actual anomalies were plotted against the residual values. These are displayed in Figures 4.11-4.15.

If no systematic errors existed in the equations, the data would be scattered about zero along the y-axis. If systematic errors were present, some type of trend in the plots would appear. None of the plots exhibited a significant trend.

The residual values for the summer season at grid point 1 (Figure 4.11) are within +/-0.30 of the actual anomalies, which appeared to have the least scatter of all the seasonal calculations. At grid point 4 (Figure 4.14), the summer season also displayed a small scatter about zero. However, the actual anomalies did not vary considerably.

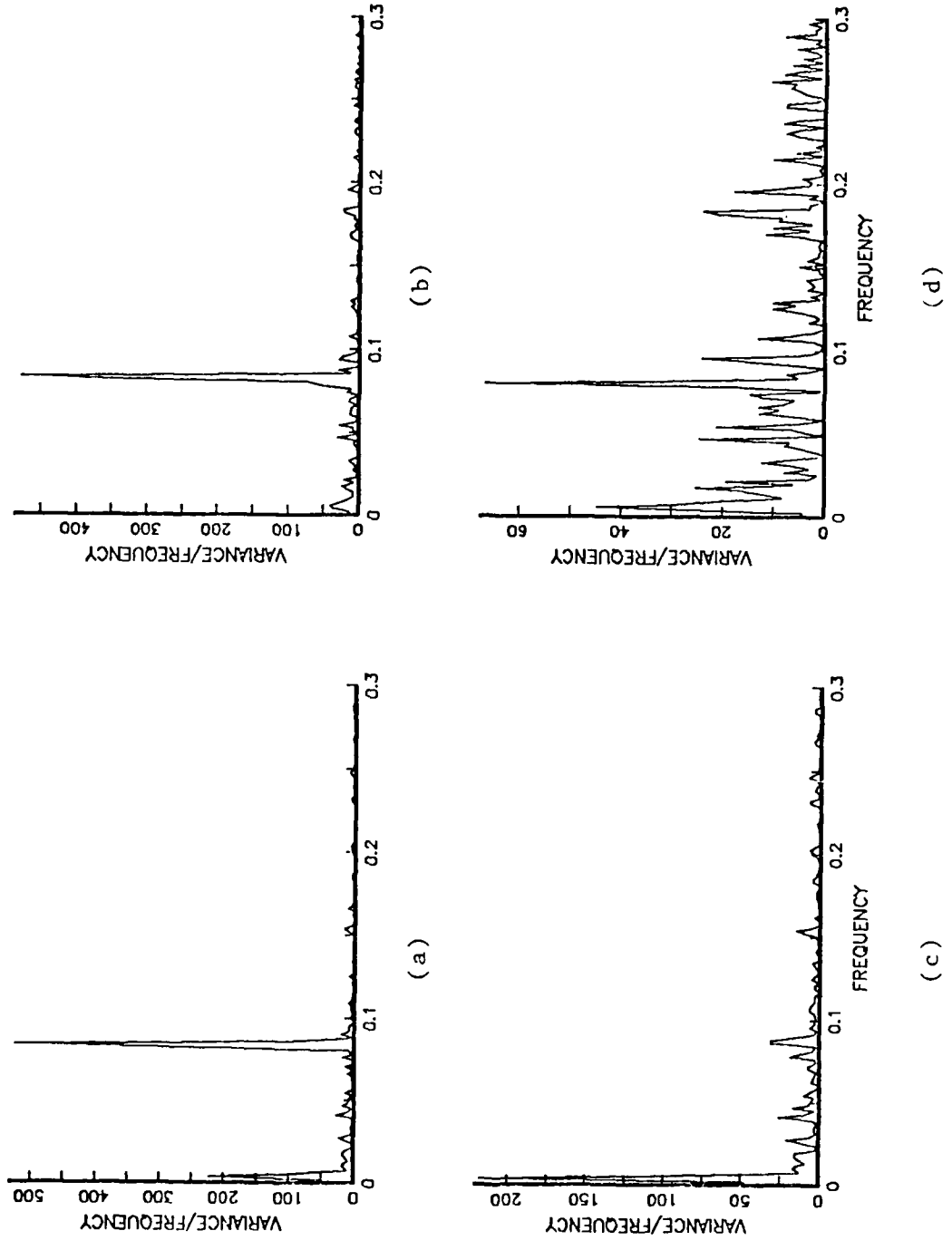

Figure 4.1 Estimated spectral density plots of spatially averaged (a) ice concentration and (b) SST and their respective detrended anomaly values (c) and (d) at grid point 2. Frequency is in cycles per month.

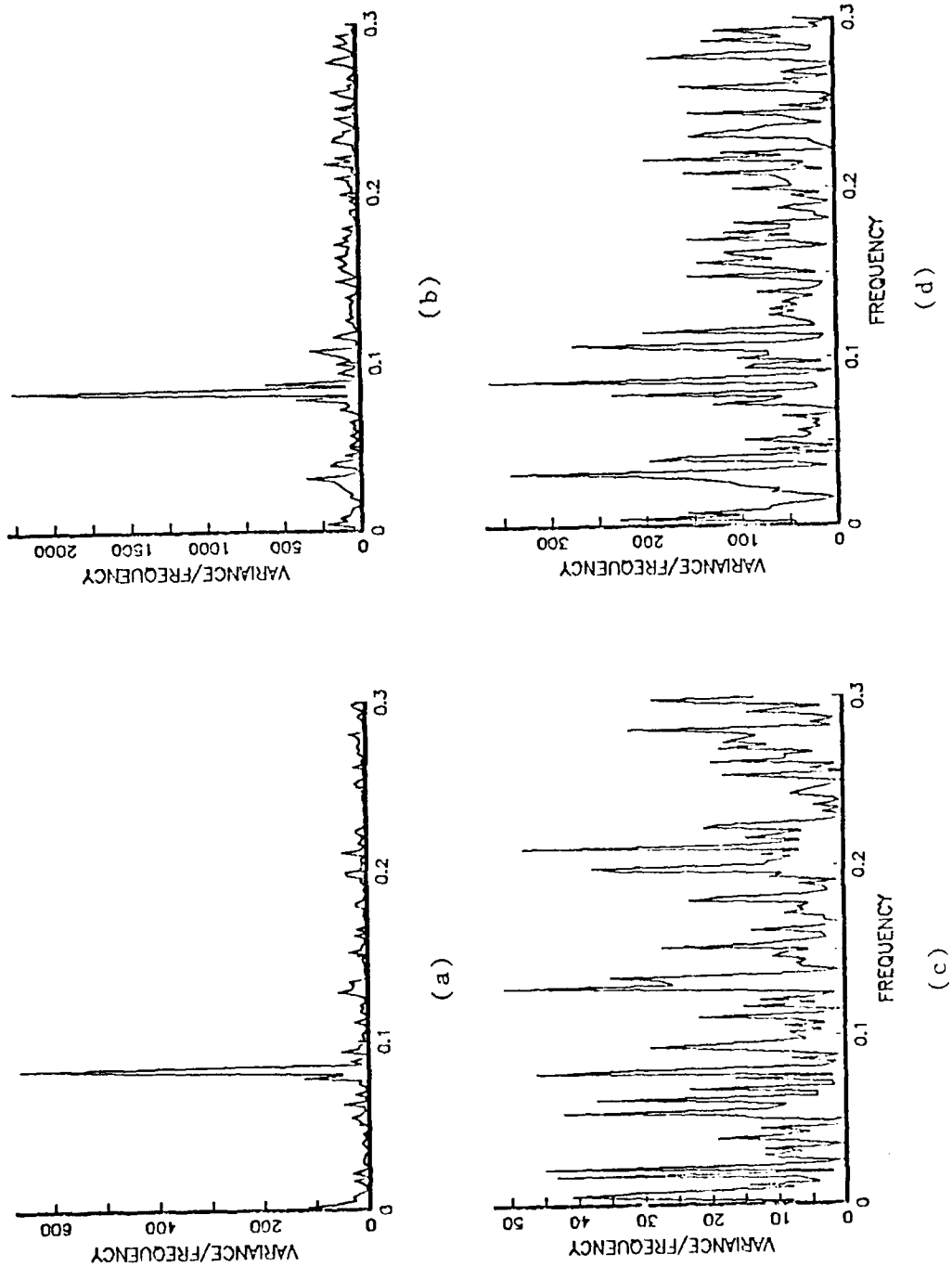

Figure 4.2 Estimated spectral density plots of spatially averaged (a) air temperature and (b) sea level pressure and their respective detrended anomaly values (c) and (d) at grid point 2. Frequency is in cycles per month.

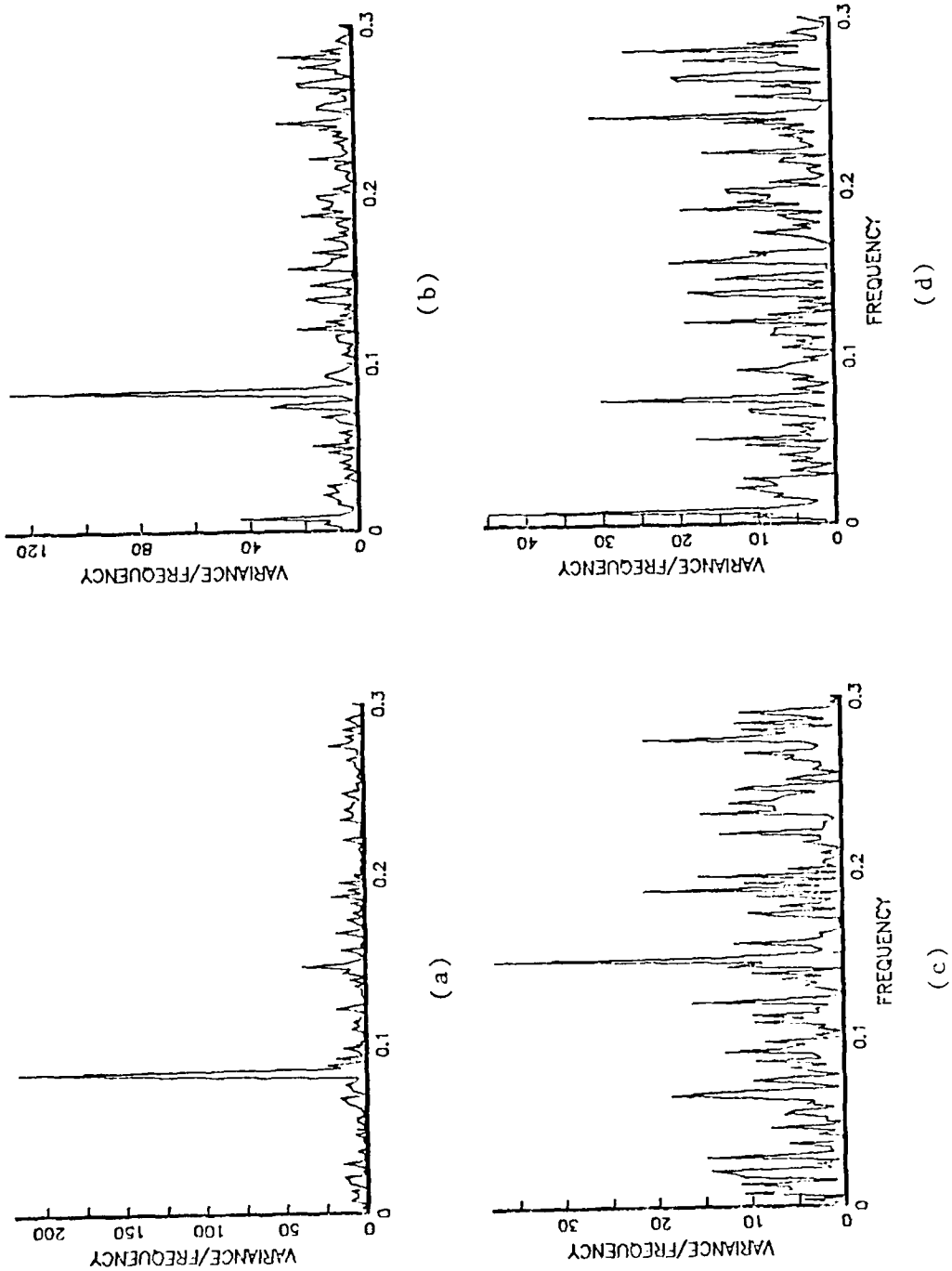

Figure 4.3 Estimated spectral density plots of spatially averaged (a) U and (b) V wind components and their respective detrended anomaly values (c) and (d) at grid point 2. Frequency is in cycles per month.

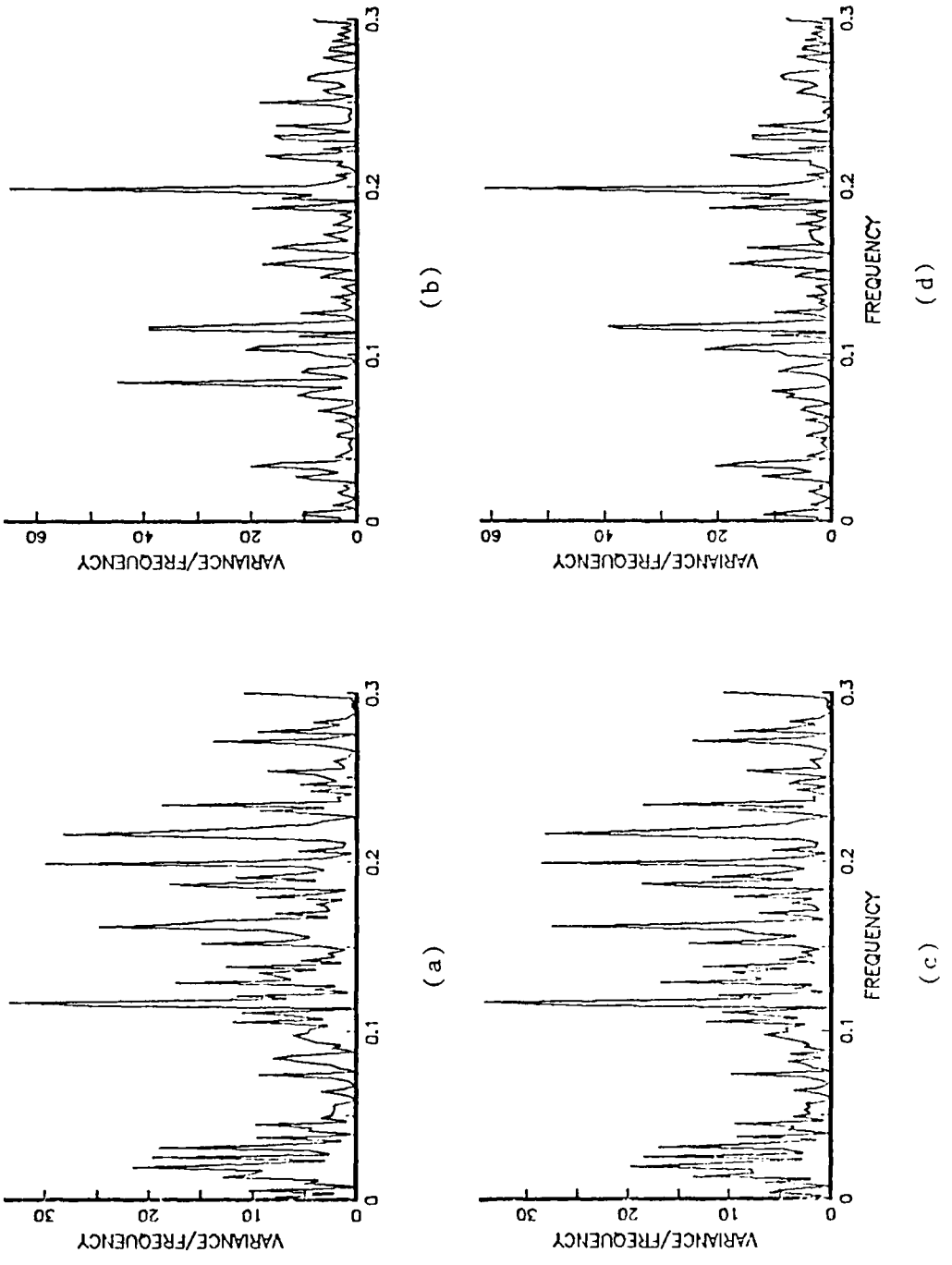

Figure 4.4 Estimated spectral density plots of spatially averaged (a) U and (b) V wind components and their respective detrended anomaly values (c) and (d) at grid point 4. Frequency is in cycles per month.

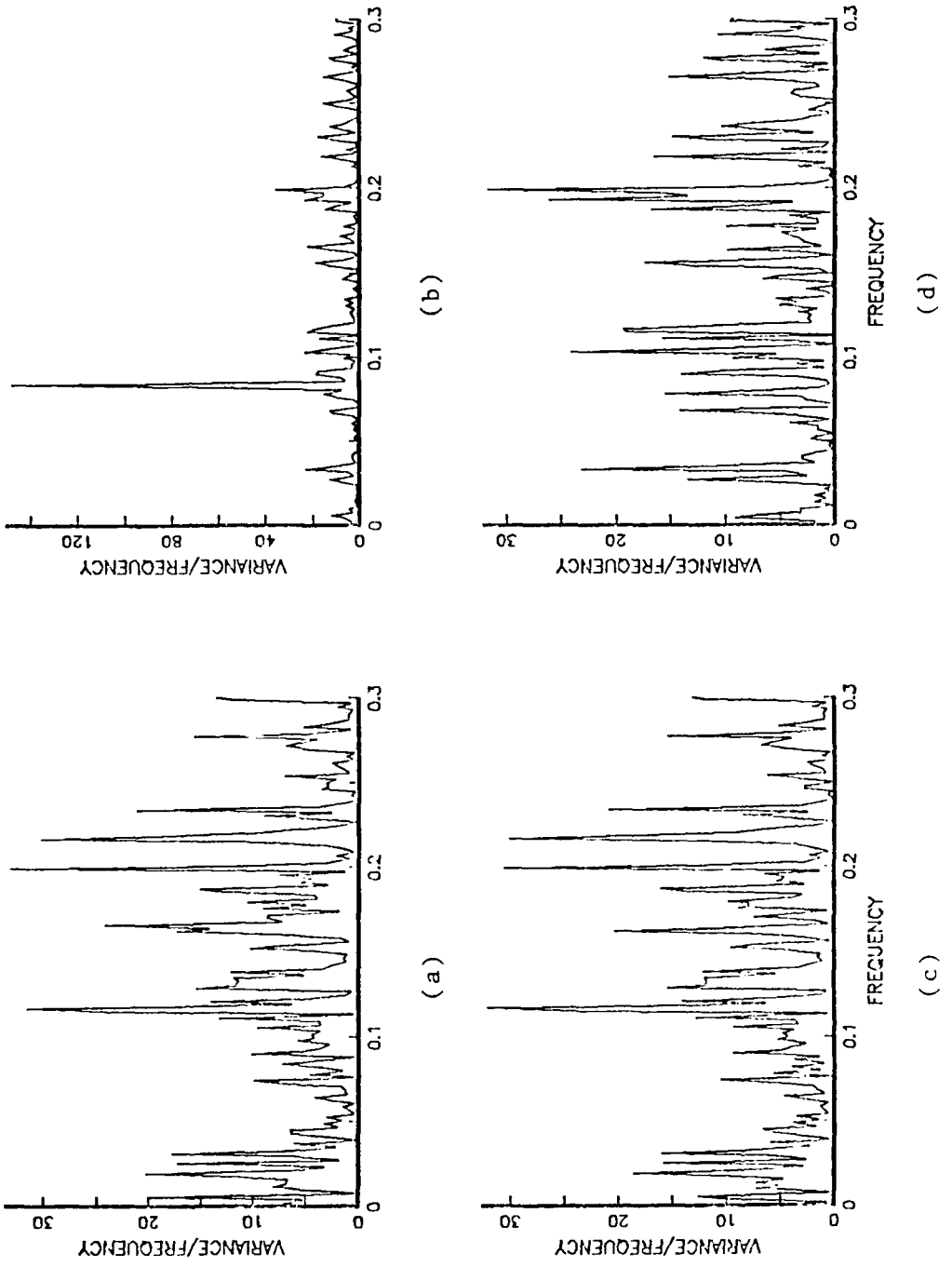

Figure 4.5 Estimated spectral density plots of spatially averaged (a) U and (b) V wind components and their respective detrended anomaly values (c) and (d) at grid point 5. Frequency is in cycles per month.

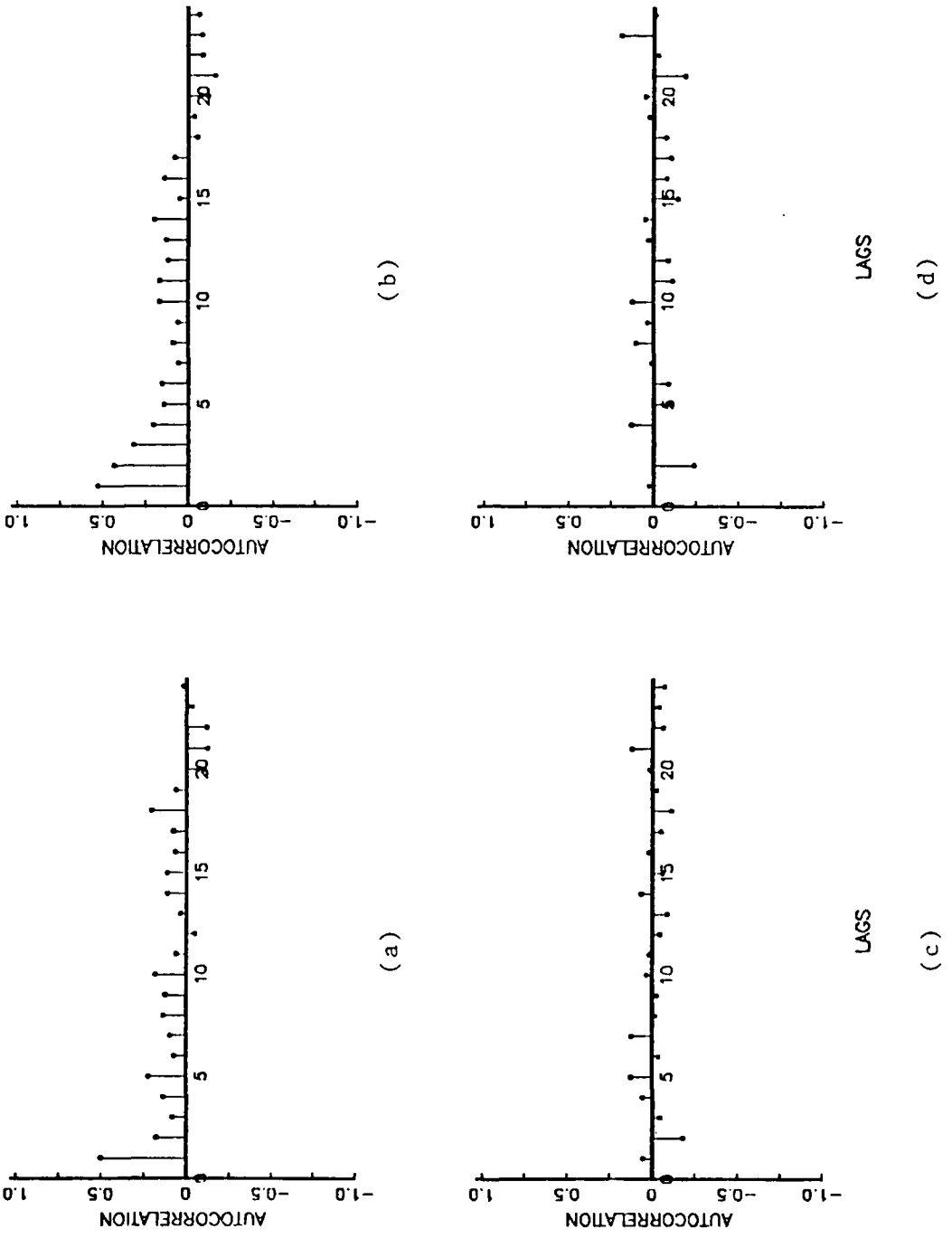

Figure 4.6 Ice concentration anomaly autocorrelation for (a) winter, (b) summer, and SST anomaly autocorrelation for (c) winter and (d) summer at grid point 1. The winter season is composed of five months and summer is composed of three months. Lags are in months.

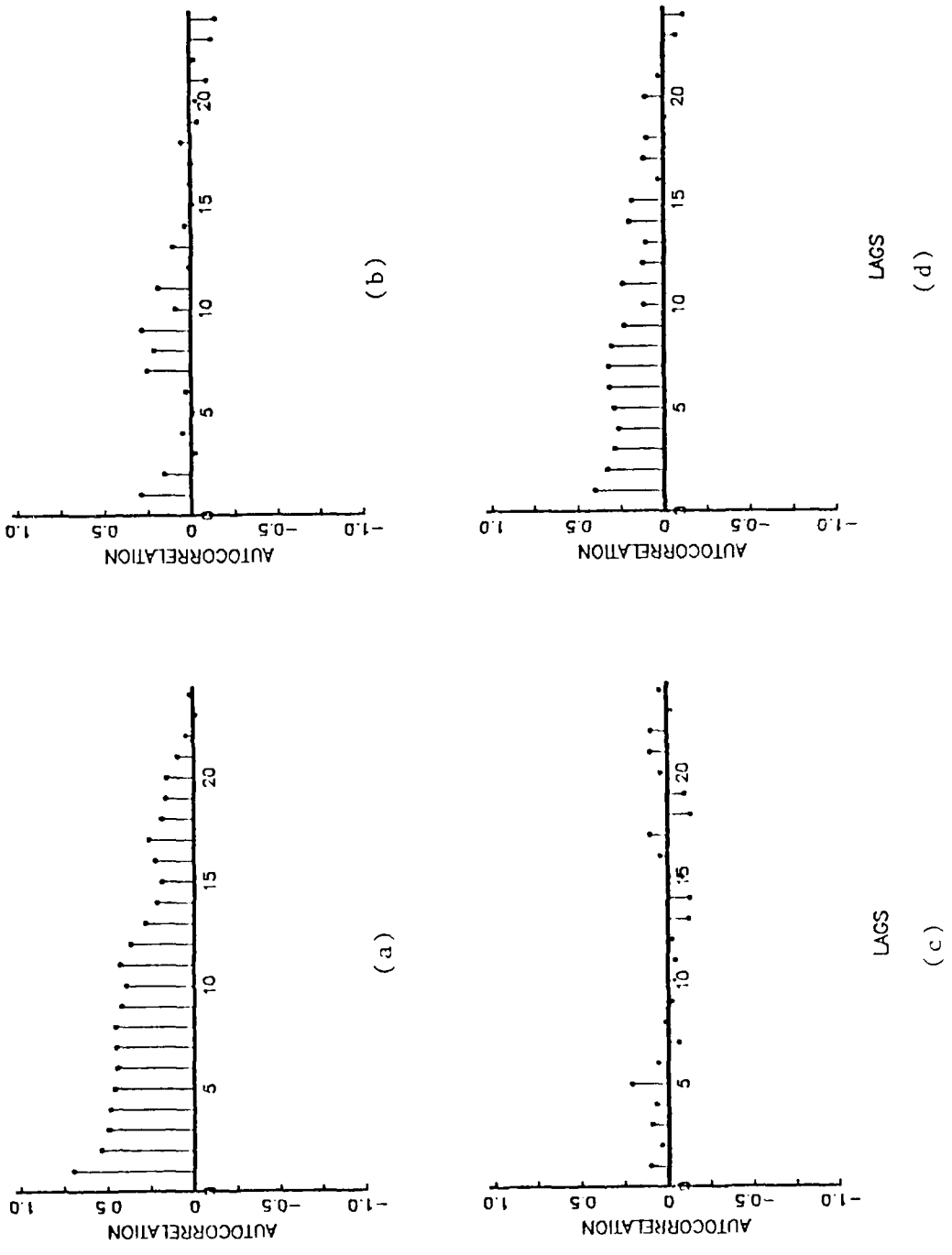

Figure 4.7 Ice concentration anomaly autocorrelation for (a) winter, (b) summer, and SST anomaly autocorrelation for (c) winter and (d) summer at grid point 2. The winter season is composed of five months and summer is composed of three months. Lags are in months.

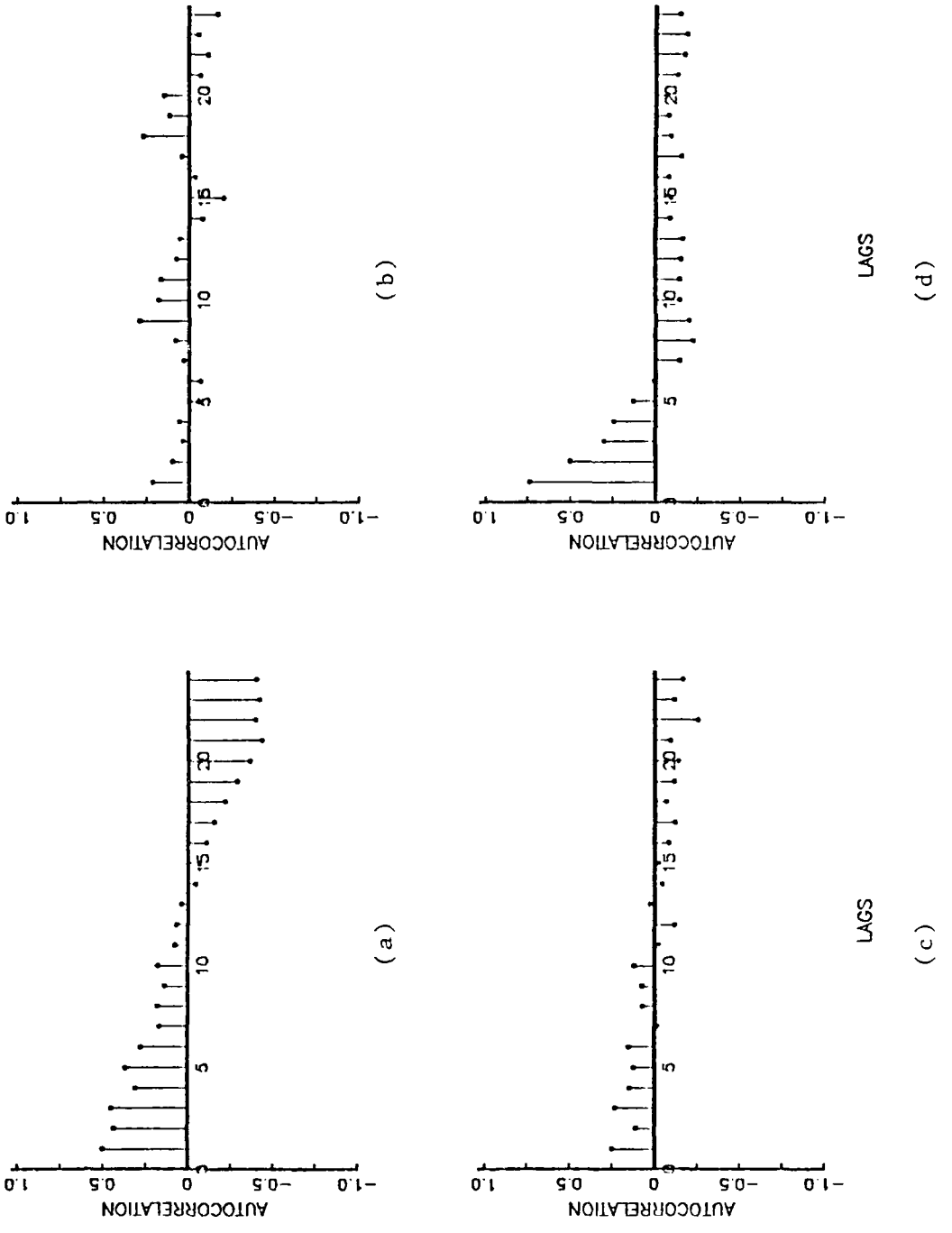

Figure 4.8 Ice concentration anomaly autocorrelation for (a) winter, (b) summer, and SST anomaly autocorrelation for (c) winter and (d) summer at grid point 3. The winter season is composed of five months and summer is composed of three months. Lags are in months.

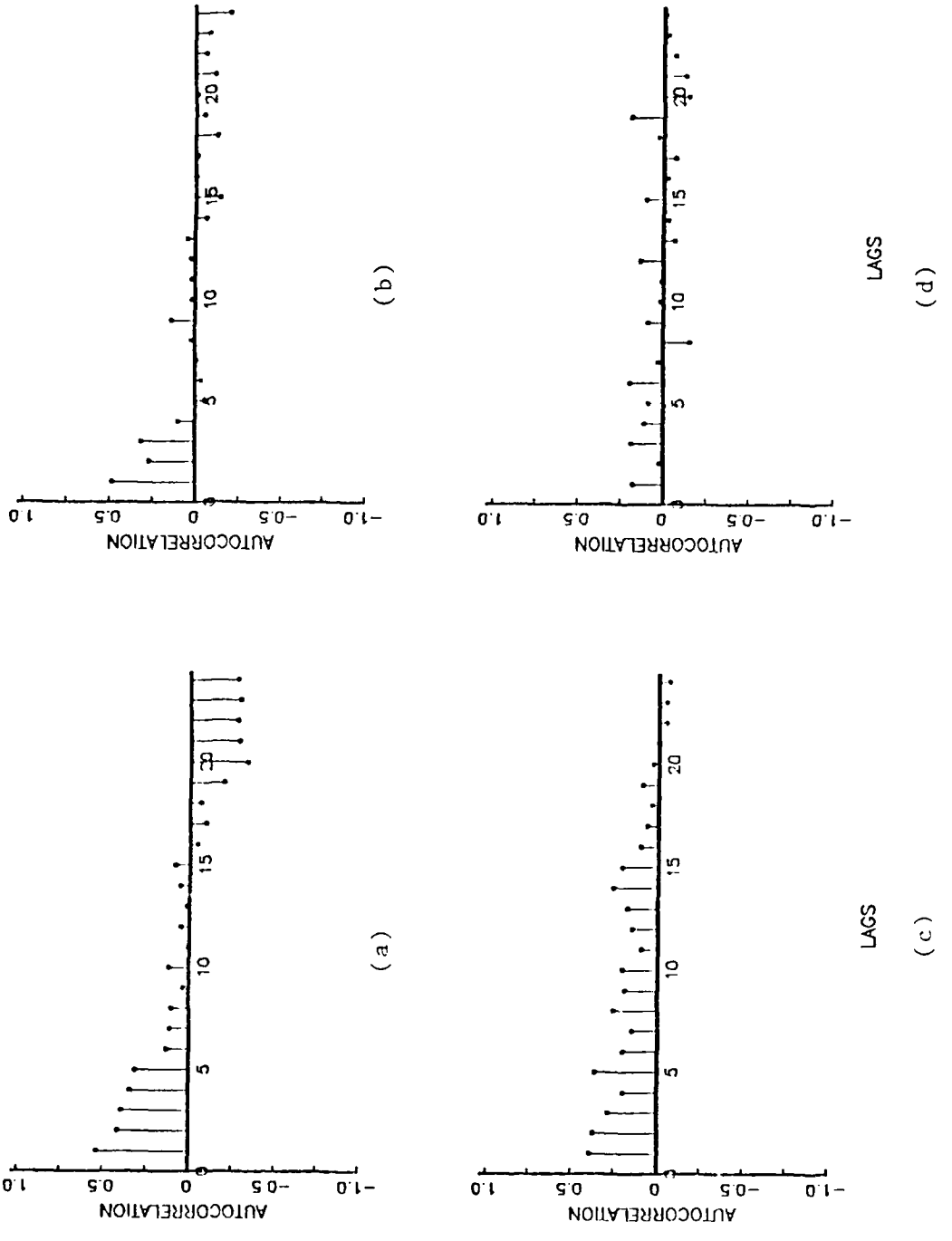

Figure 4.9 Ice concentration anomaly autocorrelation for (a) winter, (b) summer, and SST anomaly autocorrelation for (c) winter and (d) summer at grid point 4. The winter season is composed of five months and summer is composed of three months. Lags are in months.

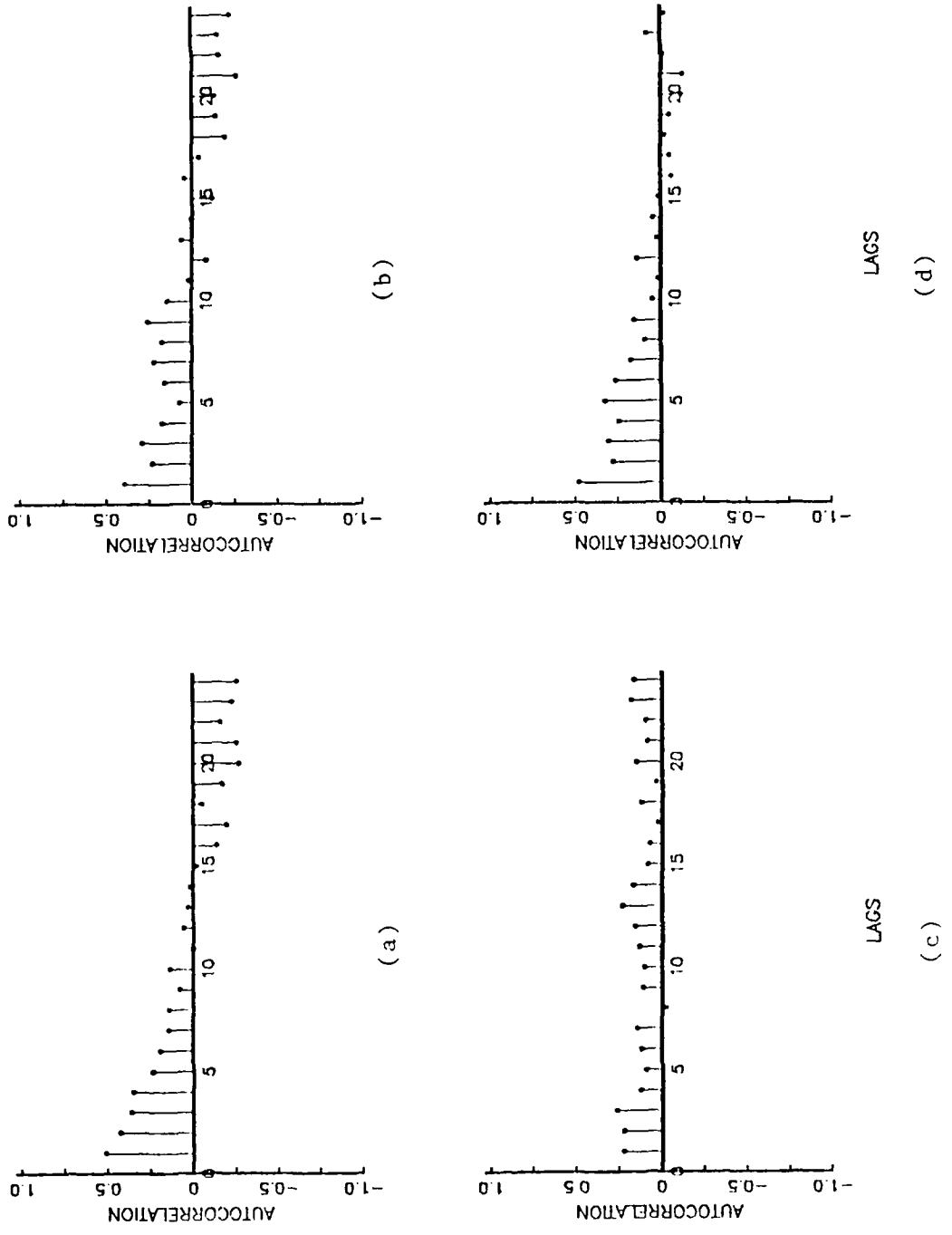

Figure 4.10 Ice concentration anomaly autocorrelation for (a) winter, (b) summer, and SST anomaly autocor relation for (c) winter and (d) summer at grid point 5. The winter season is composed of five months and summer is composed of three months. Lags are in months.

TABLE I

GRID POINT 1

SUMMARY OF STEPWISE REGRESSION PROCEDURE FOR WINTER

VARIABLE ENTERED	VARIABLE REMOVED	NUMBER IN	PARTIAL R**2	MODEL R**2	EQUATION COEFFICIENT
ICE3		1	0.3201	0.3201	0.363
SSTM8		2	0.1684	0.4885	0.617
SSTM12		3	0.0905	0.5790	-0.702
INTERCEPT					-0.043

STEP	VARIABLE ENTERED	VARIABLE REMOVED	F	PROB>F
1	ICE3		11.2987	0.0026
2	SSTM8		7.5716	0.0114
3	SSTM12		4.7305	0.0407

SUMMARY OF STEPWISE REGRESSION PROCEDURE FOR SUMMER

VARIABLE ENTERED	VARIABLE REMOVED	NUMBER IN	PARTIAL R**2	MODEL R**2	EQUATION COEFFICIENT
ICE3		1	0.3416	0.3416	0.278
V6		2	0.1747	0.5163	0.065
U10		3	0.1261	0.6424	0.379
SST7		4	0.1121	0.7545	-0.212
SLPM7		5	0.0839	0.8384	-0.069
INTERCEPT					-0.017

STEP	VARIABLE ENTERED	VARIABLE REMOVED	F	PROB>F
1	ICE3		12.4516	0.0017
2	V6		8.3061	0.0084
3	U10		7.7580	0.0108
4	SST7		9.5842	0.0055
5	SLPM7		10.3871	0.0043

TABLE II

GRID POINT 2

SUMMARY OF STEPWISE REGRESSION PROCEDURE FOR WINTER

VARIABLE ENTERED	VARIABLE REMOVED	NUMBER IN	PARTIAL R**2	MODEL R**2	EQUATION COEFFICIENT
ICEM4		1	0.5477	0.5477	1.855
V9		2	0.0812	0.6289	-1.057
SSTM13		3	0.0650	0.6939	-0.895
U9		4	0.0605	0.7544	-0.977
INTERCEPT					-0.140

STEP	VARIABLE ENTERED	VARIABLE REMOVED	F	PROB>F
1	ICEM4		29.0629	0.0001
2	V9		5.0336	0.0348
3	SSTM13		4.6716	0.0418
4	U9		5.1718	0.0336

SUMMARY OF STEPWISE REGRESSION PROCEDURE FOR SUMMER

VARIABLE ENTERED	VARIABLE REMOVED	NUMBER IN	PARTIAL R**2	MODEL R**2	EQUATION COEFFICIENT
ICE3		1	0.4720	0.4720	0.174
ICEM13		2	0.1032	0.5752	-0.651
SLP6		3	0.0780	0.6531	0.044
SSTM3		4	0.0648	0.7179	-0.168
ICE13		5	0.0708	0.7886	0.660
AIR5		6	0.0550	0.8436	0.083
INTERCEPT					0.005

STEP	VARIABLE ENTERED	VARIABLE REMOVED	F	PROB>F
1	ICE3		21.4534	0.0001
2	ICEM13		5.5859	0.0269
3	SLP6		4.9443	0.0368
4	SSTM3		4.8201	0.0395
5	ICE13		6.6951	0.0176
6	AIR5		6.6770	0.0182

TABLE III

GRID POINT 3

SUMMARY OF STEPWISE REGRESSION PROCEDURE FOR WINTER

VARIABLE ENTERED	VARIABLE REMOVED	NUMBER IN	PARTIAL R**2	MODEL R**2	EQUATION COEFFICIENT
SSTM13		1	0.4353	0.4353	0.656
U3		2	0.1456	0.5809	
SLPM9		3	0.1044	0.6853	-0.385
V12		4	0.0955	0.7808	-0.268
ICE13		5	0.0677	0.8486	
	ICE13	4	0.0022	0.9508	
	U3	3	0.0059	0.9635	
INTERCEPT					0.096

STEP	VARIABLE ENTERED	VARIABLE REMOVED	F	PROB>F
1	SSTM13		18.5034	0.0002
2	U3		7.9909	0.0096
3	SLPM9		7.2990	0.0130
4	V12		9.1480	0.0065
5	ICE13		8.9466	0.0072
9		ICE13	0.7897	0.3866
11		U3	3.3072	0.0866

SUMMARY OF STEPWISE REGRESSION PROCEDURE FOR SUMMER

VARIABLE ENTERED	VARIABLE REMOVED	NUMBER IN	PARTIAL R**2	MODEL R**2	EQUATION COEFFICIENT
ICE3		1	0.4743	0.4743	0.333
SSTM5		2	0.2169	0.6912	
SLP3		3	0.0611	0.7522	-0.051
ICE13		4	0.0574	0.8097	0.877
	SSTM5	3	0.0289	0.7807	
SLP8		4	0.0778	0.8585	-0.025
INTERCEPT					0.018

STEP	VARIABLE ENTERED	VARIABLE REMOVED	F	PROB>F
1	ICE3		21.6519	0.0001
2	SSTM5		16.1509	0.0005
3	SLP3		5.4220	0.0295
4	ICE13		6.3362	0.0200
5		SSTM5	3.1910	0.0885
6	SLP8		11.5514	0.0027

TABLE IV

GRID POINT 4

SUMMARY OF STEPWISE REGRESSION PROCEDURE FOR WINTER

VARIABLE ENTERED	VARIABLE REMOVED	NUMBER IN	PARTIAL R**2	MODEL R**2	EQUATION COEFFICIENT
ICE3		1	0.3912	0.3912	0.515
U4		2	0.1835	0.5746	0.431
SLP5		3	0.0934	0.6680	-0.086
SST4		4	0.0579	0.7259	-0.243
INTERCEPT					-0.006

STEP	VARIABLE ENTERED	VARIABLE REMOVED	F	PROB>F
1	ICE3		15.4197	0.0006
2	U4		9.9214	0.0045
3	SLP5		6.1878	0.0209
4	SST4		4.4355	0.0474

SUMMARY OF STEPWISE REGRESSION PROCEDURE FOR SUMMER

VARIABLE ENTERED	VARIABLE REMOVED	NUMBER IN	PARTIAL R**2	MODEL R**2	EQUATION COEFFICIENT
ICE9		1	0.4841	0.4841	0.343
V6		2	0.1453	0.6294	0.226
SLP10		3	0.0657	0.6952	0.115
SLPM10		4	0.0705	0.7656	-0.188
ICEM12		5	0.0786	0.8442	0.708
ICEM8		6	0.0523	0.8965	-0.223
INTERCEPT					0.031

STEP	VARIABLE ENTERED	VARIABLE REMOVED	F	PROB>F
1	ICE9		22.5220	0.0001
2	V6		9.0183	0.0064
3	SLP10		4.7441	0.0404
4	SLPM10		6.3134	0.0202
5	ICEM12		10.0955	0.0047
6	ICEM8		9.5964	0.0059

TABLE V

GRID POINT 5

SUMMARY OF STEPWISE REGRESSION PROCEDURE FOR WINTER

VARIABLE ENTERED	VARIABLE REMOVED	NUMBER IN	PARTIAL R**2	MODEL R**2	EQUATION COEFFICIENT
ICE3		1	0.3487	0.3487	1.034
AIR9		2	0.2787	0.6274	-0.588
U4		3	0.1070	0.7344	0.115
SSTM12		4	0.0664	0.8008	0.418
ICE4		5	0.0595	0.8603	-0.271
INTERCEPT					0.015

STEP	VARIABLE ENTERED	VARIABLE REMOVED	F	PROB>F
1	ICE3		12.8521	0.0015
2	AIR9		17.2051	0.0004
3	U4		8.8624	0.0070
4	SSTM12		7.0033	0.0151
5	ICE4		8.5182	0.0085

SUMMARY OF STEPWISE REGRESSION PROCEDURE FOR SUMMER

VARIABLE ENTERED	VARIABLE REMOVED	NUMBER IN	PARTIAL R**2	MODEL R**2	EQUATION COEFFICIENT
ICE11		1	0.4036	0.4036	
ICE3		2	0.1913	0.5949	1.000
ICEM3		3	0.0672	0.6621	-1.350
SST10		4	0.1012	0.7633	0.452
ICE9		5	0.0621	0.8254	0.417
	ICE11	4	0.0123	0.8131	
U6		5	0.0509	0.8640	-0.235
INTERCEPT					0.057

STEP	VARIABLE ENTERED	VARIABLE REMOVED	F	PROB>F
1	ICE11		16.2434	0.0005
2	ICE3		10.8603	0.0032
3	ICEM3		4.3743	0.0482
4	SST10		8.9751	0.0069
5	ICE9		7.1166	0.0148
6		ICE11	1.4090	0.2491
7	U6		7.4919	0.0127

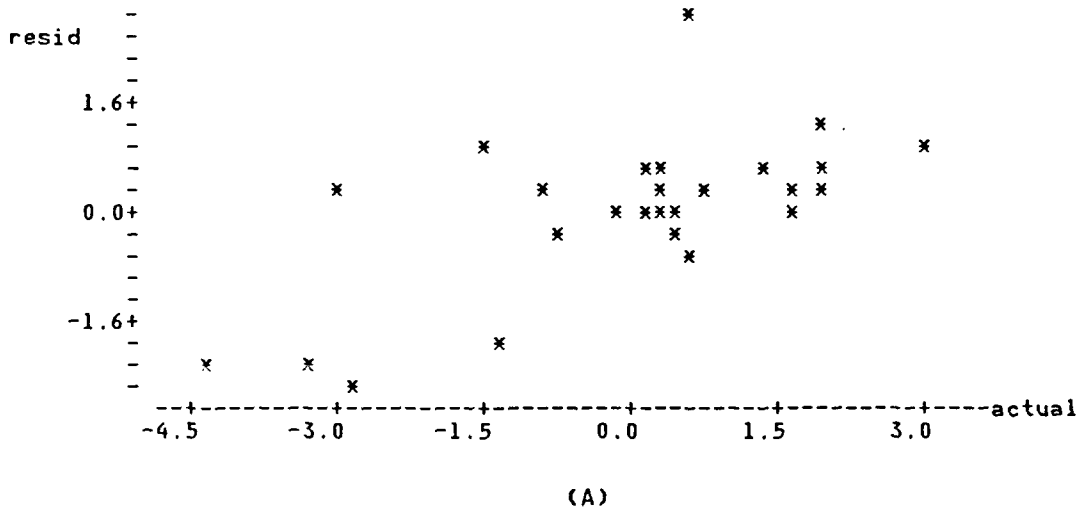

(A)

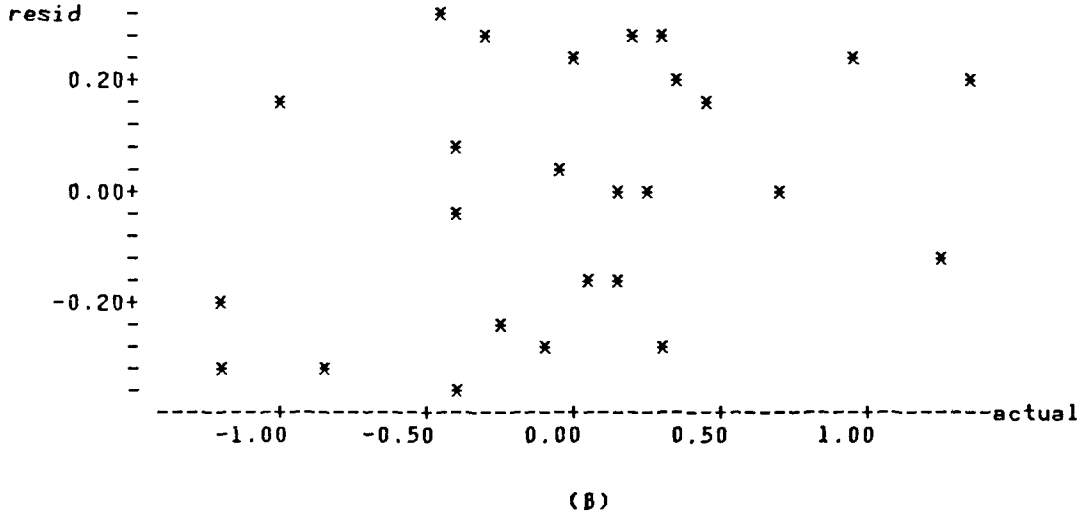

(B)

Figure 4.11 Scatter plots of actual versus residual ice concentration anomaly values for (a) winter and (b) summer at grid point 1.

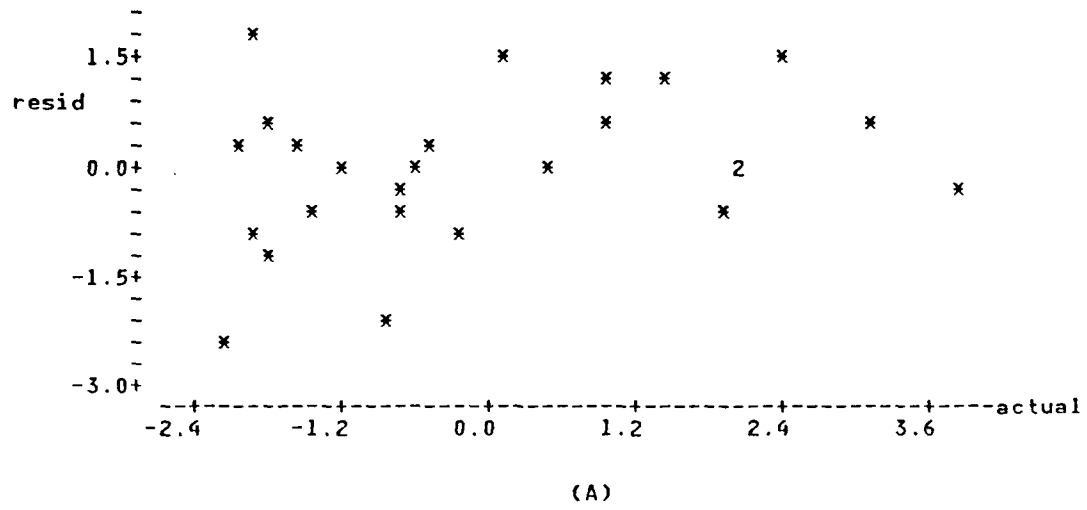

(A)

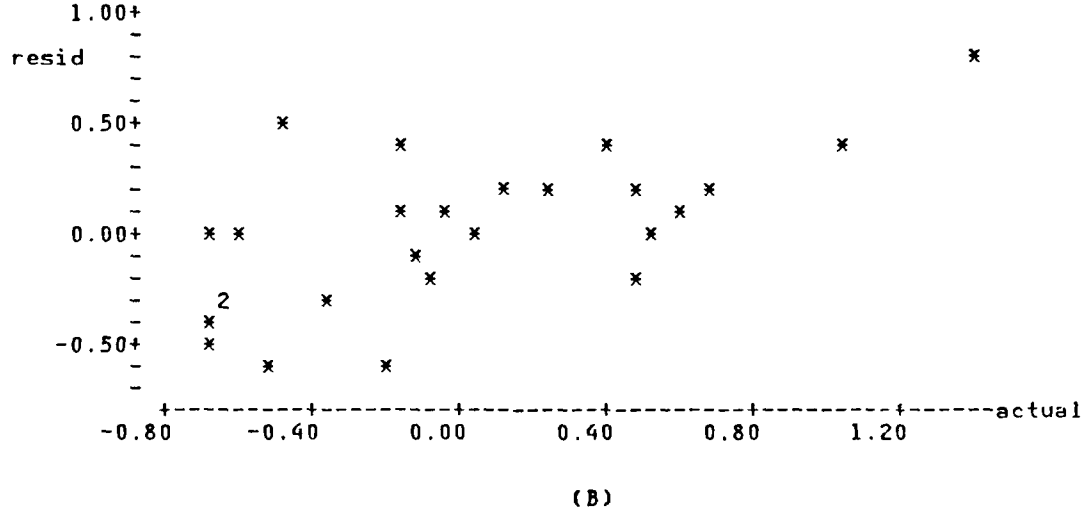

(B)

Figure 4.12 Scatter plots of actual versus residual ice concentration anomaly values for (a) winter and (b) summer at grid point 2.

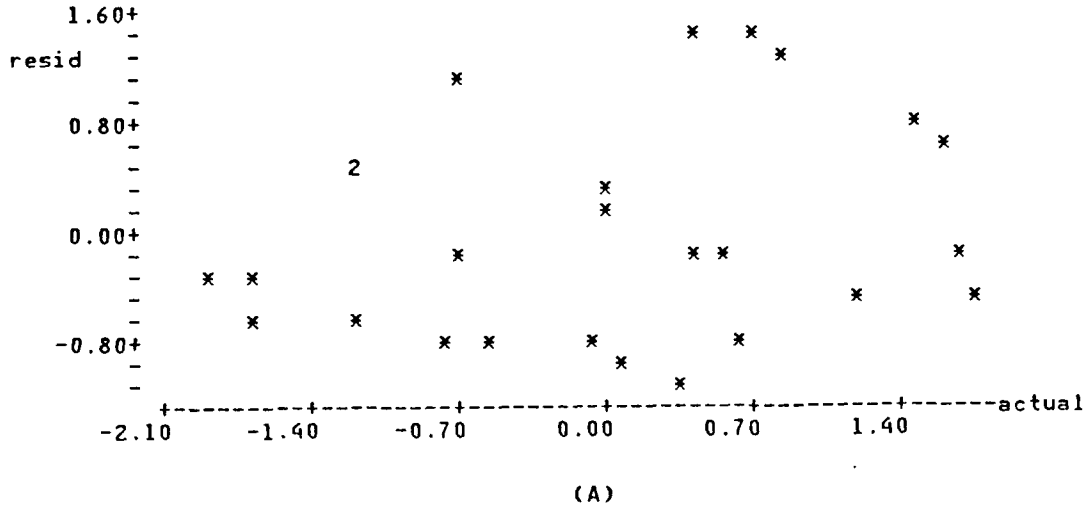

(A)

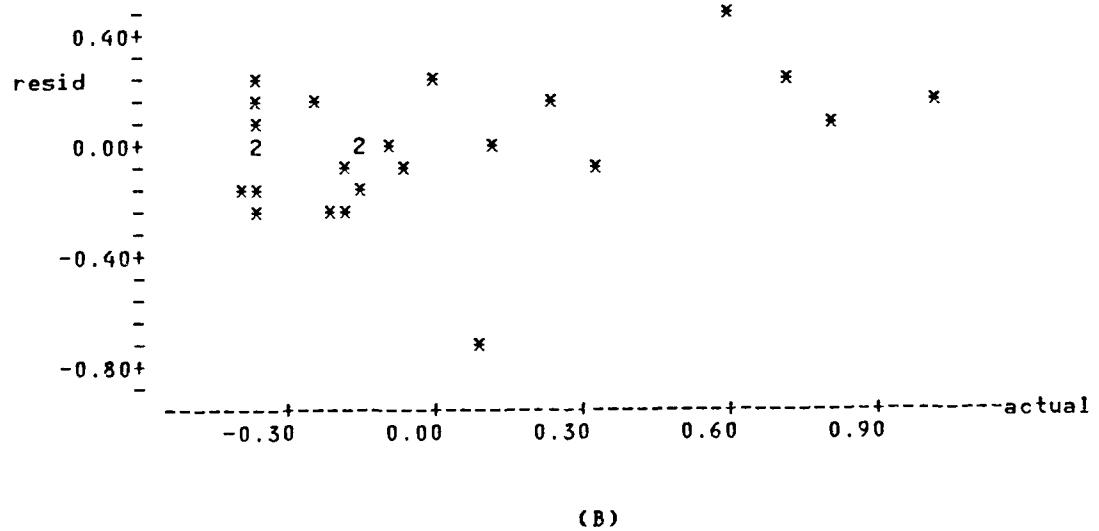

(B)

Figure 4.13 Scatter plots of actual versus residual ice concentration anomaly values for (a) winter and (b) summer at grid point 3.

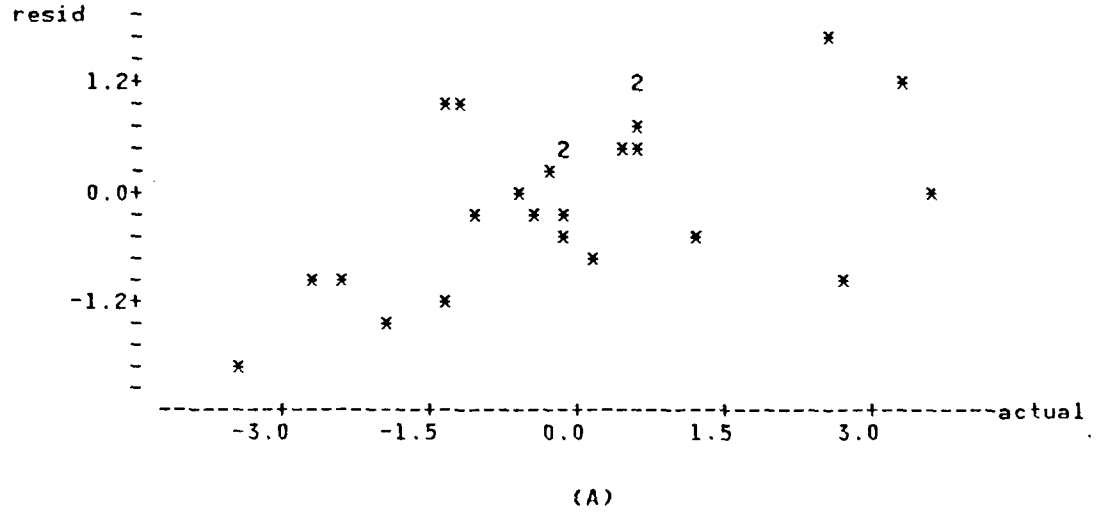

(A)

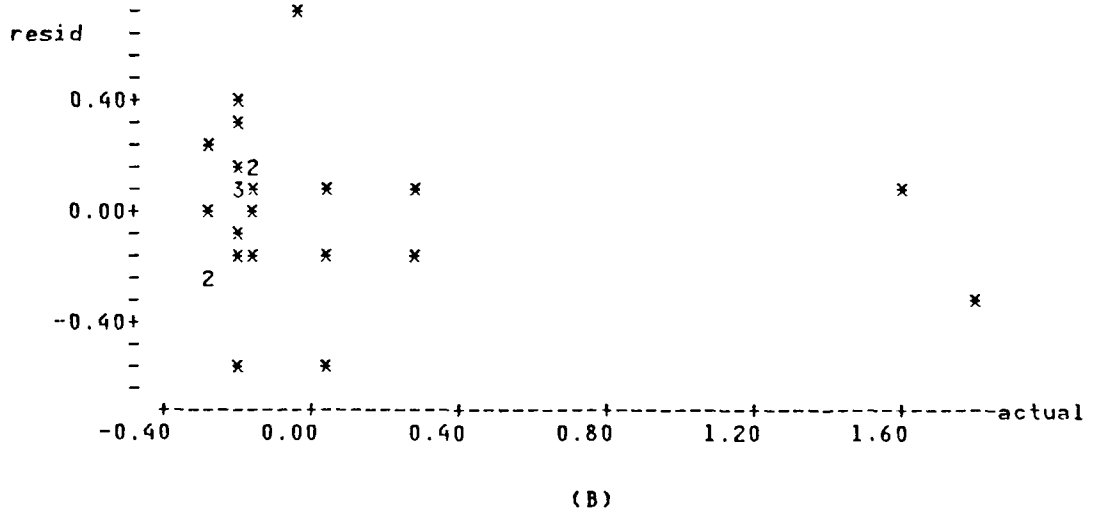

(B)

Figure 4.14 Scatter plots of actual versus residual ice concentration anomaly values for (a) winter and (b) summer at grid point 4.

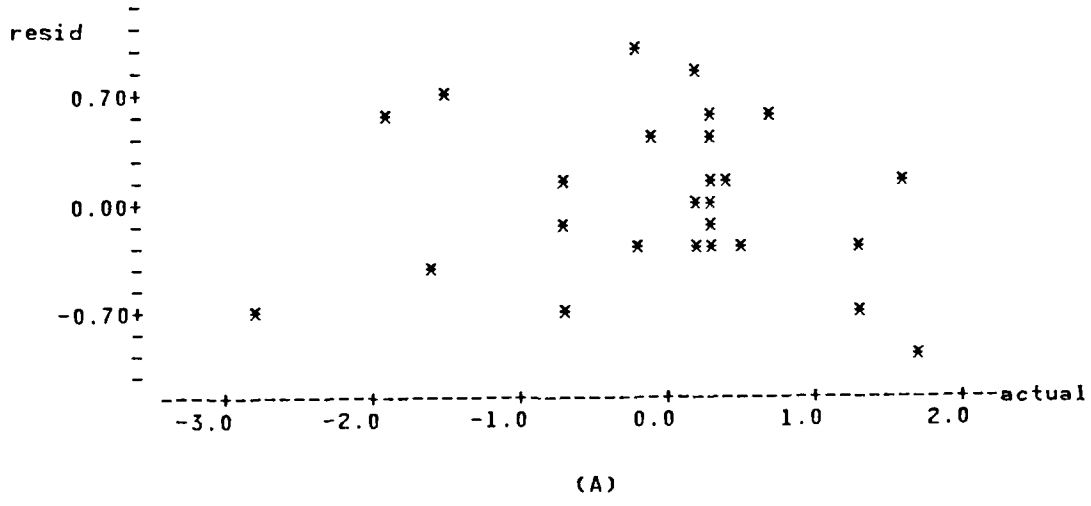

(A)

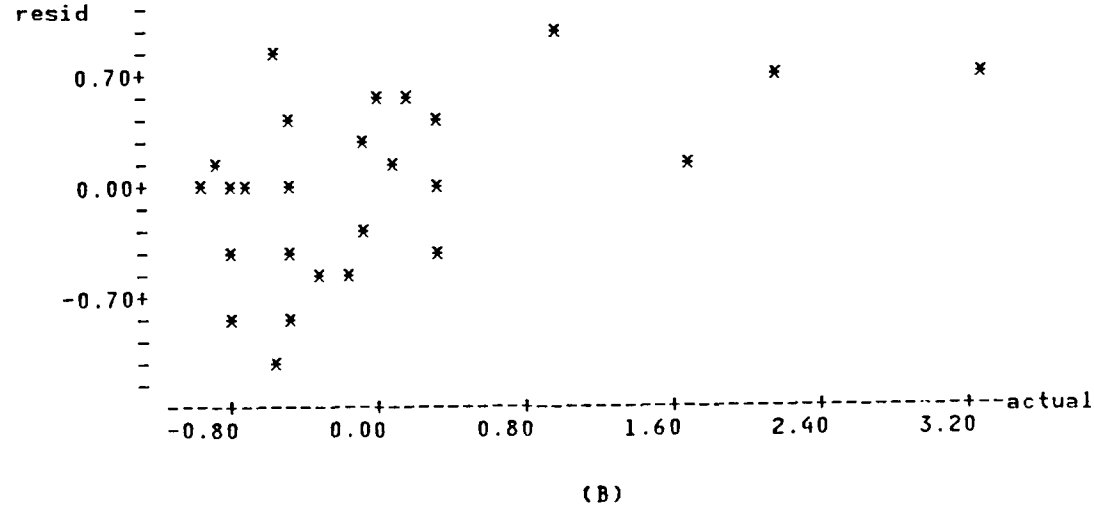

(B)

Figure 4.15 Scatter plots of actual versus residual ice concentration anomaly values for (a) winter and (b) summer at grid point 5.

V. DISCUSSION

The previous chapter established that regression equations which incorporate various forcing functions can be formulated to forecast long-term ice concentration anomalies. As might be expected, ice concentration anomalies with various lag times were the dominant predictors. Additionally, other forcing parameters influenced the evolution of ice concentration anomalies, as their contributions to the regression equations were considered to be statistically significant. This chapter will attempt to explain the variations in persistence between locations and seasons, why certain variables were included in the regression equations and how they could lead to a better understanding of ice concentration anomaly forecasting.

A. AUTOCORRELATIONS

The persistence of ice concentration anomalies has long been recognized as a useful forecasting parameter. In addition, Fleming (1987) demonstrated that the introduction of SST persistence could also be used in some areas of the Arctic Ocean to improve forecasts of ice concentration anomalies. Figures 4.6-4.11 illustrated the seasonal autocorrelations of ice concentration and SST anomalies for each area, which showed that persistence of these parameters varied quite extensively between each season and location. Although some areas displayed higher persistence during a season for one parameter, others exhibited notably weak, or no persistence. In general, the ice concentration anomaly persistence was stronger in the winter, while the SST anomaly persistence dominated in the summer.

Grid point 2, north of Iceland, exhibited the strongest persistence of the winter ice concentration anomaly, extending over two winters. The southward flowing East Greenland

point 3 is in a protected area with Svalbard and the Arctic pack serving as boundaries to the north, while Novaya Zemlya serves as a land barrier to the east of grid point 5. These barriers preclude ice dispersion to the north or to the east, respectively, resulting in confinement of the ice concentration anomalies. Although the correlation is negative, these anomalies could serve as predictors for the ice concentration anomalies into the third season.

B. REGRESSION EQUATIONS

Since the purpose of this work was to develop a statistical method to forecast ice concentration anomalies for a seasonal period over a broad area, one must consider the climatological trends of both the oceanic and atmospheric forcing parameters. Long term averages will not reflect fluctuations which occur over short periods of time. For example, ice concentrations may change considerably within a few weeks over a small region. However, the ice concentration averaged over a three month period over a broad area will not reflect these local changes.

Overall, few similarities or trends in the parameters retained by the regression equations were noted between locations. Each equation for each location and season tended to be unique. As expected, most equations for all five areas retained various ice concentration anomalies. Ice accumulation preceding a winter or summer season would directly impact the ice concentration anomaly within the next several months. If an area were subjected to extremely heavy ice buildup during a winter, it would normally take a longer period of time to melt or be advected away from the region. Conversely, conditions of light ice accumulation would tend to dissipate more rapidly, leading to lower ice concentration anomalies during the following season.

An additional similarity noted in the regression equations was that the SST anomaly from the previous winter was a component in four of the five winter equations to forecast

the following winter's ice concentration anomaly. The SST anomaly at either a 12 or 13 month lag was retained by the winter equations for grid points 1, 2, 3 and 5, with this anomaly explaining most of the equation's variance at grid point 3. Although these four geographic areas share similarities, each has its unique differences.

The effects of SST on sea ice are rather straightforward. A warm SST anomaly would delay freezing and limit ice growth, while a cold SST anomaly would promote early freezing and heavier ice production. When averaged over a period of a month, the resulting SST anomalies for these four locations are clearly highly cross-correlated with the ice concentration anomalies and serve as good predictors for the following year's ice concentration anomalies. Variations of the SST anomaly at these locations are evidently robust enough to influence ice concentration anomalies the following winter.

The SST anomaly at grid point 1 in the Greenland Sea is directly influenced by the EGC, which transports cold water and sea ice from the Arctic basin. Also, this area is located near the MIZ, which is affected by a number of physical processes. Ice-edge eddies and meanders which could modify the SST anomaly are common along this region (Gascard et al., 1988). Also, penetrating waves and swells from open waters that reach the margin could generate a shear current at the ice-ocean interface, which would increase the melt rate, and eventually alter the SST anomaly (Wadhams, 1986).

Grid point 2 near Iceland is under the influence of both the EGC and the East Icelandic Current. These currents advect sea ice into this area from much farther north. The warm waters of the Irminger Current do not influence this area during winter; hence, the waters at this location remain cold during winter. Therefore, the sea ice concentration has a sufficiently long time to respond to any SST anomaly that may develop (Fleming, 1987). These anomalies would

subsequently have a longer time period to influence the presence or dissipation of sea ice.

The winter regression equation for grid point 3 was dominated by the previous winter's SST anomaly. In addition to the EGC, ice concentration at this location is influenced by the East Spitsbergen Current. These cold currents and the more northern location of this area support cold temperatures, which would sustain the effect of the SST anomaly. Since this area is north of any warm currents, surface temperatures tend to remain more constant. Therefore, local weather effects would not change the SST significantly, and any changes in SST that may occur, would probably impact future ice concentration anomalies more significantly.

Grid point 5 is located in a region of little current activity and high ice concentration. These inherently cold waters enhance ice presence and growth. As at grid point 3, any changes in the SST anomaly would be expected to be small, and could therefore significantly impact future ice concentration anomalies.

Another common variable retained by many of the summer regression equations was the sea level pressure anomaly. All of the summer equations except for grid point 5 retained this parameter at various lags. The importance of the sea level pressure anomalies is supported by the earlier explanation of Zubov (1945). The trajectory and translation speed of cyclones entering the Arctic Seas directly effect the sea ice patterns. When the ice cover begins to melt in the spring and early summer, the presence of these storms could lead to a much more rapid breakup of the ice cover. Conversely, the lack of storm activity may lead to the ice cover enduring longer through the summer and fall seasons, which would possibly increase the ice concentration of the following winter.

The sea level pressure anomaly retained by the regression equation at grid point 1 in the Greenland Sea is not related

to any persistent storm track. However, it most probably reflects the importance of the transport of sea ice out of Fram Strait. The sea level pressure anomaly averaged from December to February could relate directly to Kirillov and Khromtsova's (1974) findings as mentioned in Chapter I. They found that including the export of Arctic ice through Fram Strait, computed from pressure differences, improved the ice concentration anomaly forecast during the summer.

At grid point 2 in the southern Greenland Sea, the sea level pressure anomaly from March is directly related to the proximity of the spring-time storm track (Figure 2.2) in this region. The location and intensity of the Icelandic low could also influence the sea level pressure anomaly.

Sea level pressure anomalies were important components in both summer and winter equations at grid points 3 near Svalbard and 4 in the western Barents Sea. As Figure 2.2 shows, the storm tracks from January and April through June greatly influence the Svalbard area. Sea level pressure anomalies from the fall transition season at grid point 4 are also related to the storm track, although the storm track from October through December is located just south of the region.

Related to sea level pressure anomalies are the wind component anomalies. These anomalies were also retained by most of the summer regression equations. Wind component anomalies from March were important contributors to the summer ice concentration anomaly forecast at grid points 1, 4 and 5. Figure 5.1 depicts the maximum, mean and minimum ice edge locations for mid-March with the mean wind from March plotted at the three grid points. As this figure shows, all three of these areas are located in the vicinity of the mean ice edge, i.e., these areas are not completely ice-covered during this time of year. Therefore, the wind anomalies could effect the ice present in these areas since it would have freedom to respond to the wind.

The March wind anomalies could significantly increase or decrease the ice extent and its degree of compactness before the breakup of the ice cover begins in April. The compactness of the ice pack at the end of March can be expected to eventually enhance or inhibit sea ice dissipation. By summer ice could still exist from a compact ice area if on-ice winds dominated over an extended period of time. Conversely, off-ice winds leading to a diffuse ice cover with lower ice concentrations would tend to break up and melt more expeditiously, resulting in lower summer ice concentration anomalies. Winds blowing parallel to an ice edge would not modify the compactness of the ice as significantly as an on/off-ice wind. Depending on the wind direction, these winds would lead to either dispersion or convergence of the sea ice due to the influence on the ice transport of the Coriolis force.

At grid point 1 in the Greenland Sea the mean ice edge tends to be oriented north/south. As depicted in Figure 5.1, the V wind component would represent a wind blowing from the north and essentially parallel to the ice edge. As noted above, this flow pattern could induce convergence of the ice pack, leading to a more compact ice cover. However, transient ice-edge eddies could generate ice streamers. Such streamers could cause more open water and enhanced melting, and eventually a lesser summer ice concentration anomaly. However, the EGC continuously transports sea ice and cold water from the Arctic basin into this region. The V wind component anomaly would enhance the drift rate of sea ice by the EGC, which could increase the ice concentration anomaly, offsetting the effects of the ice streamers and accentuating the effects of convergence.

In the Barents Sea at grid point 4 the direction of the mean ice edge varies, although climatologically it tends to lie east/west. Again, Figure 5.1 shows that the V wind component anomaly at this location represents the on-ice wind component. However, at grid point 5, the mean ice edge

extends north/south, and the U wind component represents an off-ice wind, which would tend to disperse the ice pack. Some of this ice could be blown into open ocean and warmer waters, which would infer more open water and lower ice concentration anomalies. However, grid point 5 is located in an area of high ice concentration and cold temperatures. Despite the average off-ice wind component during March, this wind blows over broad areas of ice, which could advect cold air temperatures into the region and support the continued presence of sea ice. Possibly, vertical heat exchange through the upper ocean coupled with the thermal advection of cold waters could maintain cold surface temperatures, which would support continued high ice concentration anomalies.

Noticeably absent from the regression equations are parameters from the fall transition season for grid points 1, 2 and 3. The only parameter retained by an equation was the U wind component anomaly from November at grid point 1 for the summer equation. The fall transition season tends to be volatile, causing high interannual variability of atmospheric parameters to occur.

Although the climatological sea level pressure patterns generally indicate a weak pressure gradient in October, early winter storms can occur, bringing a change in wind direction and speed. When averaged over a period of a month, short term high intensity storm winds could offset the influence of the long term climatological winds, resulting in a negligible monthly averaged anomaly.

Other fall parameters not retained by the regression equations were air and sea surface temperatures. Air temperatures also vary considerably over short time scales during this time of year. Insolation is reduced due to shorter days, increasing the amount of cooling. However, warming still occurs during daylight hours. These overall changes in the heat budget could lead to an insignificant monthly air temperature anomaly. In addition, the SST would

not be greatly affected by the small net change in air temperatures.

Conversely, at grid points 4 and 5 in the Barents Sea, parameters from October and November were important contributors to both the winter and summer forecasts. One of the major differences between the Greenland and Barents Seas is that during summer and fall in the Barents Sea the area not covered by sea ice is at a maximum (Parkinson, et al., 1987). This is due to the near total ice cover in winter and the large retreat of the ice during summer in the Barents Sea. However, in the Greenland Sea the distribution of open water is nearly uniform throughout the year, with a slight increase in late summer/early fall. This open water is attributed to the presence of leads and polynas within the ice pack.

In regions such as the Barents Sea, with little or no late-summer ice, the onset of significant seasonal ice growth could depend on the proximity of the summer ice edge to the north and on the general cooling patterns in the Northern Hemisphere (Parkinson et al., 1987). This could partially explain why the November U wind component anomaly was common to both winter equations for grid points 4 and 5. As the cooling pattern is established, colder air temperatures would be advected into the region, leading to the early formation of sea ice.

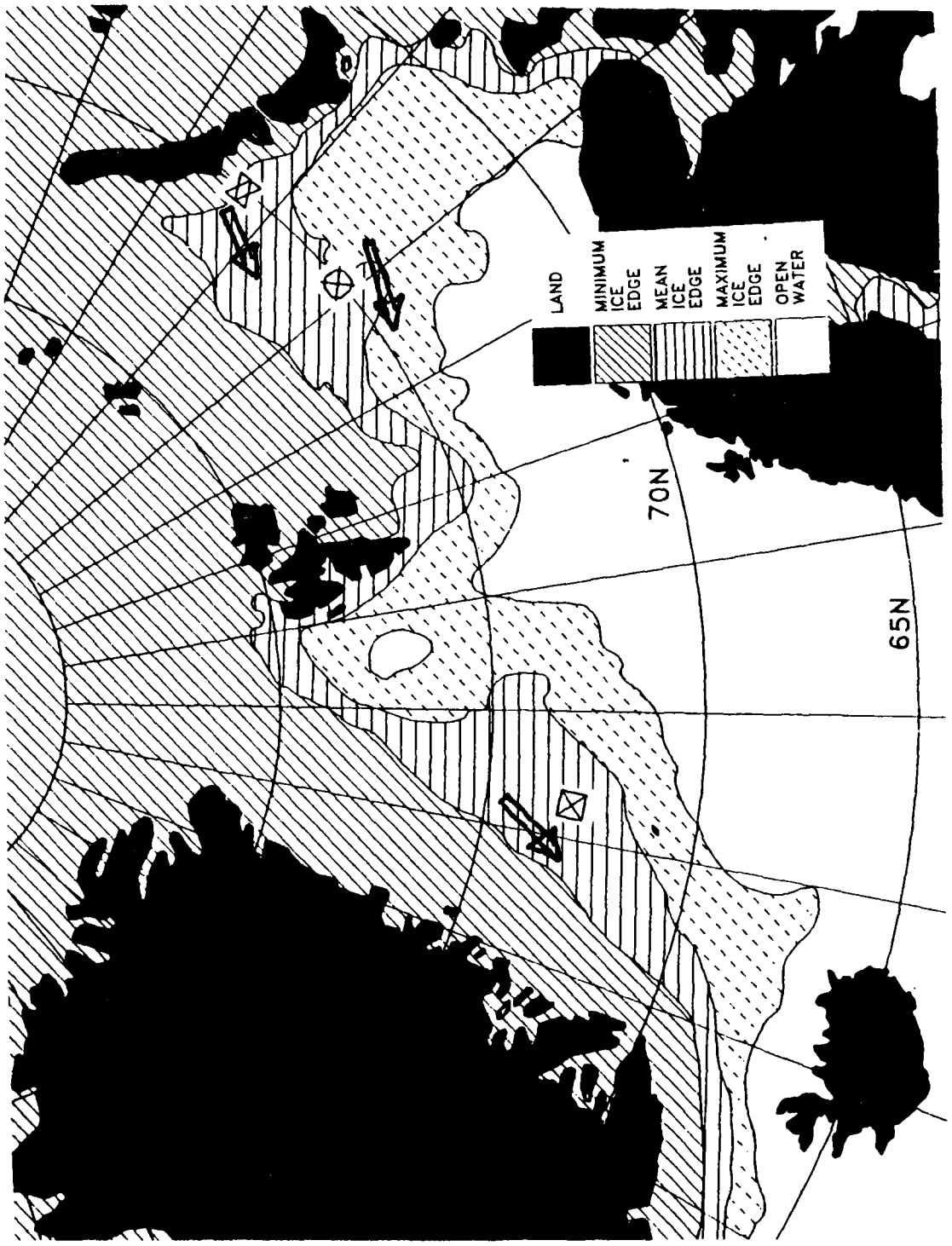

Figure 5.1 Location of maximum, mean and minimum ice edges for 15 March with the average mean wind velocity for grid points 1, 4 and 5 (from NOCD Asheville, 1986).

VI. CONCLUSIONS

Based on a 27 year data record from the COADS and SEIC data sets, a statistical analysis of ice concentration, sea surface temperature (SST), air temperature, U and V wind components, and sea level pressure anomaly data, or departures from monthly means, was conducted for five locations in the North Atlantic. These forcing functions exhibited regional dependence as they displayed various spectral density and persistence characteristics.

Regression equations were formulated based on the above data sets to calculate both the winter and summer ice concentration anomalies for the five different regions. The parameters retained by these equations indicated which forcing functions were most highly cross-correlated with the ice concentration anomaly for that location and season.

This study yielded the following results and conclusions:

1. The estimated spectral densities of both the spatially averaged and anomaly data indicated a strong annual cycle for the ice concentration, SST, air temperature and sea level pressure parameters. Shorter cycles of five and nine months were found for some of the U and V wind component parameters.

2. Persistence of the ice concentration and SST anomalies exhibited strong regional dependence. In general, the ice concentration persistence was longer in the winter and SST persistence was longer in the summer.

3. Areas near the land boundaries of Iceland, Svalbard and Novaya Zemlya exhibited enhanced ice concentration and SST anomaly persistence. These boundaries prevented strong advection of ice concentration or SST anomalies from the region, which allowed them to influence the region longer. Persistence of both the ice concentration and SST anomaly was lowest near the MIZ in the Greenland Sea, a region strongly influenced by the East Greenland Current (EGC). The volume of ice transported out of the Arctic Basin by this current fluctuates on short time scales, affecting both ice concentration and SST anomalies. The characteristics of this current led to decreased persistence.

4. The SST anomaly from a previous winter was a strong predictor of the ice concentration anomaly for the following winter in four of the five locations, which were near land, ice or shear boundaries. These boundaries allowed the SST anomaly to influence the region for an extended period of time, which eventually affected the ice concentration anomaly. This SST

anomaly had the most influence at the grid point near Svalbard, which was the most influenced of all five grid points by a boundary.

5. The on/off-ice component of wind anomalies influenced the regression equations at two locations in the Barents Sea, while the alongshore wind component anomaly (southward flow) influenced the equation in the northern Greenland Sea. These wind anomalies from March directly affected the summer ice concentration anomaly at all of the above locations.

6. Meteorological and oceanic events that occurred during the fall transition season did not affect the ice concentration anomalies at locations in the Greenland Sea or near Svalbard. However, some fall parameters were retained by the regression equations for the two locations in the Barents Sea. The short fall season is volatile, causing high interannual variability of atmospheric and oceanic parameters. Their time scales are expected to be too short to influence future ice concentration anomalies.

7. Sea level pressure anomalies were important contributors to the regression equations in both the Greenland and the Barents Sea. The passage of cyclones in the proximity of the ice cover directly effect future ice concentration anomalies.

8. Using statistical methods, regression equations which employed ice concentration, meteorological and oceanic parameters were successfully formulated to forecast ice concentration anomalies at lead times of at least one season. In general, the ice concentration anomaly at various lag times was the most influential parameter. However, since both meteorological and oceanic parameters were retained by the equations which increased the total explained model variance, the accuracy of a forecast should be improved over models based on just ice concentration anomaly persistence.

LIST OF REFERENCES

Björnsson, H., "Sea Ice Conditions and the Atmospheric Circulation North of Iceland," Jokull, v. 19, pp. 11-17, 1969.

Coachman, L.K. and K. Aagaard, "Physical Oceanography of Arctic and Subarctic Seas, In: Marine Geology and Oceanography of the Arctic Seas (Y. Herman, Ed.), Springer-Verlag, pp. 1-72, 1974.

Einarsson, T., "The Ice in the North Polar Basin and in the Greenland Sea, and the General Causes of Occasional Approach of the Ice to the Coast of Iceland," Jokull, v. 19, pp. 2-6, 1969.

Fleming, G. H., Predictability of Ice Concentration in the High-Latitude North Atlantic from Statistical Analysis of SST and Ice Concentration Data, Master's Thesis, Naval Postgraduate School, Monterey, California, September 1987.

Gascard, J. C., and others, "Diagnostic Study of the Fram Strait Marginal Ice Zone During Summer From 1983 and 1984 Marginal Ice Zone Experiment Lagrangian Observations," J. Geophys. Res., v. 93, pp. 3613-3641, 1988.

Gatham, S. G., "Climatology," In: The Nordic Seas (B. G. Hurdle, Ed.), Springer-Verlag, pp. 1-18, 1986.

Gross, C. E., "Joint Ice Center Global Sea Ice Digital Data," Snow Watch '85, Glaciological Data GD-18, World Data Center for Glaciology, Boulder, Colorado, 125 pp., 1986.

Herman, G. F., "Atmospheric Modelling and Air-Sea-Ice Interaction," In: The Geophysics of Sea Ice (N. Untersteiner, Ed), Plenum Press, New York, pp. 713-754, 1986.

Herman, G. F., and W. T. Johnson, "The Sensitivity of the General Circulation to Arctic Sea Ice Boundaries: A Numerical Experiment," Mon. Weather Rev., v. 106, pp. 1649-1664, 1978.

Hibler III, W. D., "A Dynamic Thermodynamic Sea Ice Model," J. Phys. Oceanogr., v. 9, pp. 815-846, 1979.

Hibler III, W. D., and K. Bryan, "A Diagnostic Ice-Ocean Model," J. Phys. Oceanogr., v. 17, pp. 987-1015, 1987.

Johannessen, O. M., "Brief Overview of the Physical Oceanography," In: The Nordic Seas (B. G. Hurdle, Ed.), Springer-Verlag, pp. 103-127, 1986.

Kirillov, A. A., and M. S. Khromtsova, "Many-Year Variations of the Ice Coverage of the Greenland Sea and Methods of Forecasting it," AIDJEX Bulletin, v. 303, pp. 46-55, 1974.

Lebedev, A. A., and N. S. Uralov, "Method of Ice Forecasting in the North Atlantic and Adjacent Seas," Sea Ice: Proceedings of an International Conference, National Research Council of Iceland, Reykjavik, pp. 59-61, 1972.

Naval Oceanography Command Detachment, Asheville, N. C., Sea Ice Climatic Atlas: Volume II Arctic East, pp. 1-24, 1986.

Oort, A. H., and others, "Historical Trends in the Surface Temperature Over the Oceans Based on the COADS," Climate Dynamics, v. 2, pp. 29-38, 1987.

Parkinson, C. L., and others, Arctic Sea Ice 1973-1976: Satellite Passive Microwave Observations, 296 pp, NASA, 1987.

Preller, R. H., "The NORDA/FNOC Polar Ice Prediction System (PIPS) - Arctic: a Technical Description," Naval Ocean Research and Development Activity Report 108, 61 pp., 1985.

Ramage, C. S., "Can Shipboard Measurements Reveal Secular Changes in Tropical Air-Sea Heat Flux?," J. Climate Appl. Meteor., v. 23, pp. 187-193, 1984.

Sancevich, T. I., "Methods of Long-Term Hydrometeorological Forecasts for the Arctic," In: Ice Forecasting Techniques for the Arctic Seas (B. A. Krutskih, Z. M. Gudkovic and A. L. Sokolov, Eds.), Trudy AANII, pp. 48-86, 1976.

Sanderson, R. M., "Ice-Edge Movements in the Greenland Sea," Marine Observer, v. 41, pp. 173-183, 1971.

Sater, J. E., Ronhovde, A. G. and Van Allen, L. C., Arctic Environment and Resources, Arctic Institute of North America, Washington, D.C., 309 pp., 1971.

Science Applications International Corporation, An Investigation of Soviet Capabilities in Extended Range Arctic Ice Forecasting, pp. 6-36, 1987.

Semtner, A. J. Jr., "A Numerical Study of Sea Ice and Ocean Circulation in the Arctic," J. Phys. Oceanogr., v. 17, pp. 1077-1099, 1987.

Slutz, R. J., and others, Comprehensive Ocean-Atmosphere Data Set Release 1, 268 pp, 1985.

Wadhams, P., "The Ice Cover," In: The Nordic Seas (B. G. Hurdle, Ed.), Springer-Verlag, pp. 21-87, 1986.

Walpole, R. E. and Myers, R. H., Probability and Statistics for Engineers and Scientists, 3rd ed., pp. 383-387 MacMillan Publishing Co., 1985.

Walsh, J. E., "Diagnostic Studies of Large-Scale Air-Sea-Ice Interactions," In: The Geophysics of Sea Ice (N. Untersteiner, Ed), Plenum Press, pp. 755-784, 1986.

Walsh, J. E. and C. M. Johnson, "An Analysis of Arctic Sea Ice Fluctuations, 1953-1977," J. Phys. Oceanogr., v. 9, pp. 580-591, 1979.

Welsh, J. P., and others, "A Compendium of Arctic Environmental Information," Naval Ocean Research and Development Activity Report 138, pp. 69-88, 1986.

Vinje, T., and Finnekasa, O., "The Ice Transport through the Fram Strait," Norsk Polar Institute, Oslo, Norway, 186, 36 pp., 1986.

Zubov, N. N., Arctic Ice (in Russian), Izdatel'stvo Glavsermorputi, Moscow (English translation by U. S. Naval Oceanographic Office, Bay St. Louis, MS), 1945.

INITIAL DISTRIBUTION LIST

1.	Defense Technical Information Center Cameron Station Alexandria, VA 22304-6145	2
2.	Library, Code 0142 Naval Postgraduate School Monterey, CA 93943-5002	2
3.	Chairman (Code 68Co) Department of Oceanography Naval Postgraduate School Monterey, CA 93943	1
4.	Chairman (Code 68Rd) Department of Meteorology Naval Postgraduate School Monterey, CA 93943	1
5.	Dr. R. H. Bourke (Code 68Bf) Department of Oceanography Naval Postgraduate School Monterey, CA 93943-5002	1
6.	Dr. L. D. Johnson (Code 55Jo) Department of Operations Research Naval Postgraduate School Monterey, CA 93943-5002	1
7.	LT K. S. Garcia Naval Polar Oceanography Center 4301 Suitland Rd Washington, DC 20395-5180	2
8.	Director Naval Oceanography Division Naval Observatory 34th and Massachusetts Avenue NW Washington, DC 20390	1
9.	Commander Naval Oceanography Command NSTL Station Bay St. Louis, MS 39522	1
10.	Commanding Officer Naval Oceanographic Office NSTL Station Bay St. Louis, MS 39522	1
11.	Commanding Officer Fleet Numerical Oceanography Center Monterey, CA 93940	1
12.	Commanding Officer Naval Ocean Research and Development Activity NSTL Station Bay St. Louis, MS 39522	1
13.	Commanding Officer Naval Environmental Prediction Research Facility Monterey, CA 93940	1

14.	Chairman, Oceanography Department U. S. Naval Academy Annapolis, MD 21402	1
15.	Office of Naval Research (Code 420) Naval Ocean Research and Development Activity Attn: Dr. T. Curtin Dr. L. Johnson 800 N. Quincy Street Arlington, VA 22217	2
16.	Library Scripps Institute of Oceanography P. O. Box 2367 La Jolla, CA 92037	1
17.	Library Department of Oceanography University of Washington Seattle, WA 98105	1
18.	Library School of Oceanography Oregon State University Corvalis, OR 97331	1
19.	Naval Polar Oceanography Center Attn: CDR W. Perdue 4301 Suitland Road Washington, DC 20395-5180	1
20.	University of Illinois Attn: Dr. J. E. Walsh 1101 West Springfield Avenue Urbana, IL 61801	1
21.	LCDR G. Fleming Department of Oceanography Naval Postgraduate School Monterey, CA 93943-5002	1
22.	Dean of Science Royal Roads Military College F.M.O. Victoria, B. C., Canada VOS 1BO	1
23.	Department of Meteorology McGill University Attn: Dr. L. Mysak 805 Sherbrooke St. W Montreal, P. Q., Canada H3A 2K6	1